IMPINGING JET HEAT TRANSFER WITH TURBULENCE ENHANCEMENT AT THE NOZZLE

by

Robert W. McCleave

A Thesis Submitted to the Faculty of Graduate Studies and Research in Partial Fulfillment of the Requirements for the Degree of Master of Engineering

Department of Chemical Engineering
McGill University
Montreal

October 1993

ABSTRACT

The effect of turbulence enhancement at the nozzle exit on fluid flow and heat transfer characteristics was investigated for confined jets from sharp-edged nozzles.

Average turbulence intensity of the jet flow was characterised by integrating the local turbulence intensity values over the width of the nozzle and at several axial positions from the nozzle exit to the near approach to the impingement surface. Average impingement heat transfer was obtained by integrating the local Nusselt number over an area of the impingement surface relevant to the process engineering application of impingement drying of paper.

Of the several simple methods of turbulence generation examined, the most effective was the simple expedient of placing a bar with a diameter 1/8 that of the nozzle width along the centreline of the slot nozzle. For a heat transfer averaging area equivalent to a nozzle area of 5% of the impingement surface and a nozzle to impingement surface spacing of 1.0 to 1.5 times the nozzle width, this simple method increased average heat transfer rates over those of the plain nozzle by 14%, with only a 7% increase in nozzle operating pressure. The results are presented as enhancement in average heat transfer as a graphical function of mean turbulence intensity, and as an empirical correlation between mean Nusselt number, mean intensity of turbulence and Reynolds number.

RÉSUMÉ

Nous avons étudié l'effet de l'augmentation de la turbulence à la sortie d'une tuyère sur les caractéristiques d'écoulement des fluides et de transfert de la chaleur pour le cas des jets confinés des orifices à arêtes pointues.

L'intensité moyenne de la turbulence a été caractérisée en intégrant l'intensité locale de turbulence sur la largeur de la tuyère, à plusieurs positions axiales entre la sortie de la tuyère et la surface de transfert de chaleur. Le taux moyen de transfert de chaleur a été obtenu en intégrant le nombre de Nusselt local sur un superficie de la surface de transfert de chaleur choisie en fonction de l'application du séchage de papier par jets.

Plusieurs méthodes simples de génération de la turbulence ont été examinées. De celles-ci, la plus efficace consiste à placer une barre, d'un diamètre d' un huitième de la largeur de la tuyère, le long de son centre. Prenant la moyenne sur une superficie de la surface de transfert de chaleur équivalant à une superficie de tuyère de 5% de la surface de transfert, et pour une distance tuyère - surface de transfert égale à 1.0 à 1.5 fois la largeur de la tuyère, cette méthode a augmenté le taux moyen de transfert de chaleur de 14% par comparaison à une tuyère normale, avec une augmentation de la perte de charge de seulement 7%. Les résultats sont présentés par une méthode graphique, donnant le taux moyen de transfert de chaleur en fonction de l'intensité moyenne de la turbulence, de même que par une corrélation empirique entre le nombre de Nusselt moyen, l'intensité moyenne de la turbulence et le nombre de Reynolds.

ACKNOWLEDGEMENTS

I would like to thank my supervisor Dr. W.J.M. Douglas for his guidance and support, and the other members of the research group, who have been a constant source of advice and encouragement.

Financial support from the Pulp and Paper Research Institute of Canada, for the PAPRICAN fellowship, and from Canadian Pacific Forest Products Ltd., for the F.O. Fowler Memorial Fellowship, is gratefully acknowledged.

Thanks also go to the support staff of the McGill Chemical Engineering department and PAPRICAN, including the secretaries, technicians, and shop personnel, for many jobs well done.

I would like to express appreciation to the following people, in more or less chronological order, for gratuitous acts of generosity that contributed to the completion of my thesis: Dr. M.E. Weber, Mrs. A. Prihoda, Dr. J.M. Dealy, Mr. P. McRae, Mr. T. Browne.

This thesis is dedicated to Dr. Lois Mulligan, who is very, very good at what she does.

TABLE OF CONTENTS

LIST OF FIGURES

LIST OF TABLES

NOMENCLATURE

Name	Definition	Units
CD	cross machine direction	
h	heat transfer coefficient	[w/m^2 °C]
H	distance from impingement surface to nozzle exit	[m]
I	local turbulence intensity u'/U, expressed as %	
$\bar{I}$	mean turbulence intensity expressed as %	
$\bar{I}_1$	mean turbulence intensity measured at axial position 1, the nozzle exit	
$\bar{I}_2$	mean turbulence intensity measured at axial position 2, midway between the nozzle exit and the impingement surface	
$\bar{I}_3$	mean turbulence intensity measured at axial position 3, near the impingement surface	
k	thermal conductivity	[w/m °C]
MD	machine direction	
Nu	Nusselt number hw/k	
Nu_0	stagnation point Nusselt number	
$\overline{Nu}$	mean Nusselt number	
$\overline{Nu}_{10}$	mean Nusselt number for averaging area S/w=10	
Re	jet Reynolds number $\rho\bar{U}w/\mu$	
S	length in MD of one half of averaging distance	[m]
u'	local rms fluctuating jet velocity	[m/s]
U	local jet velocity	[m/s]
$\bar{U}$	mean jet velocity	
w	width of nozzle	[m]

z	axial position between nozzle exit and impingement surface	[m]

Greek symbols

ϱ	density	[kg/m^3]
μ	viscosity	[kg/m s]

Chapter 1. Introduction

1.1 Impinging Jets in Industrial Processes

Impinging jets are widely used industrially due to their high heat and mass transfer rates and the capability of precise control of the transfer processes at the impingement surface. Large scale industrial applications range from sheet metal annealing and cooling of turbine blades to the drying of paper and textiles. As drying involves substantial energy expenditure even small improvements in heat and mass transfer efficiency may result in significant savings in capital or operating costs for drying. Thus the present study is aimed at improving the industrially important process of impingement drying of paper.

Drying paper and textiles by jets requires the use of jets confined by a hood, which is typically also the nozzle plate. The design of such a confined impinging jet system is influenced by geometric and process variables. Geometric variables include the shape, size, pitch, and spacing of nozzles, the distance between the nozzle exit and the impingement surface, exhaust port location, turbulence generation and type of confinement. Important process variables are jet Reynolds number, jet to impingement surface temperature differential, jet humidity, speed of the impingement surface i.e. of the wet sheet relative to the jets, and fluid properties.

Some of the above variables have been studied extensively and optimum conditions determined. However, the aspects of special nozzle designs and turbulence generation still present interesting challenges and opportunities as there is a great range of possibilities. The potential for impingement heat transfer augmentation at an economically acceptable additional pressure drop is the challenge examined in the present study.

1.2 Characteristics of Impinging Jets

The flow field of an impinging jet, Figure 1.1, can be considered to comprise three characteristic regions: the free jet, impingement, and wall jet regions. The free jet consists of two parts: the potential core and the developing jet.

The potential core (a, Fig. 1.1) is a region of nearly constant axial velocity with boundaries determined by the nozzle exit velocity, the turbulence intensity at the nozzle opening, and the rate of growth of the two mixing layers originating at the nozzle edges. For an unconfined slot jet, the potential core was found by Dosdogru (1969) to terminate at a distance of 6 to 8 nozzle widths (6-8 w) from the nozzle exit. In the developing flow region (b, Fig. 1.1), the axial velocity decays as the jet spreads, approaching a Gaussian distribution.

The impingement region (c, Fig. 1.1) is characterized by a sharp increase in static pressure accompanying the

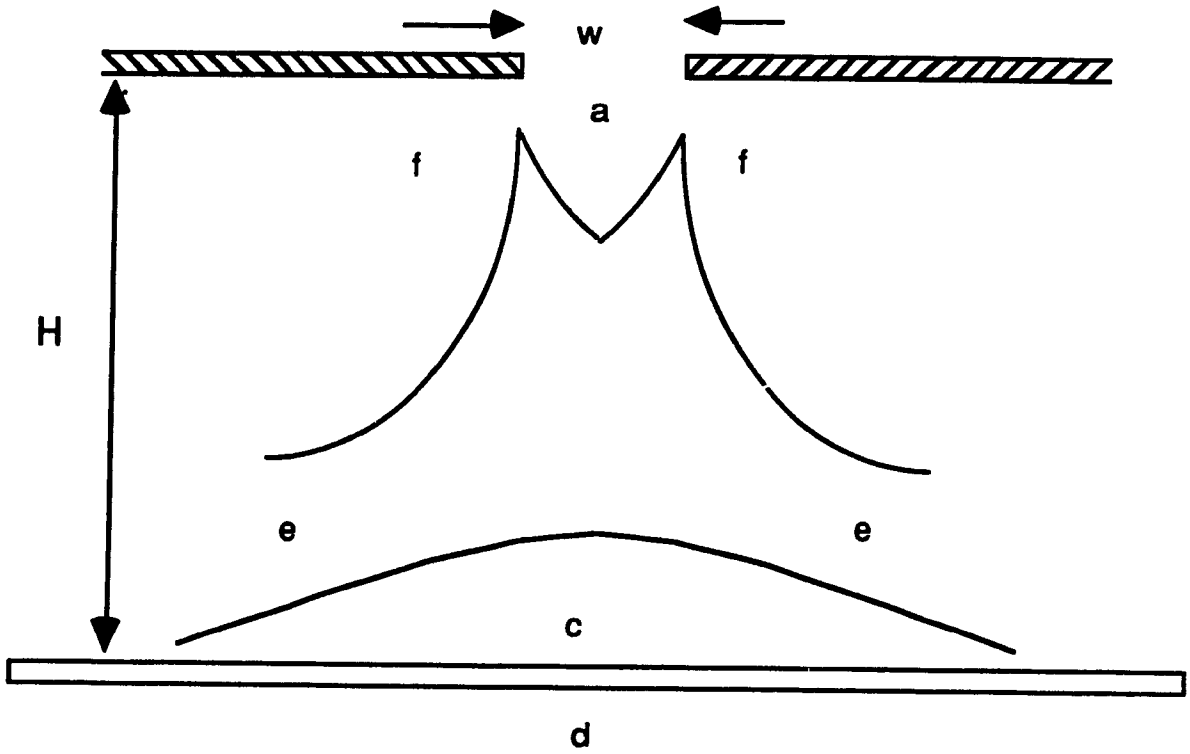

Fig 1.1 Flow field of an impinging jet.

corresponding decrease in axial velocity. This starts at a distance of about 0.21H from the impingement surface according to Saad (1981), or 1.2w from the impingement surface according to Martin (1977). The lateral extent of the impingement region depends on H/w and nozzle geometry. For a confined ASME standard slot nozzle with H/w>8, this lateral extent was reported by Gardon and Akfirat (1965) to be about 0.35H.

The flow behaviour in the wall jet region (e Fig. 1.1) is analogous to that of a free jet directed parallel to a flat plate. In this region, the static pressure increases as the flow spreads and decelerates. Although for convenience, unconfined jets have often been used by researchers, confined jets have far greater relevance for industrial heat transfer applications because energy recovery plays an important role in overall efficiency. In a confined jet, region 'f' of Figure 1.1 is typically a zone of recirculation with eddy formation.

Turbulence characteristics at the nozzle exit may have significant effect on impingement heat transfer rate. Hardisty and Can (1983) measured local impingement heat transfer rates for various shapes of slot nozzles at relatively large nozzle spacing, $6 < H/w < 8$. However, because the effect of nozzle exit flow field decreases rapidly with increasing H/w, their technique is not effective for smaller spacings, the region which is both more complex and potentially more important industrially.

Huang (1988) reported significant increases (100%) in

average heat transfer rate over those for a standard ASME nozzle for his case of H/w=3 with a confined slot jet discharging from a sharp edged re-entry channel. This significant enhancement in heat transfer was attributed to enhanced turbulence produced by his special nozzle design. However, his data are limited by having been taken for a single value of H, w, and re-entry length L of the nozzle.

Heat transfer enhancement with increase in nozzle exit turbulence has also been reported by Gardon and Akfirat (1965), Martin (1978) and Saad (1981). These studies do not however document velocity distribution or turbulence intensities. Studies of Taylor, 1961; Gutmark, 1989; Kataoka, et al. 1986 explore the effect of grids, honeycombs, cylinders, and perforated plates on the generation of turbulence. However these studies often involve flow in ducts rather than impinging jet flow, or do not include measurement of heat transfer rate at the impingement surface or of turbulence characteristics relevant to industrial applications. The above considerations were instrumental in defining the objectives of this work.

1.3 Objectives and Overview

The objectives of this work were to investigate the effect of turbulence generation at the nozzle exit on fluid flow and heat transfer characteristics for confined jets from

sharp-edged rectangular slot nozzles. Several simple methods of turbulence generation were examined. Geometric and flow parameters studied were nozzle width, nozzle to impingement surface spacing and jet Reynolds number. The effect of turbulence generation techniques on the flow field was documented by the measurement of local axial velocities at several positions between the nozzle exit and the impingement surface. As turbulence generation is at the expense of nozzle pressure drop, an important operating cost is industrial applications, the appropriate pressure was measured. The overall goal is to relate the enhancement in heat transfer rate at the impingement surface to the generation of turbulence at the nozzle exit; to document the impinging jet flow field which results from the nozzle exit jet conditions and which is the source of the heat transfer enhancement; and to quantify the cost of the enhancement in terms of the increase in pressure drop of the nozzle.

The organization of this thesis is as follows: Chapter 2 gives a critical review of the literature. Chapter 3 describes the development and use of experimental techniques used here to measure the fluid flow and heat transfer characteristics. The experimental results, analysis, and conclusions are presented in chapter 4.

Chapter 2. Literature Review

As a large volume of literature exists concerning turbulence, fluid flow, heat transfer and mass transfer with impinging jets, only a brief review of factors specifically relevant to this study is presented. General reviews on impingement jets are given in Gauntner (1970), Mujumdar and Douglas (1972), Martin (1977), Obot et al. (1979) and Polat et al. (1988).

2.1 Impinging Jet Flow Field

The development of velocity and turbulence intensity of jets has been studied by several researchers, following the early, definitive study by Corrsin (1943) for a free jet from a pipe. He found that axial turbulent velocity has the same three regions as the mean velocity, but with different limits. The potential core is much smaller for turbulent velocity than for mean velocity because of the higher rate of transport of turbulent energy. For the potential core region, turbulence intensity shows a minimum around the jet centre line and a maximum under the nozzle wall.

Gardon and Akfirat (1965) measured nozzle centre line turbulence intensities for impinging jets from long channel slot nozzles. An increase of stagnation point heat transfer was observed with increases in the nozzle to surface spacing

up to about 8w, due to increasing turbulence penetration towards the jet axis. Increase in spacing beyond the potential core length results in gradual decrease in heat transfer because of the decrease of mean velocity with increasing H. With H/w>14, the initial turbulence level at the nozzle exit contributes much less to heat transfer at the surface than does mixing induced turbulence. At the nozzle exit centre line for a long channel slot nozzle, up to 10% turbulence was measured by Gardon and Akfirat, while for an ASME contoured entry slot nozzle the measured axial turbulence intensity was less than 1% (Saad, 1981).

Gutmark et al. (1978) studied turbulent velocity profile, turbulence intensity, spectral and other statistical properties of turbulence of a 2-dimensional jet from an unconfined contoured entry slot nozzle. As the turbulence field of an impinging slot jet is quite anisotropic, the treatment of isotropic turbulence of earlier studies (Taylor, 1961) is not applicable. Turbulence intensity increases sharply with distance from the nozzle exit, then decreases sharply with approach to the surface. The effect of the impingement surface on the turbulence properties does not propagate back into the flow beyond 0.2H from the surface. Saad (1981) documented the turbulence intensity under impinging slot jets.

2.2 Impinging Jet Heat Transfer

Heat transfer from single impinging slot jets has been studied for a wide range of jet parameters: $1500 < Re_j < 110000$; $0.25 < H/w < 80$; x/w up to 750. However only Folayan (1977) and a number of studies from the laboratory of the present investigation (van Heiningen (1982), Polat (1988), Huang (1989) and Chen (1989)) considered confined jets, which have much greater significance in process industries. The heat transfer correlations and experimental conditions are summarized in table 2.1.

Gardon and Akfirat (1966) found that off-stagnation Nusselt number peaks subsided at H/w=8, marking the end of transition from the laminar stagnation flow to the wall jet turbulent boundary layer. Beyond H/w=8, the Nusselt number profiles become Gaussian.

For jets discharging from an ASME contoured-entry nozzle and including impingement surface motion, van Heiningen (1982) measured local heat transfer rate at the impingement surface with a highly sensitive, fast response heat flux sensor. The off-stagnation local heat transfer peaks were found be suppressed on the side where the impingement surface approaches the nozzle. Also, for a fixed jet flowrate, the average heat transfer was found to decrease with increasing surface motion.

Table 2.1 Heat transfer correlations

Researcher	Correlation	Limits	Nozzle
Metzger (1962)	$\overline{Nu}=0.547 Re^{0.566} f^{0.143} Pr^{0.63}$	1500<Re<5000 7/H/w<10 0.01<f<0.167	unconfined contoured
Gardon and Akfirat (1966)	$Nu_0=1.2 Re^{0.58} (H/w)^{-0.62}$ $\overline{Nu}=0.66 Re^{0.62} f^{0.38} (H/w)^{-0.31}$	2000<Re<50000 14<H/w<60 Re>2000 H/w>8 f<0.17	unconfined long channel slot
Schlünder et al. (1970)	$\frac{\overline{Nu}}{Pr^{0.42}} = \frac{3.06\ Re^{m}}{s/w+H/w+2.78}$ $m=0.695-\frac{2}{S/w+0.8\ (H/w)^{1.33}+6.12}$	1500<Re<45000 4<H/w<20 4<S/w<20	Unconfined

Table 2.1 continued

Researcher	Correlation	Limits	Nozzle
van Heiningen (1982)	$Nu_0=0.54Re^{0.5}$	5200<Re<20300 H/w=6 8.5<S/w<51	confined ASME contoured
	$\overline{Nu}=\frac{0.91}{S/w+22}Re^{0.76}$		
	$Nu_0=0.455Re^{0.5}$	9700<Re<91600 H/w=2.6	
Hardisty and Can (1983)	$Nu_0=0.43Re^{0.53}$	2000<Re<11000 H/w=8 5<S/w<20	unconfined various shapes
	$\overline{Nu}=0.42Re^{0.54}(S/w')^{-0.25}$		
	$w'=wCd$		

Table 2.1 continued

Researcher	Correlation	Limits	Nozzle
Huang (1988)	$Nu_0 = CRe^m$ $\overline{Nu} = \frac{A}{S/w + B} Re^n$	A, B, m functions of H/w 3<H/w<6	confined re-entry slot
Polat (1988)	$\overline{Nu} = 0.0938 Re^{0.679}$	8100<Re<25800 H/w=5 S/H=0.5	confined ASME contoured
Chen (1989)	$\overline{Nu} = \frac{a\ (H/w)^c}{S/w - 2H/w + b} Re^n$	a,b,c,n empirically determined 5<S/w<25 5000<Re<20000 3.1<H/w<6.2 1.3<L/w<13.3	confined re-entry slot

The enhancement of heat transfer by throughflow at the impingement surface was documented by Saad (1981) for a stationary impingement surface and by Polat (1988) for a high speed surface. In both cases standard ASME contoured-entry slot nozzles were used. For such nozzles, it was found that the average Nusselt number, $\overline{Nu}$, peaked for H/w=6, while the maximum stagnation point Nusselt number, Nu_0, occurred at a larger spacing, H/w=8. Polat determined impingement heat transfer using a sensitive porous thin film heat flux sensor in order to determine also the effect of throughflow at the impingement surface, a factor not involved in the present study. For eight unconfined nozzles, Hardisty and Can (1983) also observed similar maxima. However, at H/w>8, little potential remained for increasing $\overline{Nu}$ by varying nozzle geometry. They did not measure the jet flow field characteristics.

Korger and Krizek (1966), Cadek (1968), Kumada and Mabuchi (1970), Schlünder et al. (1970), van Heiningen (1982), and Polat (1988) all documented aspects of the size, location and Re-H/w dependency of the secondary peaks in local convective transfer rate, which are located about 5-7w from the stagnation point of single impinging slot jets.

Huang (1988) found that Nu_0 and $\overline{Nu}$ increased monotonically with decreasing spacing for 6>H/w>3 with a long channel re-entry slot nozzle, thus indicating Nu_0 and $\overline{Nu}$ maxima at H/w < 3 in contrast to previous work with other

nozzle types. For H/w=6, the difference in $\overline{Nu}$ between the re-entry and the ASME nozzles was negligible. Chen (1989) found that with variable length re-entry slot nozzles, impingement heat transfer is not significantly influenced by L/w, and that the heat transfer rates at H/w=3 and 6 match the maximum obtained at H/w=8 for ASME nozzles.

2.3 Effect of Turbulence on Heat Transfer

The relationship between the turbulent flow field and heat transfer was studied by Comings et al. (1948) who measured the influence of turbulence intensity on heat transfer rate for a cylinder in cross flow at Re=400 - 20000. Heat transfer at high Re was found to increase significantly for turbulence intensities as low as 3%. The maximum gain in Nusselt number was found to be 25% for I_j>10%. Maisel and Sherwood (1950) reported the rate of water evaporation from spheres and cylinders in cross flow. Turbulence intensity, measured with a Burgess-Dryden hot wire anemometer, was varied between 3.5-23% and the scale of turbulence between 5.1-12.7 mm. Turbulence intensity was found to have significant effect on mass transfer rate. A review on free stream turbulence and heat transfer is given by Kestin (1966).

Gardon and Akfirat (1965) varied the turbulence intensity from an unconfined slot jet with a #18 mesh screen placed at various distances upstream of the nozzle exit. The nozzle exit

turbulence intensities of 6 and 18% were obtained with the mesh placed 12.5 mm and 2.3 mm from the nozzle exit, respectively, for Re=11000 and H/w=2. The corresponding increases in Nu_0 for the above conditions were 25 and 80% respectively with an averaging distance of S/w=8. With increasing H/w, the heat transfer enhancement decreased, becoming negligible for H/w>8.

Gardon and Akfirat (1965) reported an increase in Nusselt number with nozzle width due to an increase in turbulence. Thurlow (1954) had also observed Nu enhancement (by a factor of 2.6) on increasing the diameter of a round nozzle from 1.27 to 2.54 cm. Saad (1981) likewise observed a similar dependency of heat transfer rate on the width of slot nozzles.

Gutmark et al. (1977) measured power spectra in the stagnation region for a contoured entry round nozzle. They reported an increase in turbulence intensity and mean axial velocity on forcing the jet turbulence higher than the neutral frequency of 27Hz at Re=12400, H/d=10. Forcing the turbulence structure to lower than neutral frequency had no effect on mean velocity.

Bayley and Milligan (1977) and Bayley and Priddy (1979) investigated the effect of free stream turbulence intensity and frequency on heat transfer to turbine blades. They varied turbulence frequency by the use of a variable speed motor turning a squirrel cage of horizontal bars in the flow field. For the tested frequency range they found, at the same level

of turbulence intensity, that heat transfer rates were higher at the higher frequencies . Enhancement of heat transfer by increasing free stream turbulence was also observed. They also noted a Reynolds number dependence on the heat transfer enhancement.

Hijikata et al. (1982) found a weak effect of the scale of turbulence on heat transfer around the stagnation point of a cylinder in cross flow. At Re=54000, however, the stagnation point Nusselt number, Nu_0, was found to increase by 20% for a small increase in turbulence intensity, 4.3 to 8.6%.

Yokobori et al. (1978) determined by flow visualization the structure and extent of large scale eddies in the plane stagnation flow field. Their work also indicated augmentation of heat transfer in the stagnation region through the control of streamwise vortex generation by upstream free shear layer disturbances.

Kataoka et al. (1986, 1987) reported visual observation with hot wire turbulence measurement using a hydrogen bubble technique in a turbulent free jet impinging normally on a flat plate. It was found that the large scale eddies became doubly periodic for the optimal spacing, H/w=6.7, due to the alternate impingement of fast and slow moving core fluids and sway of jet axis. The large scale eddies produced a turbulent surface renewal effect and the consequent heat transfer enhancement. The proposed surface renewal parameter, composed of the product of the Reynolds and Strouhal numbers,

correlated well with the stagnation point heat transfer augmentation. A review of the generation of nearly isotropic turbulence by several types of grids, examined by means of pressure losses, turbulence intensities, spectra, correlation functions and length scales, is given by Roach (1987).

2.4 Conclusions

Impingement heat transfer rates are sensitive to the properties of the flow field, particularly turbulence intensity and scales of eddy dissipation. However, as nozzle design is normally constrained by geometric and manufacturing cost factors, there is an incentive to investigate alternate methods to attain optimum heat transfer rates, including by turbulence generation at the nozzle. The literature survey reveals a paucity of data on local turbulence profiles for impingement heat transfer with turbulence generation. Further, most studies focused on unconfined impinging jets despite the overwhelmingly greater industrial relevance of confined jet systems. Thus the review of literature reveals little information concerning the enhancement of impingement heat transfer by turbulence generation at the nozzle, or the relation of the impinging jet flow field to the turbulence generation and to heat transfer, and nothing on the relation between nozzle pressure drop and such enhancement of turbulence and heat transfer.

Chapter 3. Experimental Equipment

3.1 Introduction

The experimental equipment consisted of a moving impingement surface, provided by a rotating cylinder 0.48m diameter by 0.22 m wide, enclosed by concentric hoods to confine the jet flow, with impinging jet nozzles and jet exhaust ports located integrally with the confinement hoods. By use of a heated jet on one side and an unheated jet on the other, the mean impingement cylinder temperature is steady at an intermediate value. The apparatus used is based on a modification of the Simtest facility, described elsewhere (van Heiningen, 1982; Huang, 1988; Chen, 1989) constructed initially to make experimental tests of computer simulations of impingement heat transfer. The equipment was originally designed for the measurement of local heat transfer rate between a slot jet and a rapidly moving impingement surface. For the present study the basic changes were the use of turbulence generation at the slot nozzles, and the installation of a hot wire anemometer to document profiles of the mean and fluctuating axial velocity of the jet flow at several planes between the nozzle exit and the impingement surface. Precise positioning of the anemometer was accomplished with a specially designed probe holder incorporating a micrometer.

The other principal modifications carried out for this

study included reversing which jet was heated and which was unheated, changing the air heater position, fabrication of a new heat flux sensor, installation of new nozzle plate-jet confinement hoods and modification of one nozzle plenum chamber.

Although the Simtest facility has the capability to measure local heat flux with the impingement surface moving at high speed, as is the case in the drying of paper, the effect of impingement surface motion has been well documented by previous studies in this laboratory. For the present study, therefore, a single value of relatively low surface speed was used, obtained by fixing at approximately 75 rpm the rotational speed of the impingement cylinder, resulting in an impingement surface speed of approximately 2.0 m/s.

The equipment construction and calibration are now described.

3.2 Simtest Equipment

A schematic diagram of the Simtest apparatus is shown in fig 3.1. The basic concept is to achieve heat transfer operation which is, overall, steady state, at a rotating cylindrical impingement heat transfer surface. The design accomplishes this objective through the use of two air jets, one heated and one unheated, which impinge at positions 180° apart, on top and bottom of the rotating heat transfer

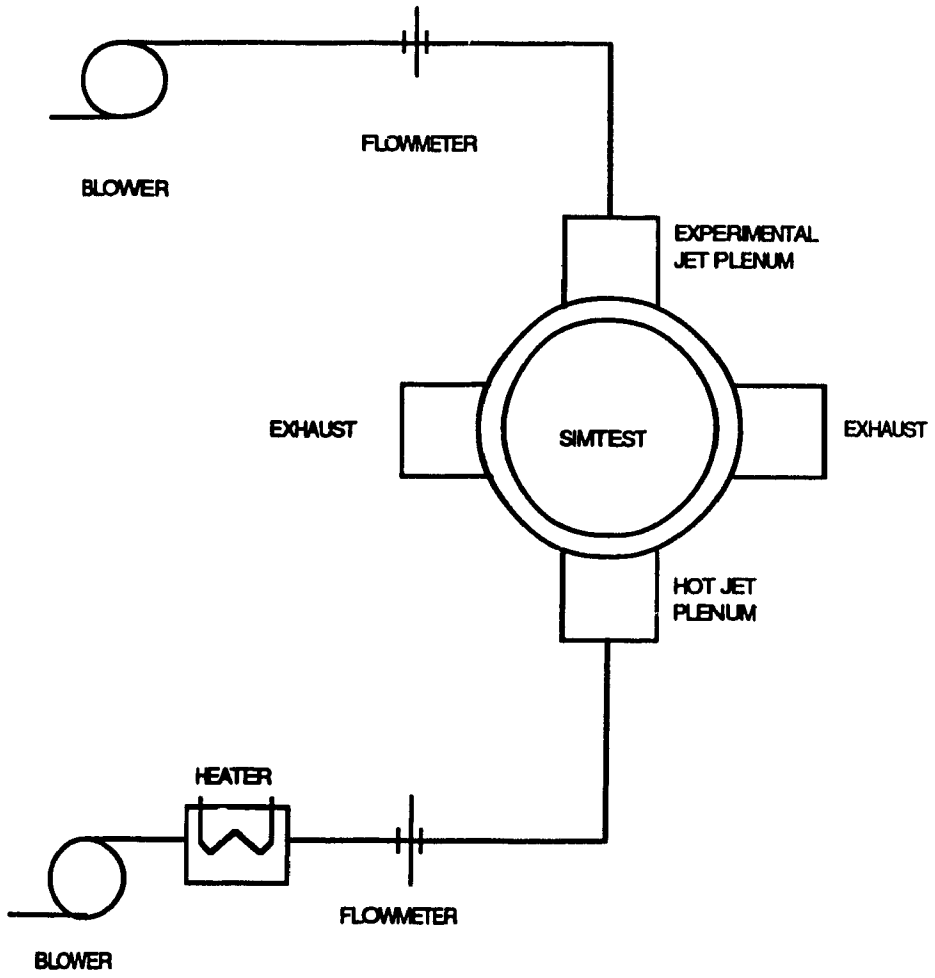

Fig 3.1 Flowsheet of the Simtest apparatus.

cylinder. Previously it was the air flow to the experimental nozzle directed at the top of the impingement cylinder thatwas heated. With that arrangement, flow and temperature non-uniformities in the experimental jet were a problem, as described by Huang (1988) and Chen (1989). The apparatus was modified for this study by installing a 6kW, 12-stage heater in the air duct supplying the nozzle directed at the bottom of the impingement cylinder. As the lower jet is not used for experimental measurements, but serves only to maintain the heat transfer cylinder at a steady temperature, this change eliminated the difficulty previously experienced. The heater in the line supplying the upper nozzle was replaced by a 200mm square duct for a distance of 2 metres upstream of the upper plenum chamber, providing a transition from the 200mm round duct used in the orifice flowmeter section, to the 200mm square plenum chamber above the experimental nozzle. This change eliminated some flow restrictions and reduced pressure drop.

The slot nozzles were mounted 180° apart on the vertical centre line of the impingement cylinder. The lower nozzle, producing the heated jet, was an ASME standard, elliptically contoured entrance nozzle, of width 14mm, unchanged from previous work. The upper (unheated jet) experimental nozzle was a rectangular slot machined from a removable 3.2 mm thick plate. There were three interchangeable confinement hoods for the upper section, giving values of the nozzle to surface

spacing, H, of 12, 24, or 37mm.

The flow exit side of all nozzles were flush with their respective confinement hoods. The lower 180° section had a single confinement hood, giving a fixed nozzle to impingement surface spacing H of 37mm, as detailed by van Heiningen (1982) and Huang (1988). The exhaust ports were located on the horizontal centre line of the drum, on diametrically opposite sides, so that each flow exhausted 90° from the respective nozzle. The exhaust ports were divided along their centre lines by skimmer plates which extended to within 1mm of the impingement cylinder surface. The skimmer plates thereby isolated the top half of the impingement cylinder, where all the experimental measurements were made, from any effects from the bottom half of the apparatus.

Air was provided by a separate blower for each line. A 3.7 kW blower delivered unheated air to the upper jet, while a 22.4 kW blower supplied air through the duct heater to the lower jet. The flow rate to each nozzle was measured using an orifice plate flowmeter constructed to ISO specifications (ISO ,1983).

The impingement surface was the outer side of a 3 mm thick stainless steel cylinder, 0.48 m in diameter and 0.22 m in the cross machine direction (CD). The confinement hood slightly reduced the exposed CD length of the drum to 0.20 m. Thus over one complete revolution of the cylinder, the 1.51m of machine direction (MD) length of the impingement surface

passes successively under a heating jet and a cooling jet. The impingement cylinder, mounted on a hollow drive shaft, was belt driven by a variable speed electric motor (3.75 kW).

3.2.1 Design of Experimental Upper Nozzle

Figure 3.2 shows the top view of a typical nozzle plate and the relative position of the sensor on the impingement surface when it is aligned directly under the nozzle centre line. The dimensions of the square nozzle plate, 200 mm, are those of the cross section of the plenum chamber and of the unheated air duct. The CD dimension of the nozzle plate and the plenum chamber matches that of the exposed impingement cylinder surface.

The experimental nozzle was a sharp edged slot orifice cut in the nozzle plate. The plate thickness of 3.2 mm was chosen to closely match the 10 gage (3.4 mm) steel plate used for the nozzle plate-confinement hood units of industrial Yankee dryers for drying paper under impinging jets.

Five nozzle plates were fabricated: one for each of the four nozzle widths used: 6, 12, 18 and 25mm, and one for a nozzle of width 24mm and containing 3 bars. Each nozzle had a CD slot length of 0.18 m, centred in the nozzle plate, thus covering essentially all of the 0.20m CD dimension of the impingement cylinder surface.

The 6,12,18, and 25mm nozzles were designed so that

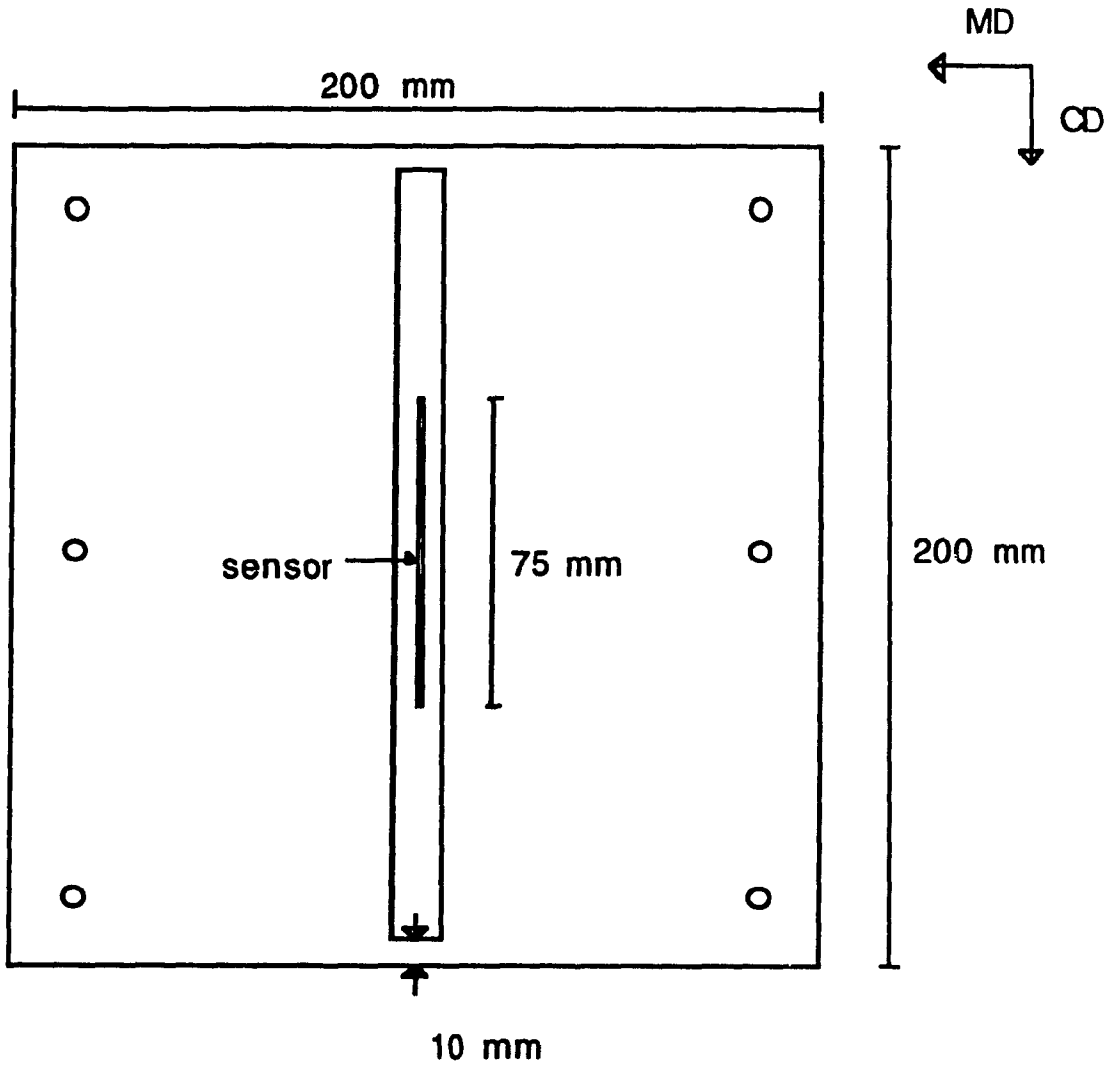

Figure 3.2 Nozzle plate layout and sensor alignment

alternate methods of turbulence enhancement could be used. For all nozzle widths, wire screen of #10 or #18 mesh size could be clamped to the air inlet side of the nozzle plate. The #10 mesh screen was formed of 0.66 mm diameter round wire woven in a square mesh with hole openings 1.9 mm per side. The #18 mesh screen was similarly formed using 0.44 mm diameter wire and 1.0 mm square openings. The nozzle plate of 25 mm slot width was constructed so that a single round bar could be placed along the nozzle centre line on the air inlet side of the nozzle, with the bar resting on top of the plate (fig 3.3). The fifth nozzle plate (fig 3.4) had a slot width of 24 mm, but with three rectangular bars spaced equally across the nozzle width. The bars were each 1 mm wide, with the same thickness (3.2mm) as the nozzle plate.

Three sets of hoods were used for the confinement of the unheated jet flow over the upper 180° of the impingement cylinder. These hoods had radii of curvature to provide the required values of H: 12 mm, 24 mm and 37 mm. Each set of 180° hoods comprised two symmetrical halves which, when installed, were separated by a gap of 30 mm in order to accommodate the slot nozzle of maximum width, 25 mm. The nozzle plates (Figs 3.2, 3.3, and 3.4) were attached across the top of the confinement hoods so that the slot nozzle was centred in this gap between the two curved confinement surfaces (fig 3.5) and with the nozzle centre line coincident with the vertical centre line of the impingement cylinder.

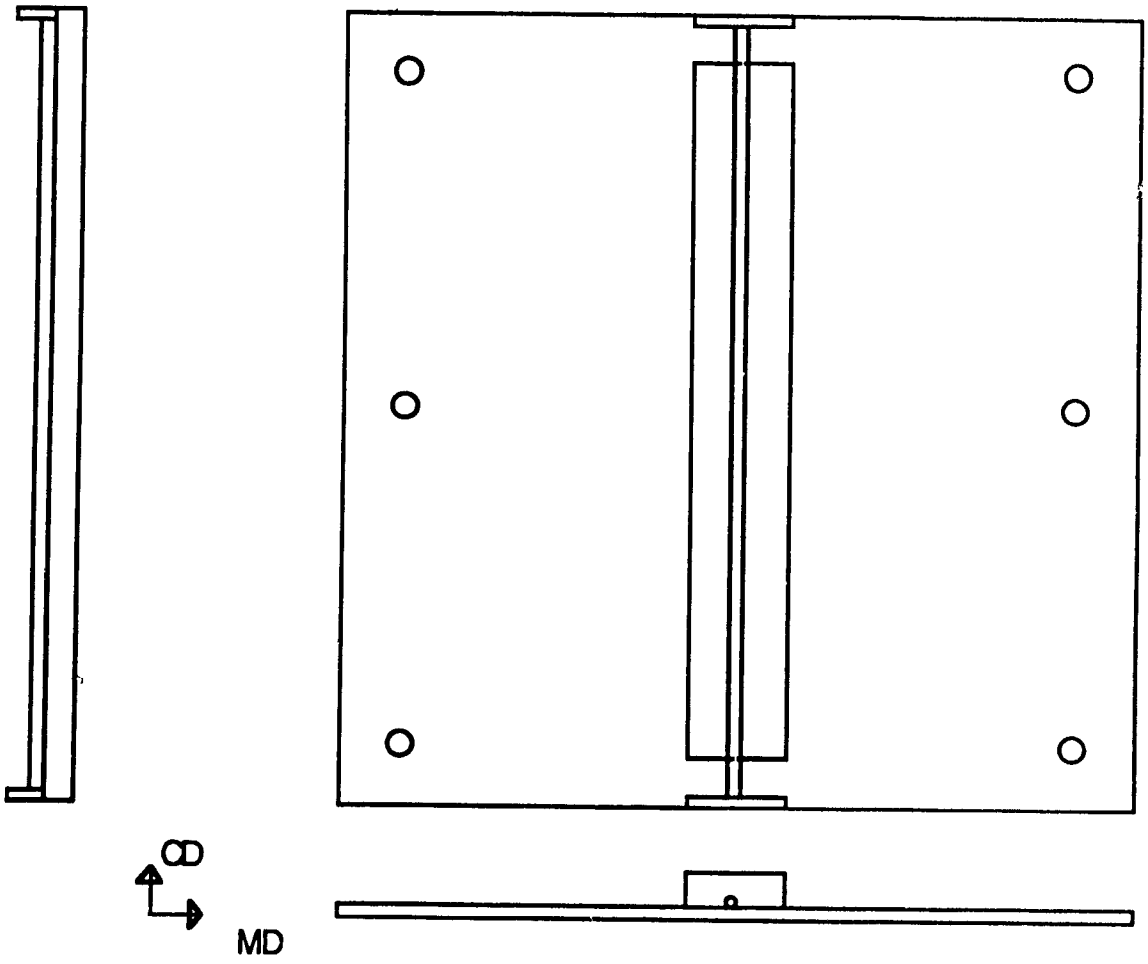

Figure 3.3 Nozzle plate with 1 bar turbulence generator

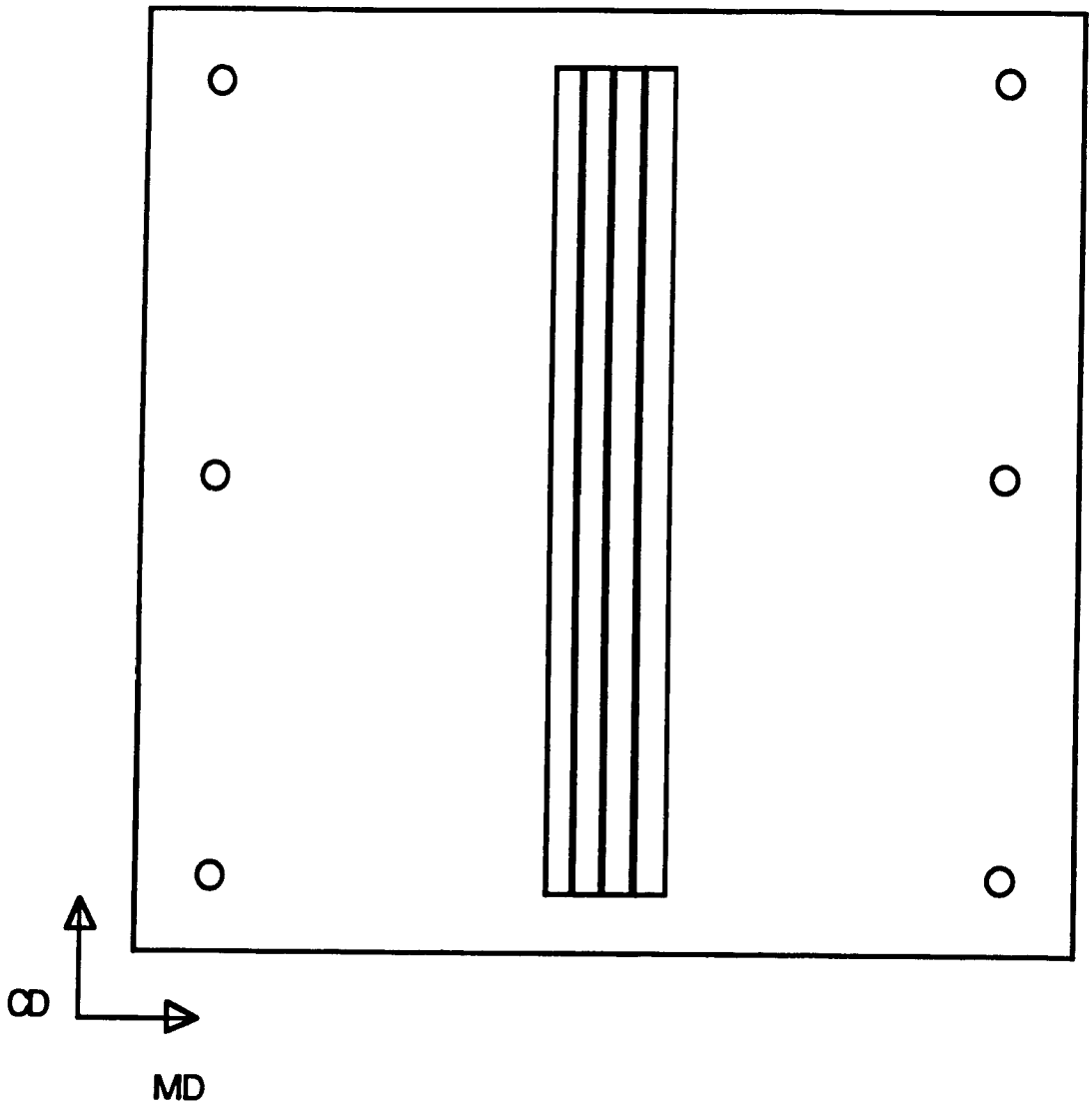

Figure 3.4 Nozzle plate with 3 bar turbulence generator.

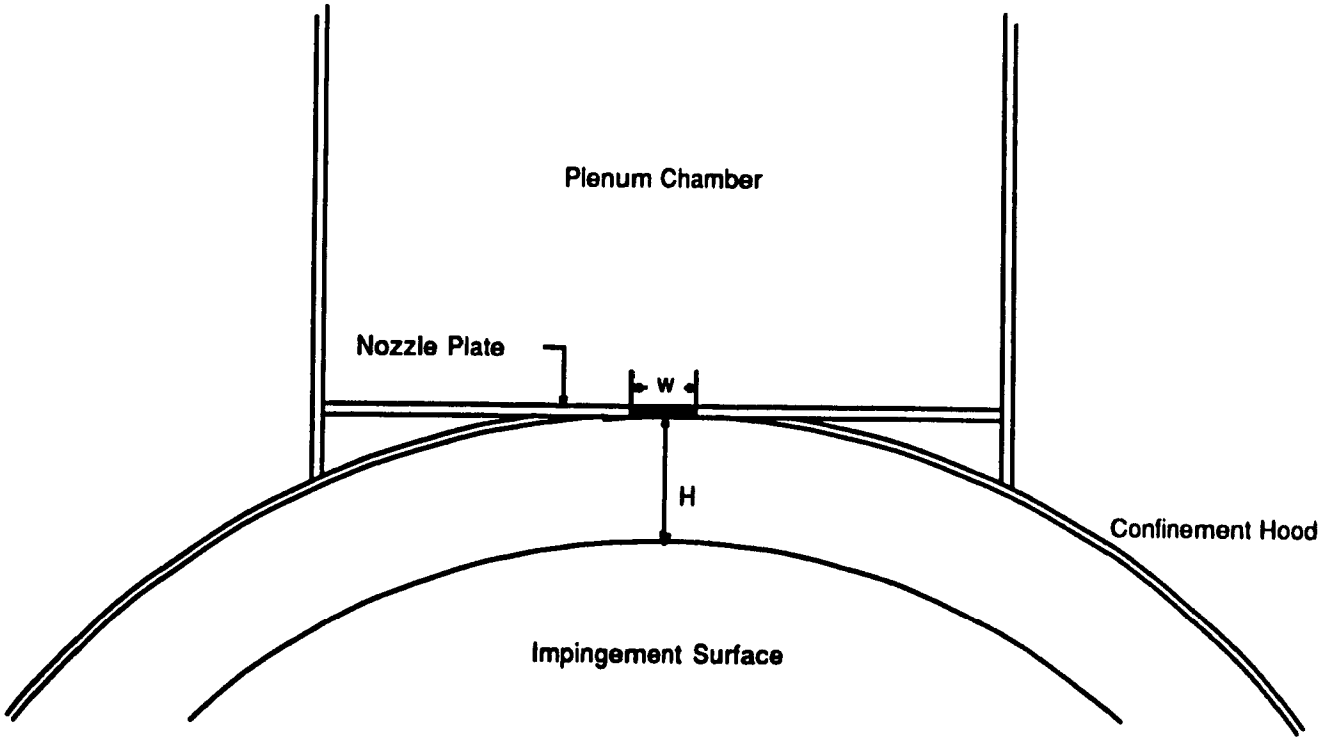

Figure 3.5 Nozzle - confinement hood - plenum chamber layout.

3.3 Measurement of Local Mean Velocity and Turbulence Intensity

3.3.1 Measurement Sensor

Local values of mean and turbulence axial velocities in the jet flow field were measured using a hot wire anemometer (HWA) made by DISA (now Dantec), operated as a constant temperature anemometer. The apparatus consisted of a probe (type P14) with a 0.5 μm diameter hot wire attached to a constant temperature bridge (type 55 M 10), linearizer (type 55 D 10) and RMS voltmeter (type 55 D 35). As the flow field characteristics measured do not vary with impingement surface motion, for convenience all measurements with the HWA were carried out with the impingement cylinder stationary.

A positioning device (fig. 3.6) was constructed to enable accurate two-dimensional positioning of the probe. Each traverse of the anemometer probe in the nozzle width dimension was carried out with the probe located at the CD centre line and at a selected position in the axial dimension between the nozzle exit and the impingement surface. Accurate positioning for traversing in the MD was accomplished using the micrometer and linear stage to which the probe support was attached.

This documentation at the CD centre line of the flow field in the nozzle width dimension was carried out at three axial positions: at the nozzle exit, at the midpoint between the nozzle exit and the impingement surface, and at the

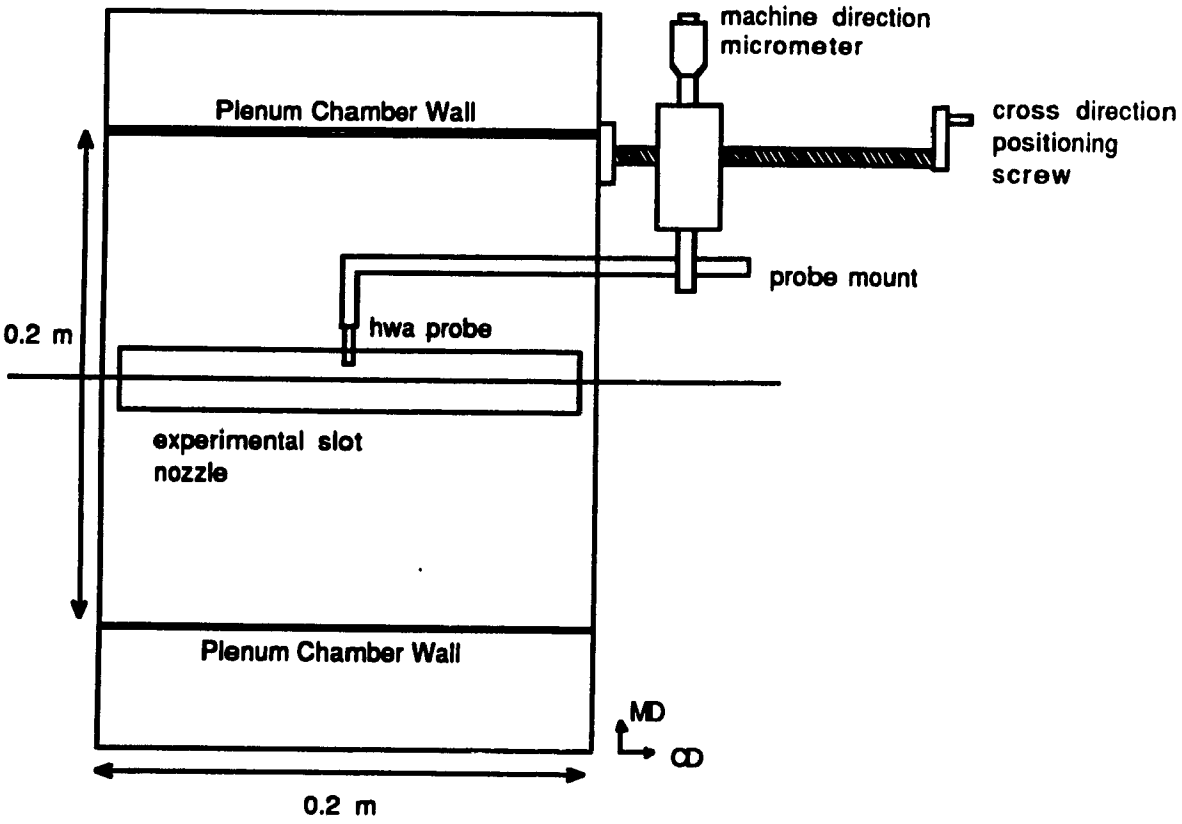

Figure 3.6 Hot wire anemometer probe positioning device.

closest approach to the impingement surface allowed by the shape of the probe. The type P14 probe is a right angle design, and with the probe base as close as possible to the impingement surface the probe tip was 7mm above the impingement surface. The axial position was set by rotating the probe mount until the probe tip was at the desired axial location.

3.3.2 Measurement Procedure

The hot wire of the probe was electrically heated to a temperature higher than that of the air in the duct, determined by the overheat ratio setting. In the constant temperature operating mode, the air flowing over the wire cools the heated probe and a feedback loop changes the current to keep the probe at the setpoint temperature. The average voltage across the probe is converted to the average velocity of the fluid across the probe, while the fluctuations of the probe voltage correspond to the fluctuating fluid velocity.

Following standard practice (Disa, 1962), the probe resistance was measured at two known air velocities. Parameters were calculated from a linear regression of the logarithms of this pair of resistance-velocity values. This slope and intercept were entered into the analog computer as the constant and exponent of an exponential voltage-velocity relationship, according to King's law (Lomas, 1986).

For characterizing the flow field, the impingement cylinder was kept stationary and there was no heat transfer, thus only the experimental jet was used. Because of the temperature sensitivity of the electronics, the anemometer was kept powered on, in stand-by mode, for at least 24 hours before an experiment. The blower was operated for at least an hour with the butterfly valve adjusted to provide the required flowrate, until the outlet air temperature became constant, usually 4-5°C above the ambient temperature due to internal heating by the blower.

The hot wire anemometer was switched to measurement mode and the local axial jet velocity was read as the linearized voltage on a voltmeter, while the local fluctuating velocity was determined from the RMS component of the linearized voltage, read from an RMS voltmeter. The local turbulence intensity is the ratio of the fluctuating velocity to the average velocity.

For the traverses in the nozzle width dimension, readings were taken at 1 mm intervals. At the nozzle exit plane, these traverses were continued to within 1 mm of the nozzle edges. For traverses made at the two lower levels, i.e. at the midpoint between the nozzle exit and the impingement surface, and at the closest approach to the impingement surface allowed by the probe, traverses were continued past the projection of the nozzle edges.

3.4 Heat Transfer Rate Measurement

3.4.1 Measurement Sensor Description

Heat transfer rate was measured using a fast responding heat flux sensor (fig 3.7) based on resistance thermometry (van Heiningen, 1982). A new sensor was made for this study, as described in Appendix A. It was mounted flush with the impingement surface in the cross machine direction, parallel with the nozzle. The sensor was connected to the monitoring and data acquisition system through a slip ring assembly (IEC Corporation model IEC-BK-14) on one end of the hollow drive shaft of the impingement cylinder. Figure 3.8 shows the electronics used with the sensor.

The sensor was connected to a constant voltage supply built by Huang (1988), through a Wheatstone bridge (James G. Biddle Co. model 601022). As the temperature of the sensor changes, its resistance and hence its voltage changes. The voltage signal was amplified 2500 times by a low noise amplifier (Dana model 2820). The amplified signal was passed through a variable low pass filter (Frequency Devices Inc. model 901F) to produce a signal that was sampled by the data acquisition system, consisting of an IBM PC compatible computer equipped with an analog to digital data acquisition board (Data Translation model 2801A).

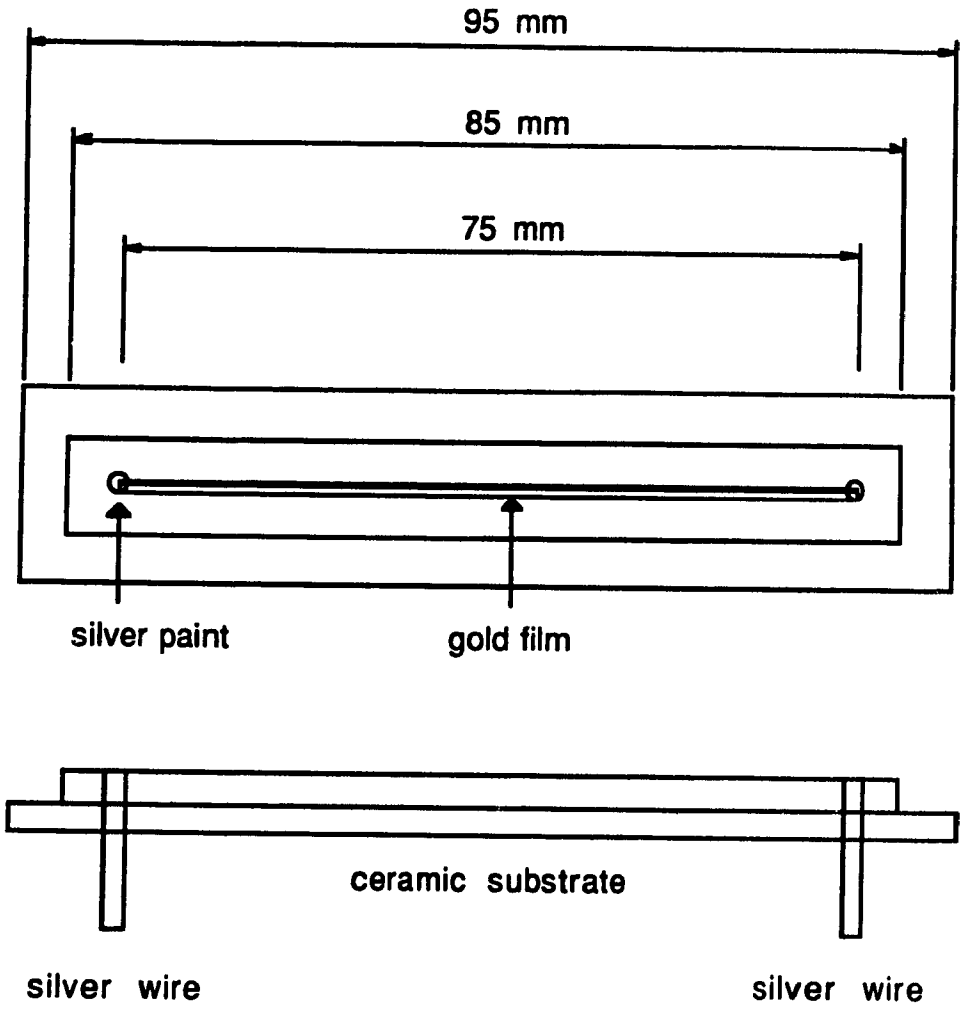

Figure 3.7 Heat flux sensor detail.

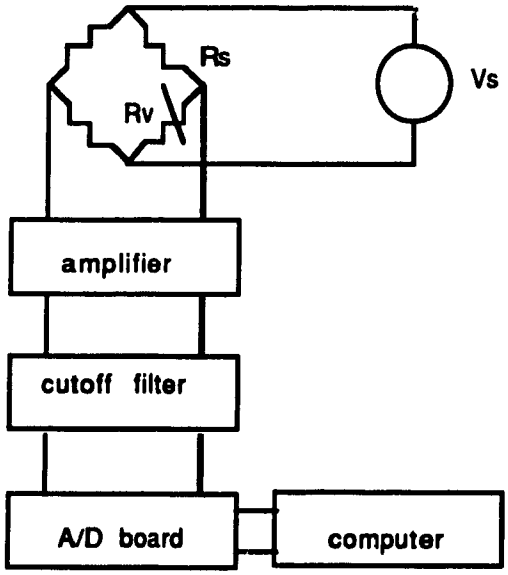

Figure 3.8 Heat flux sensor electronics schematic

The digitized voltage signal was sampled and stored for further analysis. By using a calibration equation described in Appendix B, each voltage reading across the sensor at a given point in the cylinder rotation was converted to a temperature at the corresponding point on the impingement surface.

Previous work established that with the very short duration of the alternate heating and cooling of the rotating impingement surface, the fluctuations in temperature never reach the inside surface of the impingement cylinder, which therefore remains isothermal and adiabatic. Heat transfer within the impingement cylinder may then be considered as one-dimensional unsteady state heat conduction in a semi-infinite slab (van Heiningen, 1982). Therefore the measured transient impingement surface temperature becomes one boundary condition, and a zero heat flux on the inside of the impingement surface the other, to solve for the one dimensional transient heat flux at the impingement surface. This solution was carried out on a computer using the finite difference method. From these values of local heat flux, values of local Nusselt number were produced, and were integrated to give average Nusselt number, as both local and average Nusselt number were used in analysis of the experimental results.

3.4.2 Measurement Procedure

The value of jet Reynolds number and nozzle width for the unheated jet determined the flow rate and temperature required for the heated jet on the opposite side of the impingement cylinder. The heated jet flowrate was set at the same jet Reynolds number as the unheated jet. The heater was adjusted to produce a sufficiently large amplitude in impingement surface temperature and hence in the sensor signal as it was alternately heated and cooled during each rotation. The signal amplitude was required to be larger than background noise, and limited by the output range of the low noise amplifier. The equipment was operated with the blowers and heater on and allowed to attain steady state. The equipment was considered to be at steady state when the voltage oscillated around a steady mean value. A period of 1-2 hours operation was sufficient to eliminate all transient effects in the flow and heat transfer aspects and in the electronic instruments.

The rotational speed of the impingement cylinder, fixed at approximately 75 rpm, was measured using an optical sensor connected to the computer A/D board and the heat flux sensor sampling rate was adjusted to give 500 samples per rotation. The Butterworth filter cutoff frequency was set to half the sampling frequency, the Nyquist criterion for digital sampling.

This optical switch also triggered the start of the

sampling program, and 50 rotations were sampled and averaged to produce a profile of local impingement surface temperatures. This temperature profile was then converted to one of local Nusselt number using a finite difference computer algorithm (van Heiningen 1982, Polat 1989). The surface temperature and Nusselt number profiles and the experimental conditions were stored in a data file for further analysis.

Chapter 4. Results and Discussion

4.1 Introduction

Turbulence flow field characterization and impingement heat transfer rate measurements were conducted for a turbulent confined slot jet, using the apparatus described in Chapter 3. The experiments were carried out using several techniques for turbulence generation at the nozzle exit. A range of nozzle widths, nozzle to surface spacings and jet Reynolds numbers were used to document the effects of turbulence generation on the flow field and impingement heat transfer. As the effects of impingement surface motion, multiple jets, and jet angle relative to the impingement surface have been documented in other theses from this laboratory (van Heiningen, 1982; Polat 1988; Huang, 1989; Journeaux, 1990), these parameters were not included in the present study.

Profiles of mean and turbulent axial velocities of the jets, and thereby the local axial turbulence intensities were measured across the nozzle width, at several axial positions, z/H, between the nozzle exit and impingement surface. These measurements were conducted with the impingement surface stationary.

Profiles of local and average heat transfer rates were determined using a heat flux sensor of very fast response. These measurements were used to calculate heat transfer in terms of Nusselt number.

Three values of nozzle to impingement surface spacing, H,

were obtained by the use of flow confinement hoods of three diameters. Nozzles of five widths, w, were used, with each of the three values of H. The measurements were made at three levels of jet Reynolds number, Re_j. Thin (3.2 mm) sharp edged orifice nozzles were used first without turbulence generation. The effect of turbulence generation was then investigated by the addition across the nozzle entrance of wire mesh for all of the nozzles used and, for the largest nozzles used, the addition of one or three bars along the nozzle slot as detailed in section 3.2.1. The values of these parameters are shown in table 4.1. The designation of turbulence generation, tg, as 10 or 18 corresponds to the wire mesh size, while tg of 1 and 3 indicate the use of that number of bars in the nozzle, with 0 denoting a plain nozzle without turbulence generation.

Table 4.1 Values of Parameters

H	12, 24, 37 mm
w	6, 12, 18, (24) 25 mm
tg	0, 1, 3, 10, 18
z/H	0, 0.5, 0.7, 0.8
Re_j	12000, 24000, 40000

For air at 20°C and using open nozzles i.e. without turbulence generation, table 4.2 shows the values of mean nozzle exit velocity $\bar{U}$ [m/s], corresponding to the nozzle widths and jet Reynolds numbers used.

Table 4.2 Jet Mean Velocity, m/s

w [mm]	Jet Reynolds Number		
	12000	24000	40000
6	32	64	
12	16	32	51
18	11	22	36
25	8	16	26

4.2 Turbulence

For each combination of confinement hood spacing, nozzle width, jet Reynolds number, and type of turbulence generation, traverses were made across the nozzle width with a hot wire anemometer to measure the mean and fluctuating axial velocity of the jet. A total of 67 combinations of H, w, and tg were used, for each of which the profiles were measured at the nozzle exit (z/H=0). With the confinement hood giving the maximum spacing, H=37 mm, traverses were also conducted at a plane midway between the nozzle exit and impingement surface (z/H=0.5), and at 7 mm from the impingement surface, as close as permitted by the anemometer probe (z/H=0.8). For the intermediate spacing, H=24 mm, traverses were conducted at the nozzle exit and at 7 mm from the surface (z/H=0.7); at the closest spacing, H=12 mm, only traverses at the nozzle exit could be made. Thus 67 profiles were determined at the nozzle exit (position 1), 27 at the midpoint plane (position 2), and 45 at a close approach to the surface (position 3), for a

total of 139 profiles.

4.2.1 Flow Field Characterization without Turbulence Generation

Figure 4.1 shows a set of measurements obtained for one nozzle geometry, H=37 mm; w=25 mm; tg=0; at three Reynolds numbers. All hot wire anemometer measurements were taken at the discrete points so indicated on the graphs. The connecting lines, shown for the convenience of the reader, have no other significance. Figure 4.1a shows the profiles of U, the local mean axial velocity; figure 4.1b shows the corresponding profiles of u', the rms or fluctuating component of the axial velocity; figure 4.1c shows the corresponding profiles of local turbulence intensity I, the ratio u'/U for each point across the nozzle opening.

For the base case of no turbulence generation, figure 4.2 compares, for one value of H and Re, the profiles at the nozzle exit for nozzles of several widths. The profiles of mean velocity (fig 4.2a) have the characteristic flat shape for thin, square edged slot nozzles. The fluctuating velocity and turbulence intensity (fig. 4.2b and c) are nearly zero except where the jet flow is affected by the presence of the nozzle edges. Although the nozzle width varies by slightly more than a factor of two in fig 4.2, the profiles roughly superimpose when plotted in terms of the non-dimensional

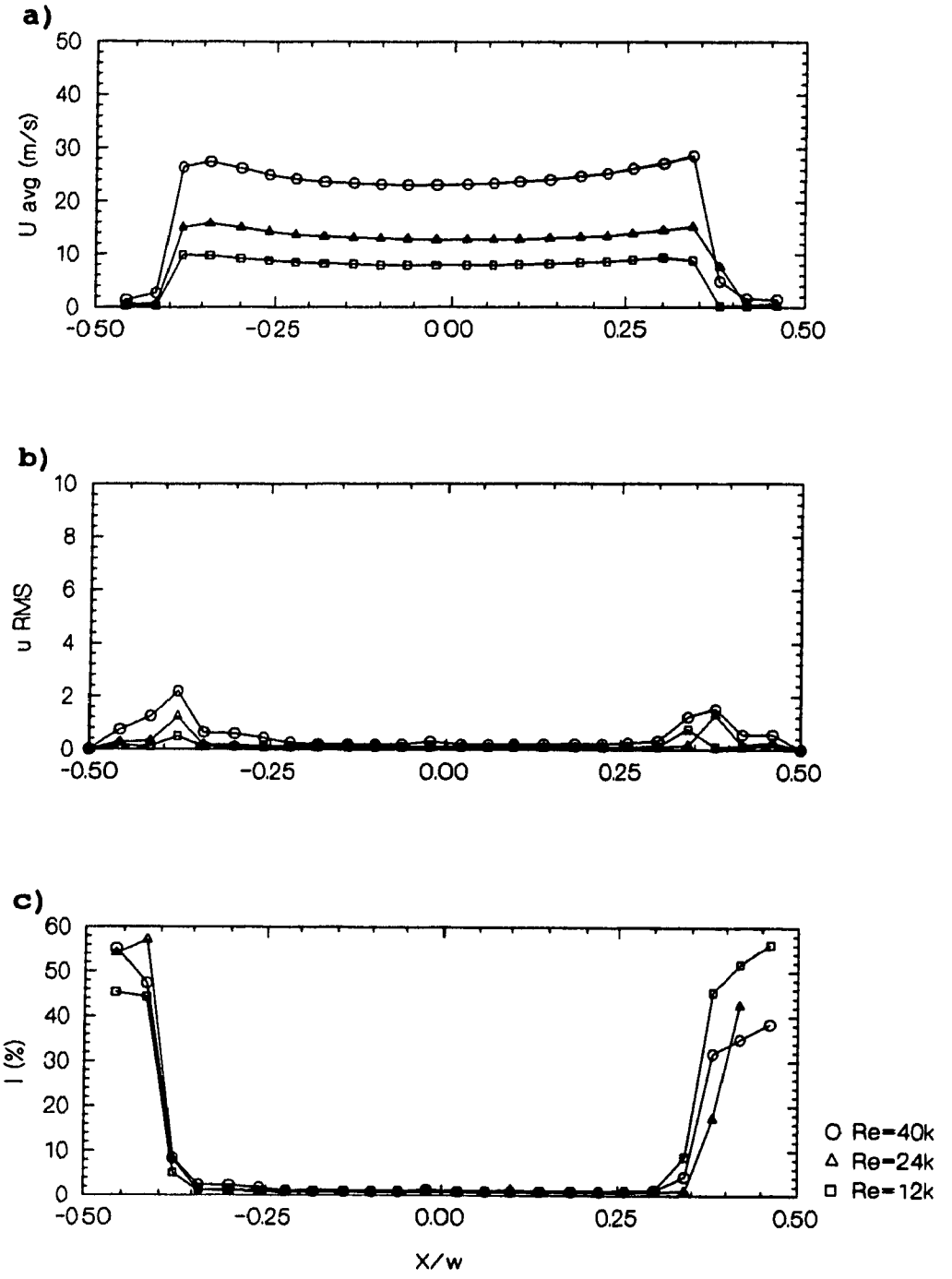

Figure 4.1 Nozzle exit profiles for H=37mm, w=25mm, tg=0: a) U, local mean velocity; b) u' local rms velocity; c) I, local turbulence intensity.

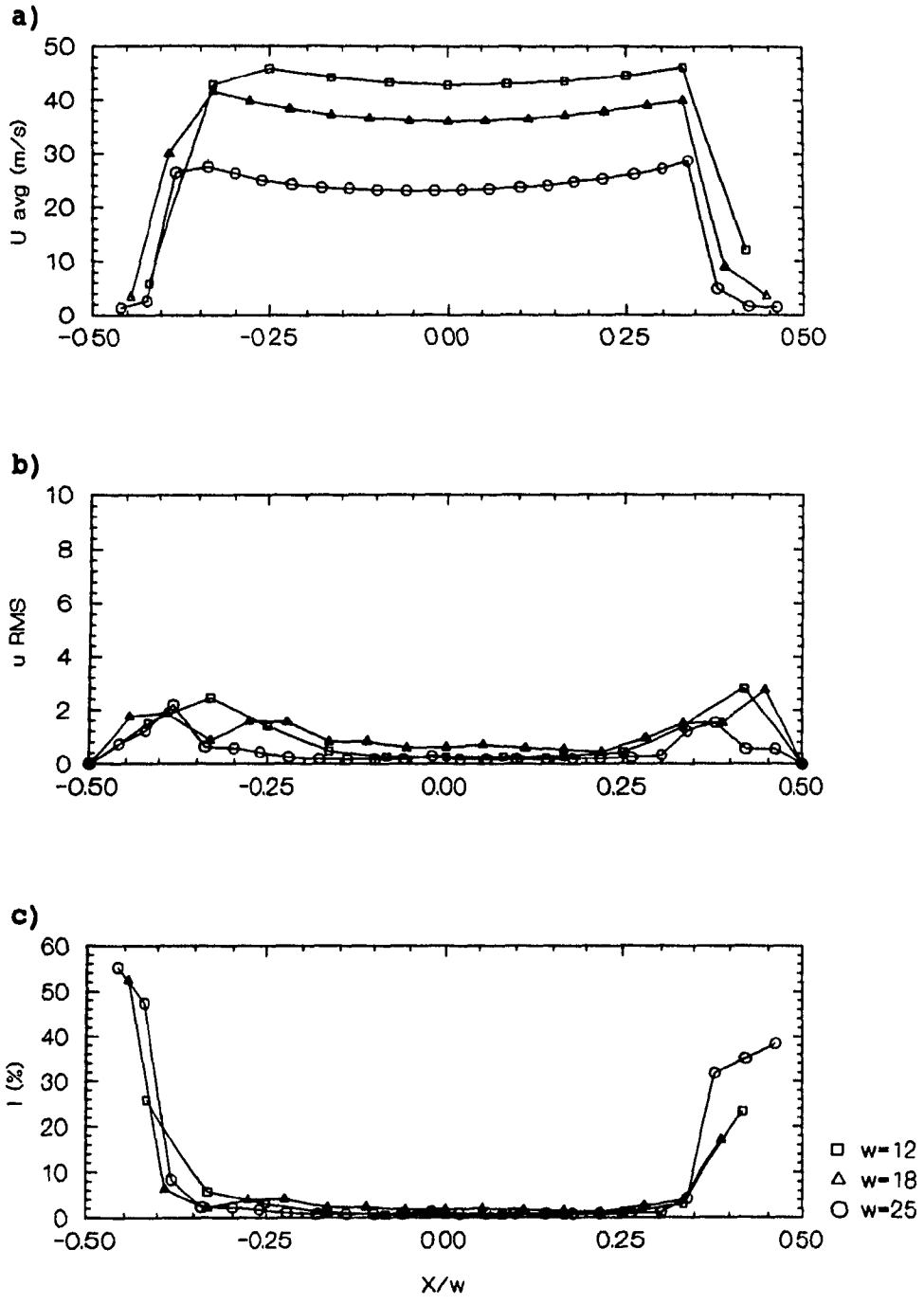

Figure 4.2 Nozzle exit profiles for H=37mm, tg=0, Re_j=40000: a) U, local mean velocity; b) u' local rms velocity; c) I, local turbulence intensity.

position variable X/w.

Figure 4.3 records profiles at the nozzle exit for nozzles of the same w, at similar Re_j, but different H. As nozzle exit profiles should be independent of H, fig. 4.3a confirms satisfactory reproducibility of the measurements. In the regions of steep gradient in U or u' near the nozzle edges, a very small uncertainty in lateral position produces a large effect on the near-wall profiles.

For the widest nozzle (w=25 mm) at the largest nozzle to surface spacing (H=37 mm), figure 4.4 shows the development of the profiles from the nozzle exit to near the impingement surface. For this combination of widest w and highest H, the nondimensional spacing is very low (H/w=1.5). Thus in this case the midway location (axial position 2), is only 0.7w from the nozzle exit and from the impingement surface, while axial position 3 is just 0.3w or 0.2H from the impingement surface.

The stagnation region is quoted by Martin (1977) as beginning 1.2w from the impingement surface, while Saad (1981) gives a value of 0.21H as the limit for this region where the presence of the impingement surface begins to affect the flow. Within the stagnation region the flow begins to accelerate laterally as it approaches the obstruction of the impingement surface. With the single wire probe used in the hot wire anemometer, the instrument cannot discriminate between axial jet flow and lateral flow. At the nozzle exit and above the stagnation region, the axial velocity is the only important

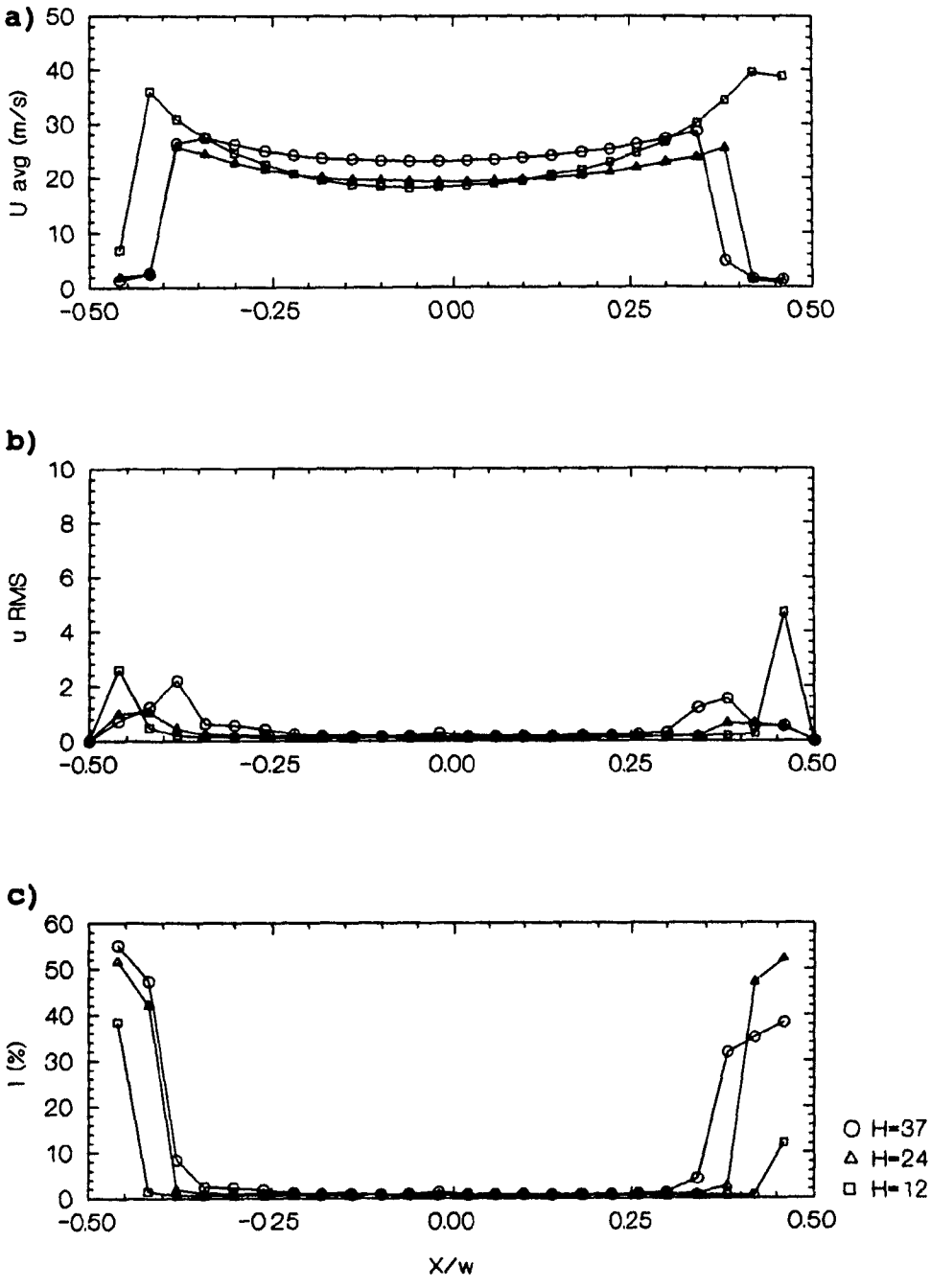

Figure 4.3 Nozzle exit profiles w=25mm, tg=0, Re_j=40000: a) U, local mean velocity; b) u' local rms velocity; c) I, local turbulence intensity.

component. For the widest nozzle, 25 mm, the near surface traverse is just 0.28w from the impingement surface. The apparent increase in velocity measured at points away from the nozzle centreline shown in figure 4.4a is evidence that the measurements at the plane closest to the impingement surface are affected by the lateral as well as axial flow. The profile at axial position 2, 0.7w from the impingement surface, is unaffected, indicating that the flow at the midpoint plane is not yet within the impingement region.

Figure 4.5 shows the near surface profiles of mean velocity for three plain nozzles; 12 mm, 18 mm, and 25 mm. The 25 mm nozzle profile is affected as described above. The 18 mm nozzle, for which axial position 3 is 0.4 w from the impingement surface, also shows an apparent increase in mean velocity at points away from the centreline. For the 12 mm nozzle, axial position 3 is 0.7 w from the surface, and examination of the profiles shows no effect comparable to the two larger nozzles. Thus, it may be concluded that the impingement zone extends at least 0.4 w above the impingement surface, but less than 0.7 w.

4.2.2 Flow Field Characterization with Turbulence Generation

Turbulence generation at the nozzle exit was produced by the three methods detailed in Chapter 3. For tg= 10 and 18, a mesh of round wires woven in a square grid, 10 or 18 per inch,

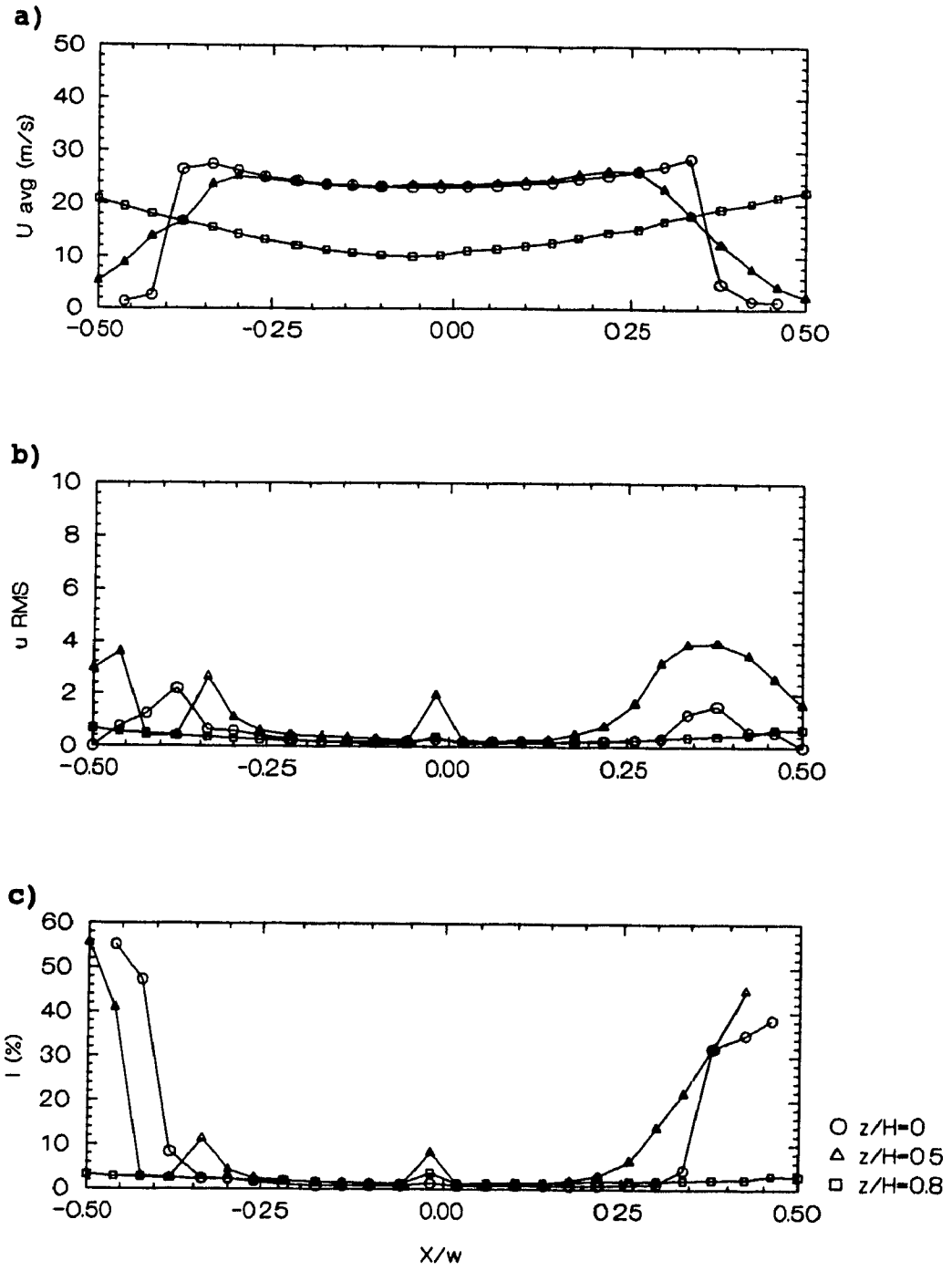

Figure 4.4 Profiles for H=37mm, w=25mm, tg=0, Re_j=40000: a) U, local mean velocity; b) u' local rms velocity; c) I, local turbulence intensity.

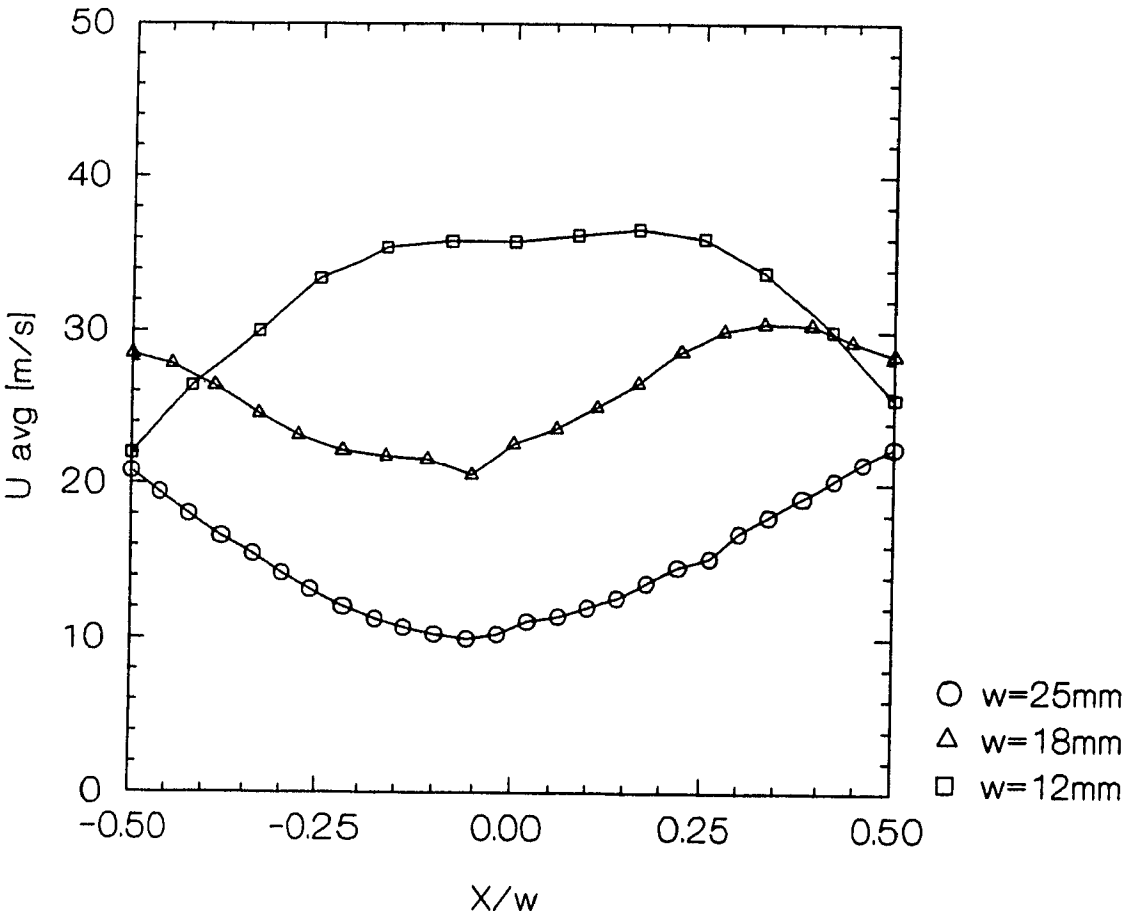

Figure 4.5 Near impingement surface mean velocity profiles for H=37mm, tg=0, Re_j=40000.

was laid over the nozzle plate. For the widest nozzle, tg=1 was achieved by mounting a single 3 mm diameter bar along the nozzle centreline in the cross machine direction, while for tg=3 a plate was constructed with a nozzle width of 24 mm subdivided into four sections by three rectangular bars, each 1 mm wide.

Figure 4.6 shows the effects of the different types of turbulence generation. The velocity profiles reflect the presence of the turbulence generators (fig. 4.6a), while the data for tg=0 are reproduced for reference from fig. 4.1. Although the effects from turbulence generation by three bars are most clearly seen, the results of the other methods are also apparent. In all cases the locations of lower values of U in figure 4.6a correspond to higher values in u' in fig. 4.6b (and consequently of I in 4.6c).

For the three bar nozzle set at H=37 mm from the impingement surface, figures 4.7, 4.8, and 4.9 show the development of the profiles at three axial positions for the three values of jet Reynolds number used. The profiles at the nozzle exit (z/H=0) show clearly the effects of the bars in the nozzle, with decreases in mean velocity corresponding with increases in fluctuating velocity. When the flow has reached the midpoint between the nozzle exit and the impingement surface (z/H=0.5), disturbances in the mean velocity profile of figs 4.7a, 4.8a, and 4.9a have largely disappeared. At Z/h=0.5, the midpoint, the peaks in the fluctuating velocity

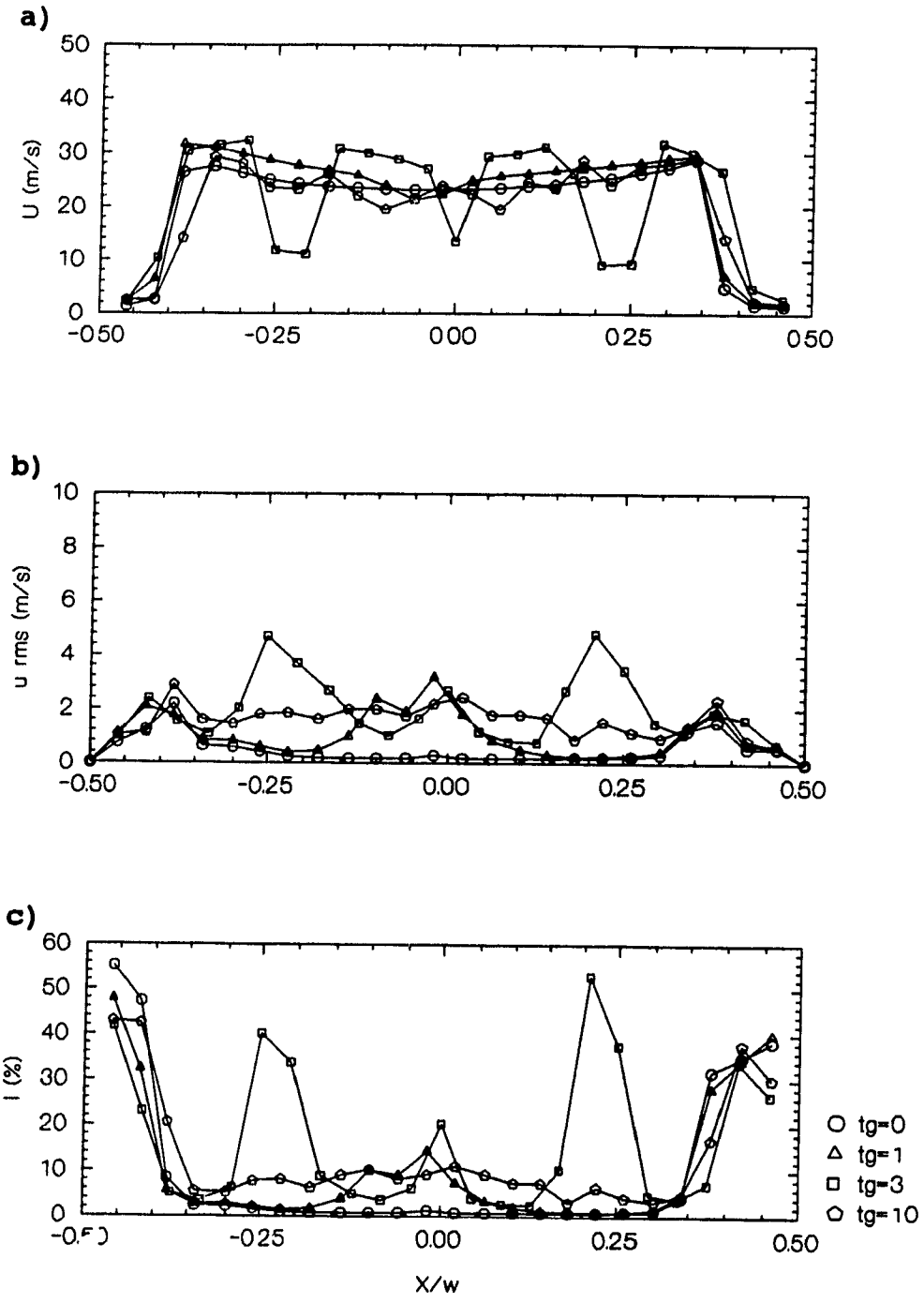

Figure 4.6 Nozzle exit profiles for H=37mm, w=24mm, Re_j=40000: a) U, local mean velocity; b) u' local rms velocity; c) I, local turbulence intensity.

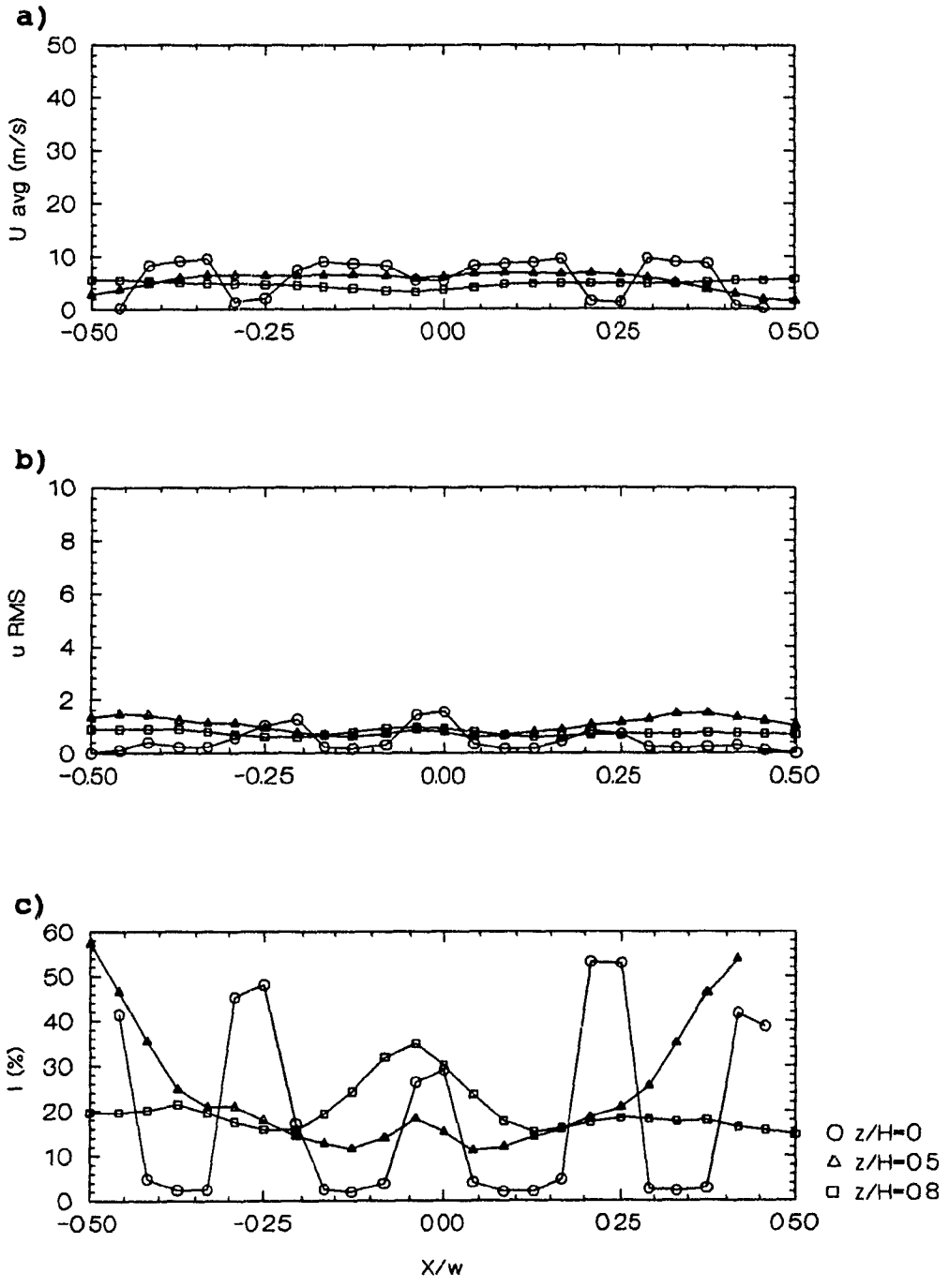

Figure 4.7 Profiles for H=37mm, w=24mm, tg=3, Re_j=12000: a) U, local mean velocity; b) u' local rms velocity; c) I, local turbulence intensity.

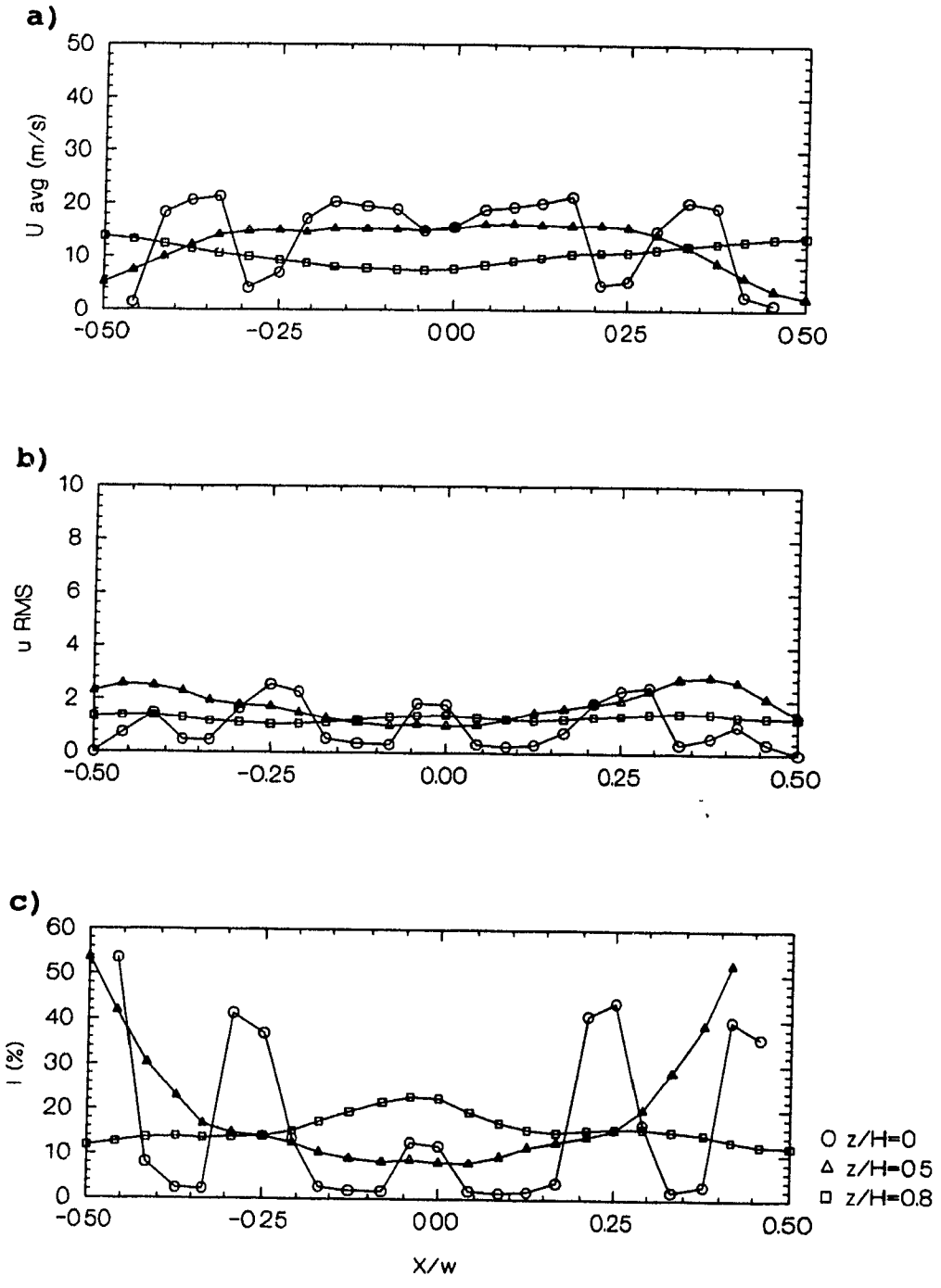

Figure 4.8 Profiles for H=37mm, w=24mm, tg=3, Re_j=24000: a) U, local mean velocity; b) u' local rms velocity; c) I, local turbulence intensity.

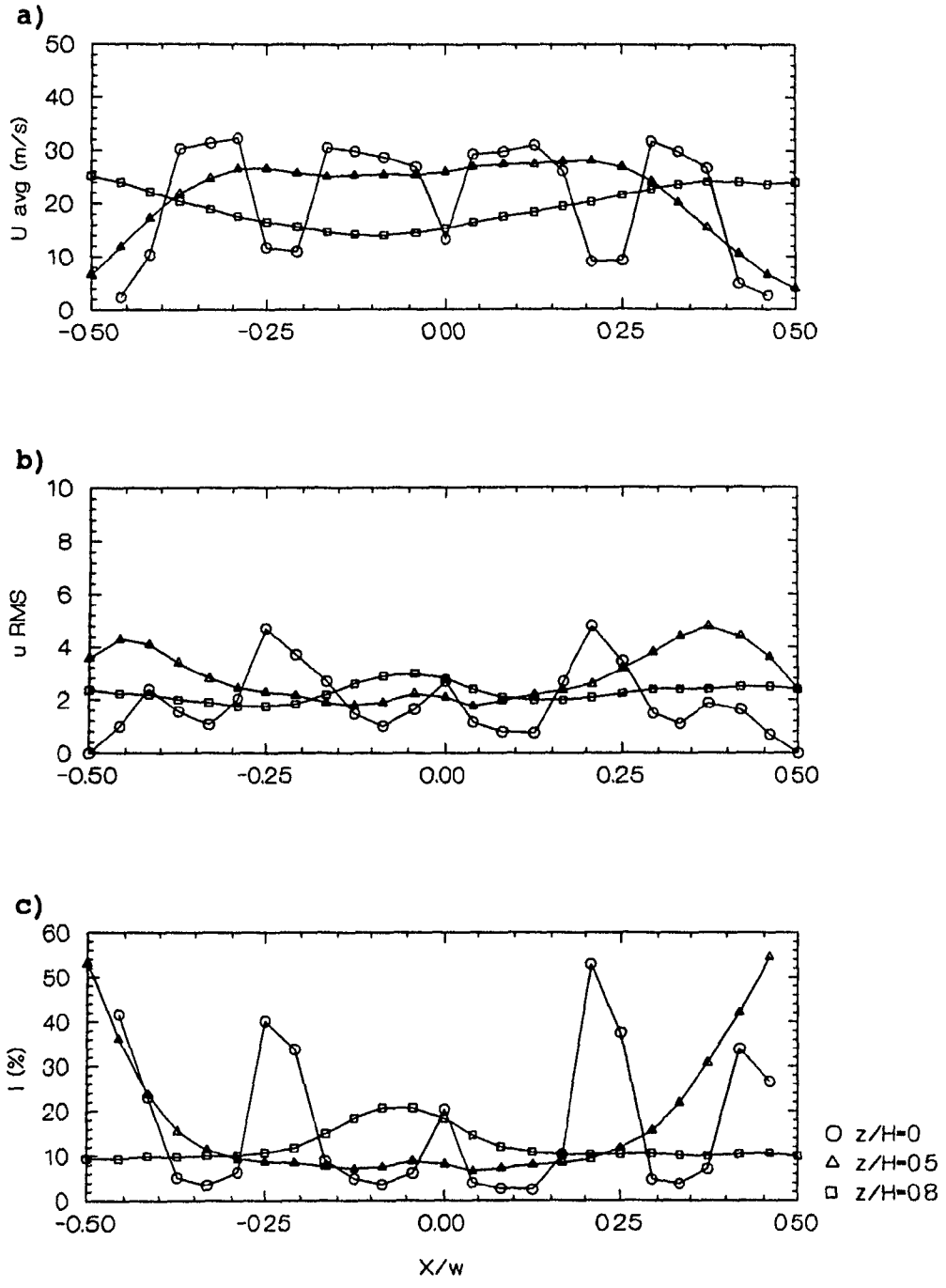

Figure 4.9 Profiles for H=37mm, w=24mm, tg=3, Re_j=40000: a) U, local mean velocity; b) u' local rms velocity; c) I, local turbulence intensity.

profiles (figs 4.7b, 4.8b, and 4.9b) persist but the two peaks from the outside bars have diffused outward. Rapid diffusion of axial turbulence in the direction perpendicular to the mean flow is a well known phenomenon. This lateral diffusion outwards from the flow centreline is also apparent in the turbulence intensity profiles at the nozzle to surface midpoint (figs 4.7c, 4.8c, 4.9c). As the flow approaches the impingement surface, z/H=0.8 when H/w=1.54, only the nozzle centreline peak in turbulence intensity is still visible in figs 4.7-4.9, the peaks from the two outside bars having diffused laterally outside the limits of measurement.

For H=37 mm, w=12 mm, H/w=3.1, the flow field described above as produced by a small number of large scale turbulence generators, i.e. 3 bars, is now contrasted with that from a large number of small generators, i.e. #10 wire mesh. The three sets of profiles, figs 4.10-4.12, show that the turbulence velocity profiles look similar regardless of Re. The profiles of rms velocity and turbulence intensity produced using a #10 mesh are naturally more uniform than those shown in figs 4.7-4.9 for three bars across the nozzle.

For the case of the single bar nozzle, the flow field is more completely mapped as the measurements at the midpoint and surface were extended beyond the positions directly under the nozzle edges (X/w = 0.5), thus figs 4.13-4.15 have wider lateral (X/w) limits. The disturbance in the centreline at the nozzle exit caused by the presence of the bar may be discerned

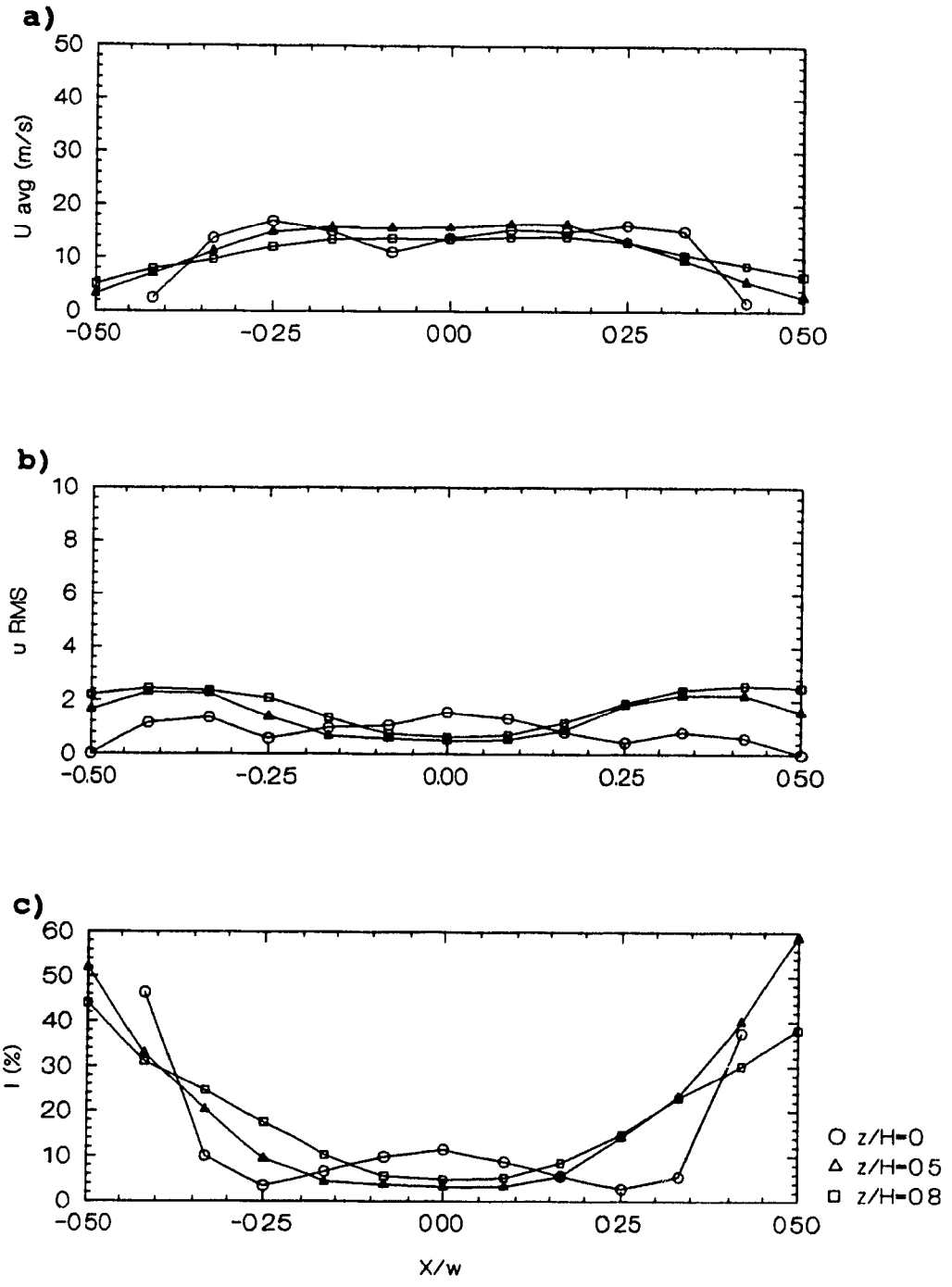

Figure 4.10 Profiles for H=37mm, w=12mm, tg=10, Re_i=12000: a) U, local mean velocity; b) u' local rms velocity; c) I, local turbulence intensity.

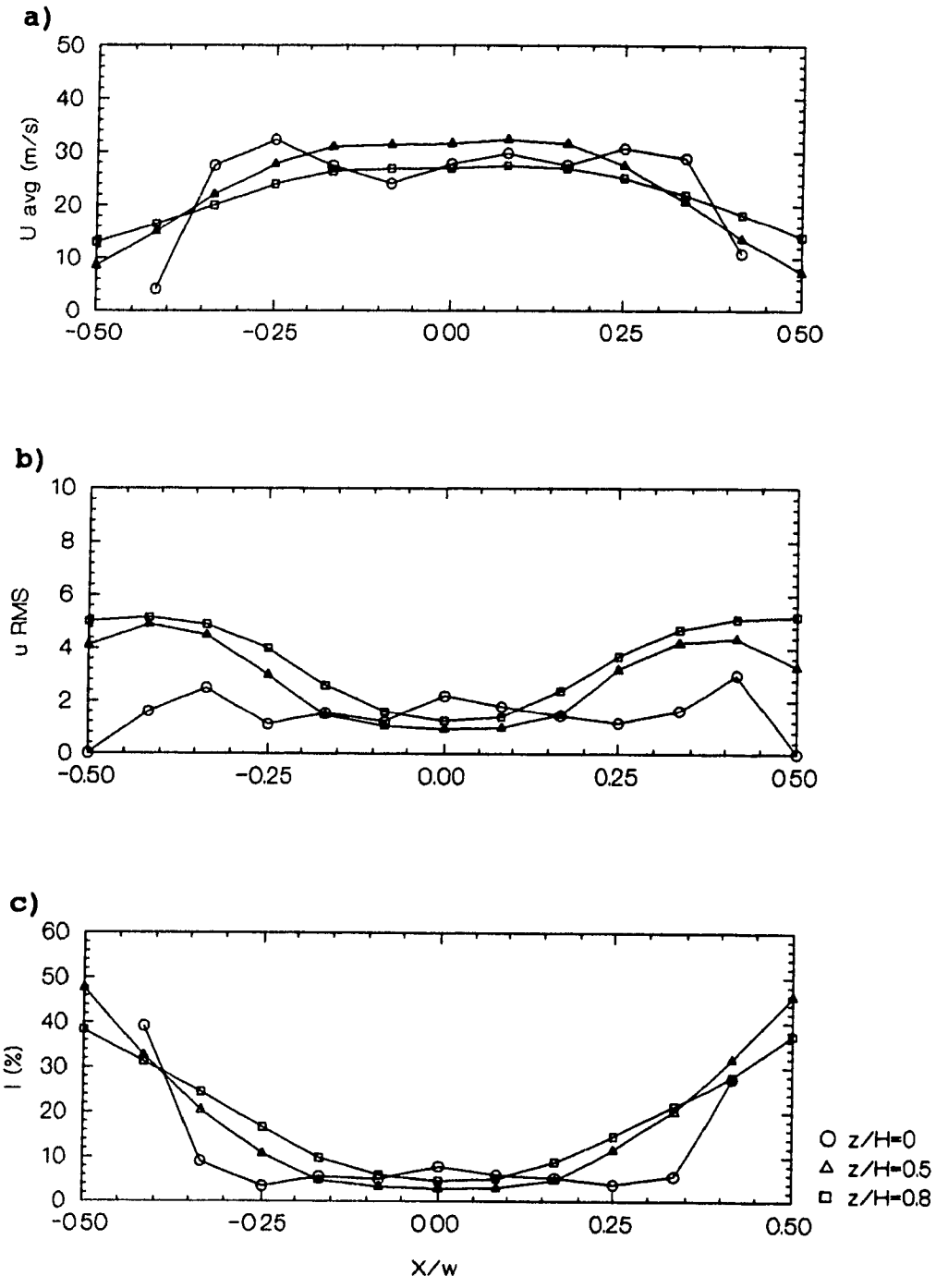

Figure 4.11 Profiles for H=37mm, w=12mm, tg=10, Re_i=24000: a) U, local mean velocity; b) u' local rms velocity; c) I, local turbulence intensity.

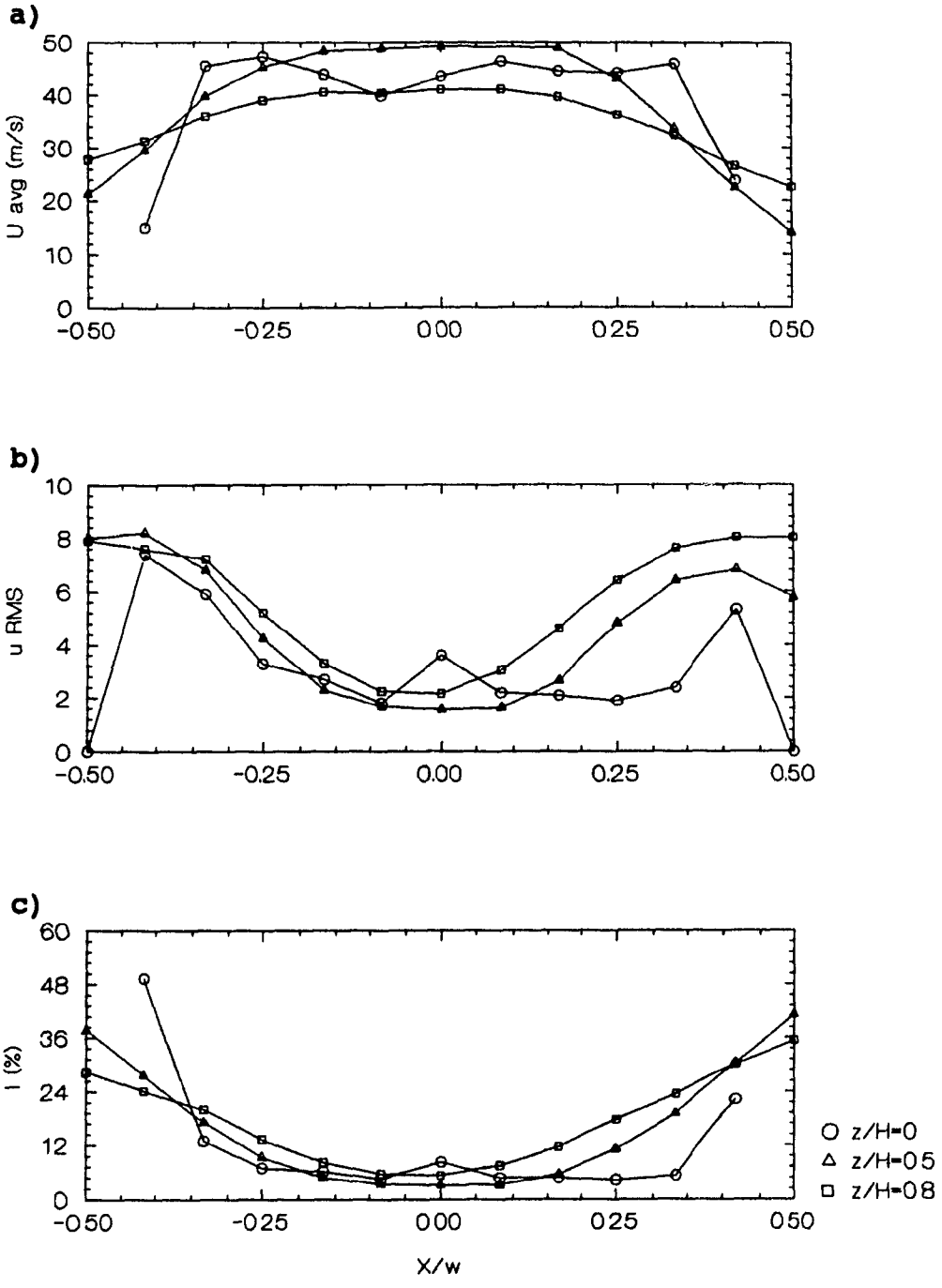

Figure 4.12 Profiles for H=37mm, w=12mm, tg=10, Re_i=40000: a) U, local mean velocity; b) u' local rms velocity; c) I, local turbulence intensity.

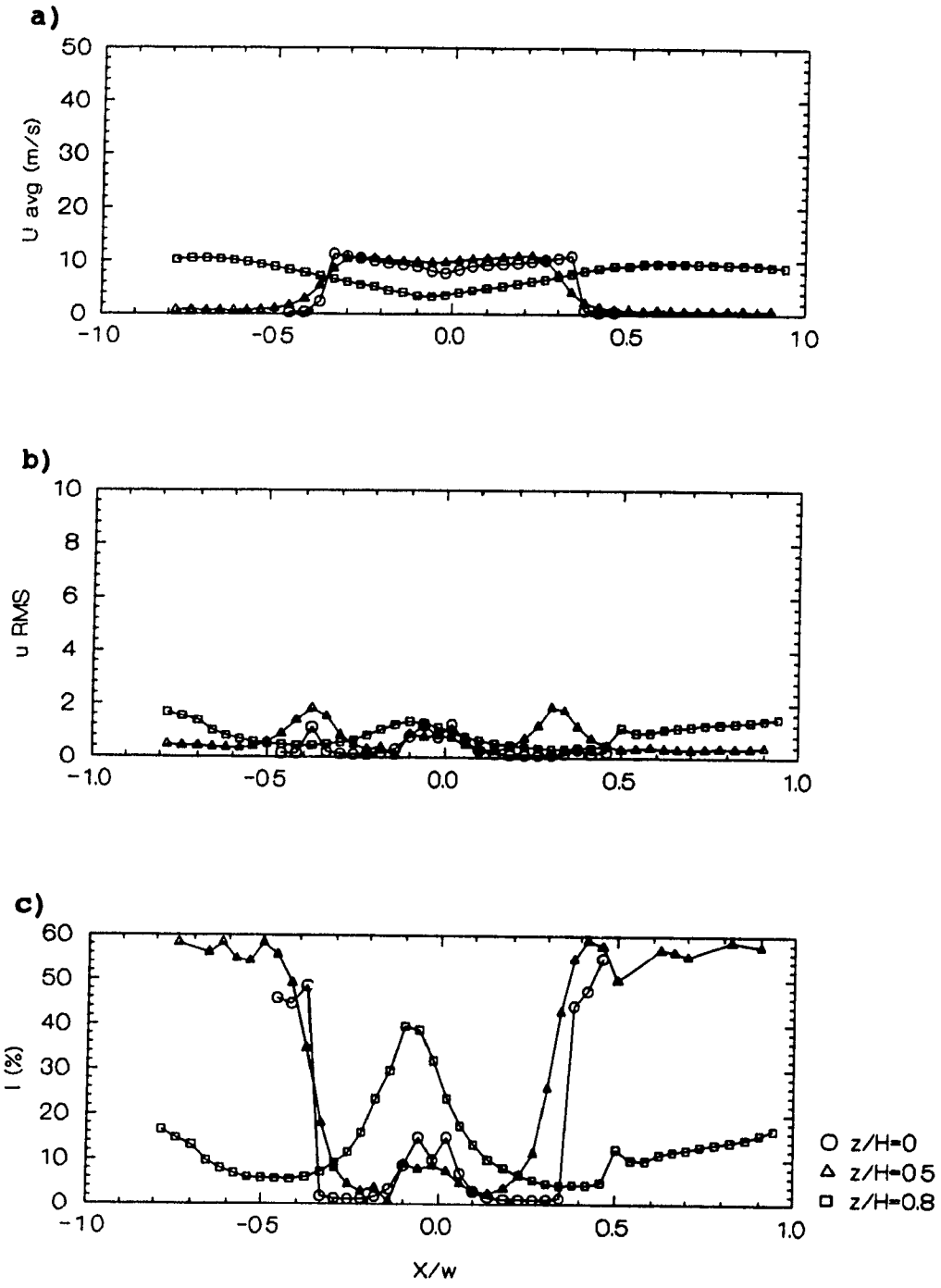

Figure 4.13 Profiles for H=37mm, w=25mm, tg=1, Re_j=12000: a) U, local mean velocity; b) u' local rms velocity; c) I, local turbulence intensity.

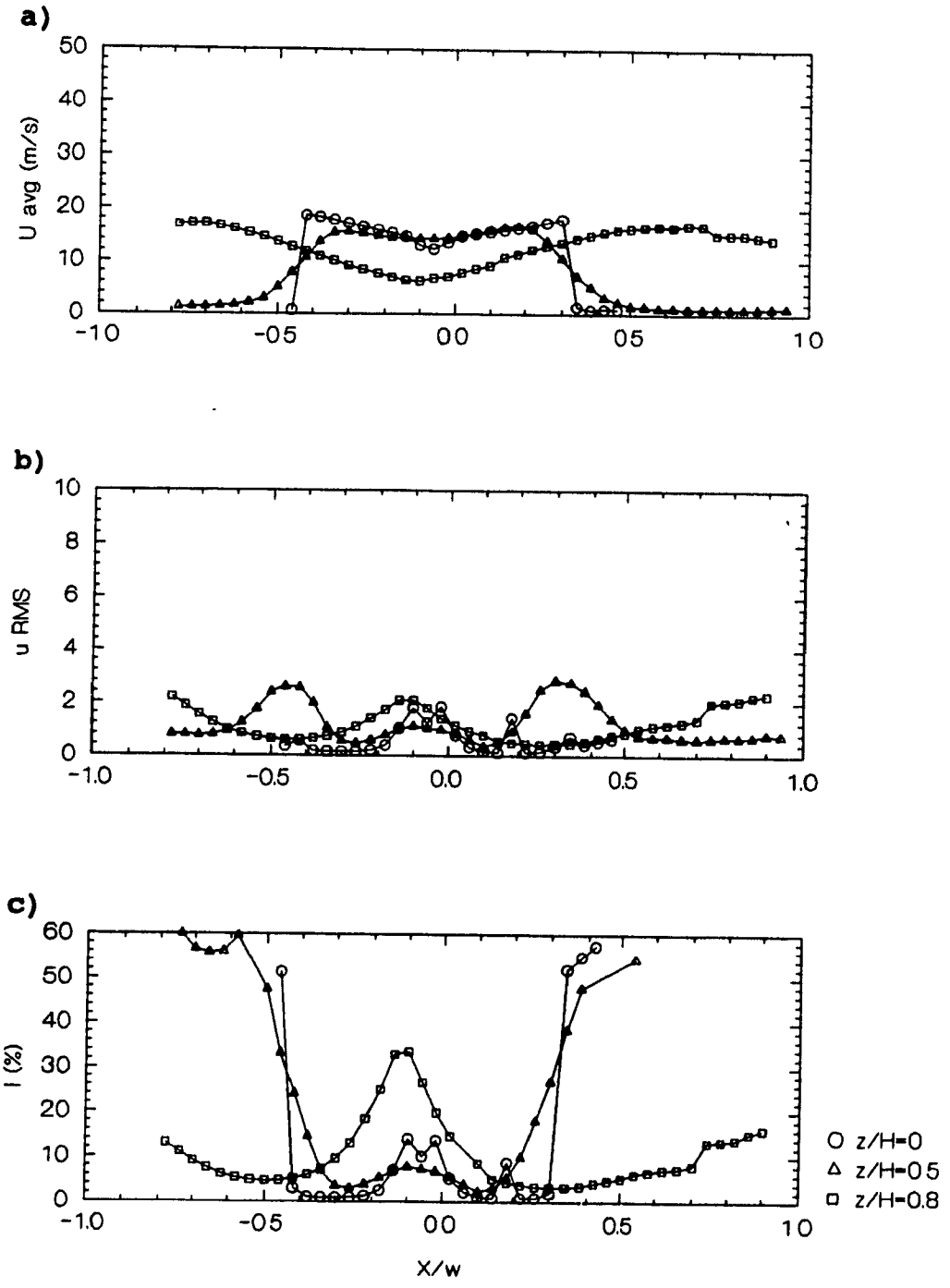

Figure 4.14 Profiles for H=37mm, w=25mm, tg=1, Re_j=24000: a) U, local mean velocity; b) u' local rms velocity; c) I, local turbulence intensity.

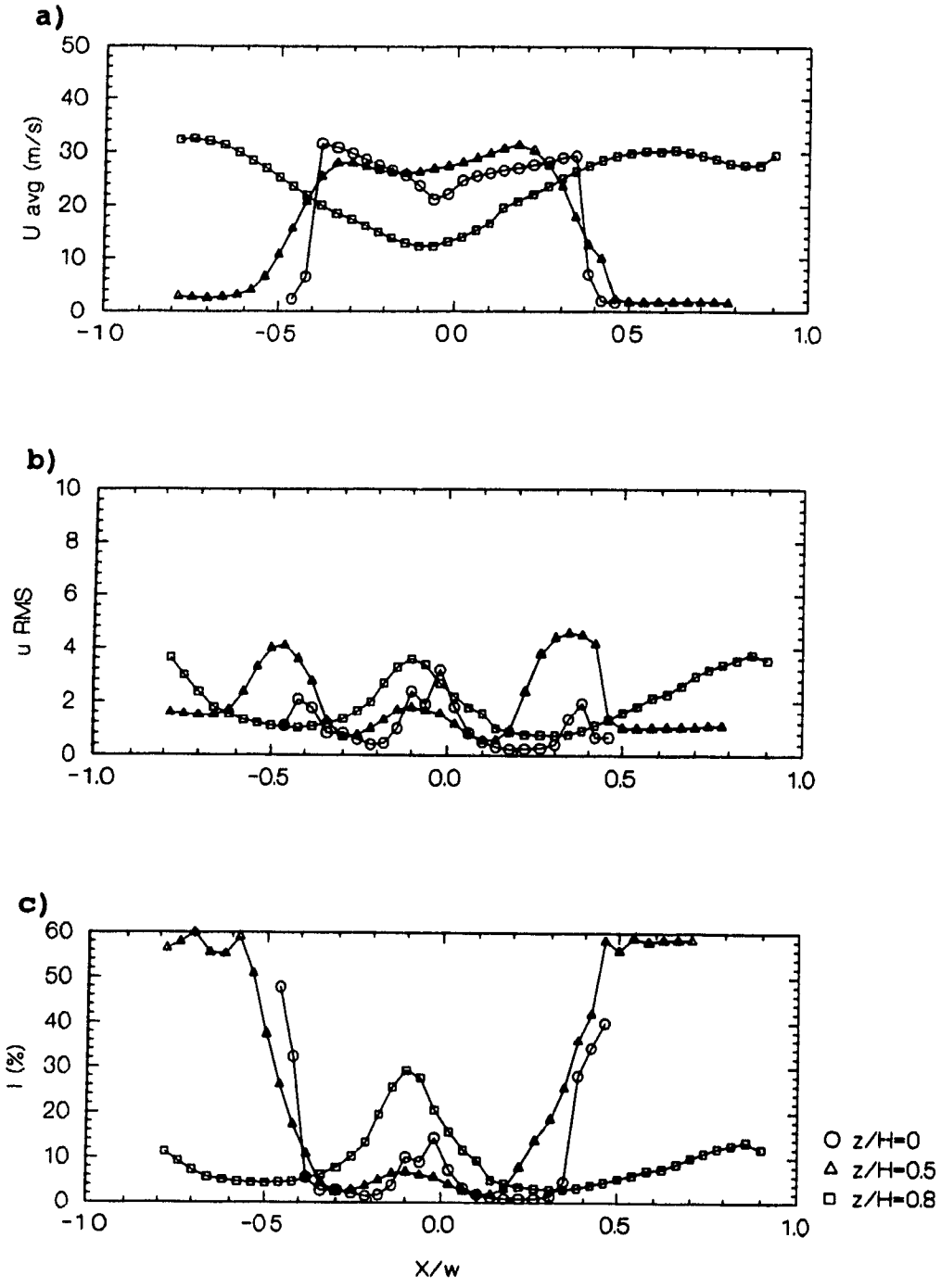

Figure 4.15 Profiles for H=37mm, w=25mm, tg=1, Re_j=40000: a) U, local mean velocity; b) u' local rms velocity; c) I, local turbulence intensity.

in the profile of mean velocity (part a in the figures), but is prominent in the profiles of u' (part b) and I (part c). At the midpoint, the effect of the single bar on mean velocity has all but disappeared. The rms fluctuating velocity and turbulence intensity profiles however show the development of progressively higher and broader peaks from the nozzle exit to the midpoint, z/H=0.5, to the approach to the impingement surface, z/H=0.8. At the midpoint position, z/H=0.5, figs 4.13-4.15 show clearly the development of axial turbulence velocity generated from two sources: the bar across the nozzle centreline, and from the nozzle edges. With the wider flow field mapped in figs 4.13-4.15, comparison of peaks in u' for this central bar with complete u' peaks from the nozzle edges shows the latter to be quite effective generators of axial turbulence.

By the approach of the impingement surface, z/H=0.8, u' from the central bar has continued to increase, while the u' peaks from the nozzle edges have been displaced laterally from the impingement region by the mechanism of turbulence diffusion and the lateral acceleration away from the nozzle centreline of the jet flow as it approaches the impingement surface. This latter effect, the formation of the wall jet region, well known from other studies, was not documented further. With regard to the measurements at z/H=0.8, it should be noted that these near-surface measurements are affected by the experimental limitation discussed previously, i.e. the

fact that the anemometer measurements are affected by the lateral as well as the axial component of the flow.

4.2.3 Average Turbulence Intensity

As the ultimate objective of this study is the effect of turbulence generation at the nozzle on rate of heat transfer at the impingement surface, the profiles of the turbulence intensity of figs 4.1c-4.15c do not provide a practical means of comparison. Although the profiles of figs 4.1-4.15 provide a detailed understanding of the impingement flow field, what is needed is a single index of axial turbulence intensity to represent the complex reality shown in these figures. These profiles establish that it would not be adequate simply to use the centreline values of turbulence, as is frequently done with fully developed turbulent flow. Simply averaging the values of local turbulence intensity across the nozzle has no theoretical significance. Moreover, in the nozzle exit region near the orifice wall where both u and u′ are approaching zero, the local intensity of turbulence is not known as there are no measurements of u and u′. Although the complete profile of local intensity of turbulence at the nozzle exit is not known, the turbulence velocity, u′, is well behaved in the near-wall regions, going to zero at the wall. Hence complete profiles of u′ at the nozzle exit are available as shown as in fig. 4.1b-4.15b. Thus a mean value, $\bar{u}'$, can be defined as

$$\overline{u'} = \int_{-.5}^{.5} u' d(x/w) \qquad (4.1)$$

As the mean velocity of the jet at the nozzle exit, $\bar{U}$, is known from the flowmeter measurements, an effective average turbulence intensity, $\bar{I}$, can be defined as

$$\bar{I} = \frac{\overline{u'}}{U} \qquad (4.2)$$

Appendix B contains the results for all of the runs conducted. Apart from the case of the smallest nozzle width, 6 mm, at the lowest Reynolds number, the level of average turbulence intensity, $\bar{I}$, is seen to be greater in nozzles with turbulence generation than with plain nozzles.

With this single numerical index, $\bar{I}$, to represent each profile, the effect of geometric and flow variables on turbulence may now be more conveniently examined. With the variables indicated in Table 4.1, the turbulence data provided by the present study may be represented as $\bar{I}$=f(H,w,Re,tg, axial position). Of the 67 profiles measured at the nozzle exit (position 1) 23 were for tg=0, 9 each for tg=1 and 3, 23 for tg=10 and 3 profiles for tg=18.

As the objective is to examine the effect of turbulence generation on impingement heat transfer, the effect on $\bar{I}$ of all parameters except turbulence generation is examined first.

Average turbulence intensity at the nozzle exit, $\bar{I}_1$, should not depend on H. Examination of the complete data , Appendix B, confirms that $\bar{I}_1$ is indeed independent of H, and moreover, it is independent of w as well. This fact greatly facilitates examination of the effect on $\bar{I}_1$ of the remaining variables - Reynolds number, turbulence generation and axial position. Table 4.3 summarises the results for the effect of turbulence generation and axial position on $\bar{I}$ at each of the three levels of Re. Of these three parameters, the effect of jet Reynolds number is the least significant. At lower levels of $\bar{I}$, i.e. below 5-6%, $\bar{I}$ is essentially independent of Re. At levels of $\bar{I}$ higher than this, there is a slight dependence of $\bar{I}$ with Re, as described below, but this effect is small compared to the effect of other parameters noted. As discussed in section 4.2.1, the near-surface measurements (axial position 3) for nozzles of width of 18 and 24-25 mm were affected by the impingement region. Therefore these data were not combined with data for the narrower nozzles for determining the values for position 3 but appear separately in the tables on the bottom line, identified as 3*.

For the base case of a single sharp-edged nozzle, the development of $\bar{I}$ with axial distance from the nozzle exit to the near-impingement surface position shown in Table 4.3 shows the behaviour well known from previous studies. Thus $\bar{I}$ first increases rapidly downstream of the nozzle exit, reaches a maximum value at an intermediate position, not far from the

Re=12000	turbulence generation				
axial position	0	1	3	10	18
	$\bar{I}$, %				
1	1.6	3.7	5.6	3.4	2.7
2	9.5	10.3	12.4	4.8	4.4
3	7.9			4.3	4.7
3*	2.4	6.7	9.7	2.3	

Re=24000	turbulence generation				
axial position	0	1	3	10	18
	$\bar{I}$, %				
1	1.6	2.6	6.7	2.9	2.5
2	8.1	9.3	11.1	4.3	4.8
3	6.9			4.2	4.5
3*	1.1	6.6	7.8	2.0	

Re=40000	turbulence generation				
axial position	0	1	3	10	18
	$\bar{I}$, %				
1	2.0	3.5	5.2	3.4	3.0
2	7.7	8.4	10.8	4.7	4.2
3	6.3			4.1	4.3
3*	1.1	5.9	8.4	2.4	

Table 4.3 Effect of turbulence generation and axial position on average turbulence intensity.

mid-point axial position 2, then is suppressed as the flow approaches the impingement surface, position 3. For turbulent jets the turbulence velocity u' does not increase in direct proportion to the mean velocity, $\bar{U}$, so the mean turbulence intensity, $\bar{I}$, at positions 2 and 3 decreases slightly with increasing Reynolds number. Relative to this base case, addition of either #10 or #18 mesh screen increases $\bar{I}$ at the nozzle exit by a factor of 50-100%. However, in spite of this substantial screen induced increase in $\bar{I}$ at the nozzle exit, it is notable that at axial positions 2 and 3 the level of $\bar{I}$ with screens is only half to two thirds of the value of $\bar{I}$ for the open nozzle. It is believed that this result is the consequence of effects of scale of turbulence, not measured in this study, in that the smaller scale turbulence generated by the screens decays much more rapidly than the larger scale turbulence from the edges of the open, sharp-edged orifice.

The single and 3-bar turbulence generation results are sharply different from those described above for screens. With one or three bars, $\bar{I}$ at the nozzle exit is generally higher than with screens, if only slightly for the single bar case. The major difference is in the downstream development of $\bar{I}$. In contrast to the nozzles with screens, the nozzles with one or 3 bars produce levels of $\bar{I}$ near the impingement surface (axial position 3) which at all three Reynolds numbers are significantly greater than those of the open nozzle.

At the closest approach to the impingement surface,

position 3, comparative data for nozzles with and without bars could only be obtained for the widest nozzles, i.e. w=18 or 24-25 mm. These data appear in Table 4.3 as position 3* because the two dimensional flow affects the significance of the measurements. Although the figures in row 3* cannot be directly compared with the remainder of the values in the table, the row 3* data show that $\bar{I}$ at the near approach to the impingement surface is substantially higher with bars than with either the simple sharp-edged nozzle or a #10 mesh screen. Comparison of the data with tg=0 and tg=10 for the narrow nozzles (line 3) with that for the wider nozzles (line 3*) leads to the conclusion that the correct value for the turbulence intensity for the larger nozzles is substantially higher than that shown on line 3* as measured with the single wire probe. As for the comparison between the 1-bar and the 3-bar nozzles, an important conclusion is that at all 3 axial positions the level of $\bar{I}$ is higher for the nozzles with 3 bars.

In summary, it is established that screens in the range of 10-18 mesh are not attractive for turbulence generation because the turbulence generated by the screens with 0.66 mm (#10 mesh) and 0.44 mm (#18 mesh) diameter wire decay faster than turbulence from a plain sharp edged orifice. By contrast, turbulence generated by one 3 mm round bar or 3 rectangular bars 1 mm wide in the nozzle, which is of larger scale than the turbulence from these screens, increases to a higher level

than that from a plain nozzle, decays less quickly than for a plain nozzle and, at the key position near the impingement surface, remains substantially higher than the turbulence generated by a simple sharp edged slot nozzle. Thus adding one or three bars to a slot nozzle substantially enhances turbulence where it counts, near the impingement surface.

These results are subsequently combined with the impingement heat transfer measurements to provide a comprehensive perspective of the turbulence/heat transfer relationship for impinging slot jets.

4.3 Pressure Drop Increase due to Turbulence Generation

Inserting obstructions such as bars or wire mesh into the nozzle blocks some of the area available for flow, thus increasing pressure drop. This effect was monitored by measurement of the jet plenum pressure. Any increase in impingement heat transfer obtained by turbulence generators in the nozzle is at the expense of increased pressure drop across the obstructed nozzle. The present study therefore monitored the latter in order to facilitate a cost/benefit analysis of increased heat transfer vs. increased pressure drop.

Figure 4.16 compares the jet plenum pressure for the largest nozzle with the three turbulence generation methods. From the base case of the plain nozzle, the increase in plenum pressure is least for the 1 bar nozzle, next highest for the

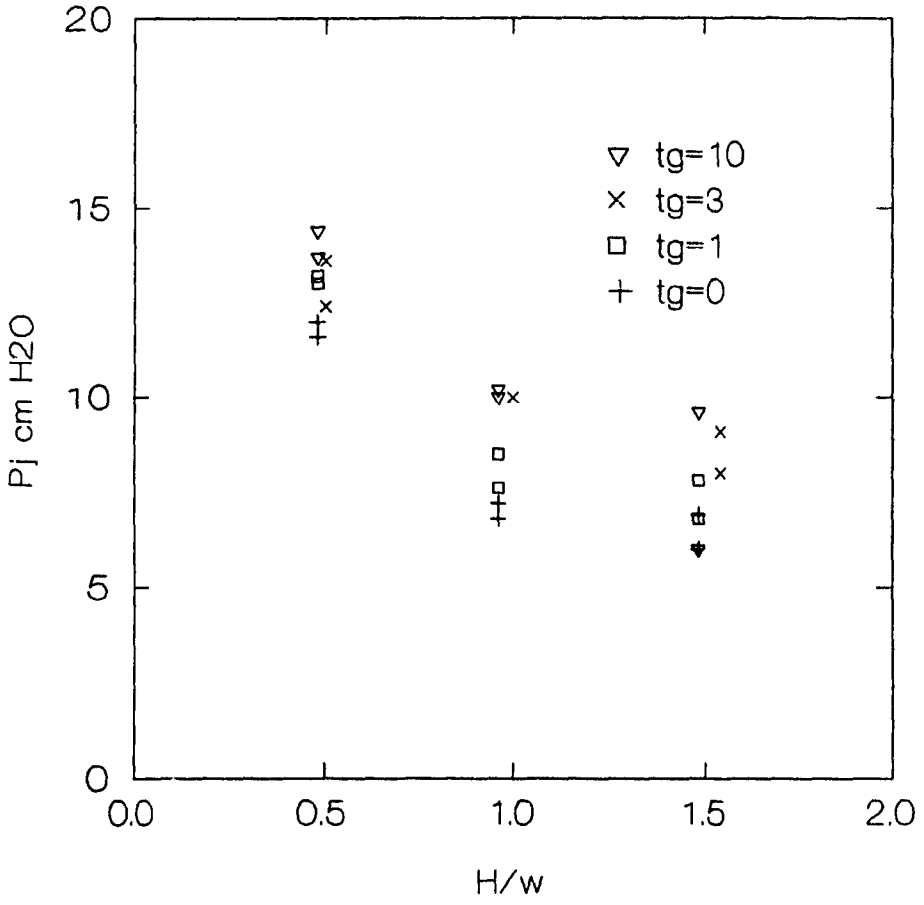

Figure 4.16 Plenum pressures for H=37mm, w=25mm, Re_j=40000.

3 bar nozzle, while the wire mesh produces the highest plenum pressure. Using the widest nozzle, w=25 mm, at the closest spacing, H=12 mm, H/w=0.5, the nozzle is wider than the 12 mm spacing from the impingement surface. As the wall jet velocity at the position X/w=0.5 is in this case twice the nozzle exit velocity, the system pressure drop is correspondingly very high, as reflected in the plenum pressures for all cases at H/w=0.5. Appendix B contains a complete set of plenum pressure data for all of the nozzle setups.

Plenum pressures are used instead of a pressure drop across the nozzle because of the pressure recovery phenomenon. This effect occurs for impinging jets which are contained by a confinement hood as in the present study, and as in the process industry application, the drying of paper under confined impinging jets. The pressure recovery phenomenon was described by van Heiningen (1982). The static pressure in the high velocity jet flow just downstream of such nozzles is below that at the exhaust ports. With dissipation of the jet velocity, the static pressure rises to that at the exhaust port discharge. It is of more practical significance therefore to measure the static pressure in the plenum chamber upstream of the nozzle, and to indicate the effects on operating pressure of the changes in the nozzle geometry made to increase impingement heat transfer rates.

4.4 Heat Transfer

Profiles of heat transfer rate for confined slot jets from several designs of orifice nozzles were calculated from high speed, high resolution heat flux sensor measurements taken at the impingement surface. For all combinations of the geometric parameters, three levels of Reynolds number were used, except for the smallest nozzle width, 6mm, for which the highest Reynolds number was beyond the equipment capability. Nozzle configurations representing 22 combinations of H, w, and tg were used, covering the range given for each variable listed in Table 4.1. With three levels of Re used, except as noted above, 64 Nusselt number profiles were determined for combinations of the flow and geometric parameters.

4.4.1 Heat Transfer without Turbulence Generation

4.4.1.1 Local Heat Transfer

The results are produced in terms of a local Nusselt number calculated from each of the 500 measurements of the heat flux sensor taken per revolution of the cylinder.

For the base case of the plain, sharp edged nozzle with no additions for turbulence generation, figure 4.17 shows local heat transfer profiles for w=12 mm at the three values of H. At H/w=3 (fig. 4.17a), a close nozzle to surface spacing, although this is the largest spacing used, the

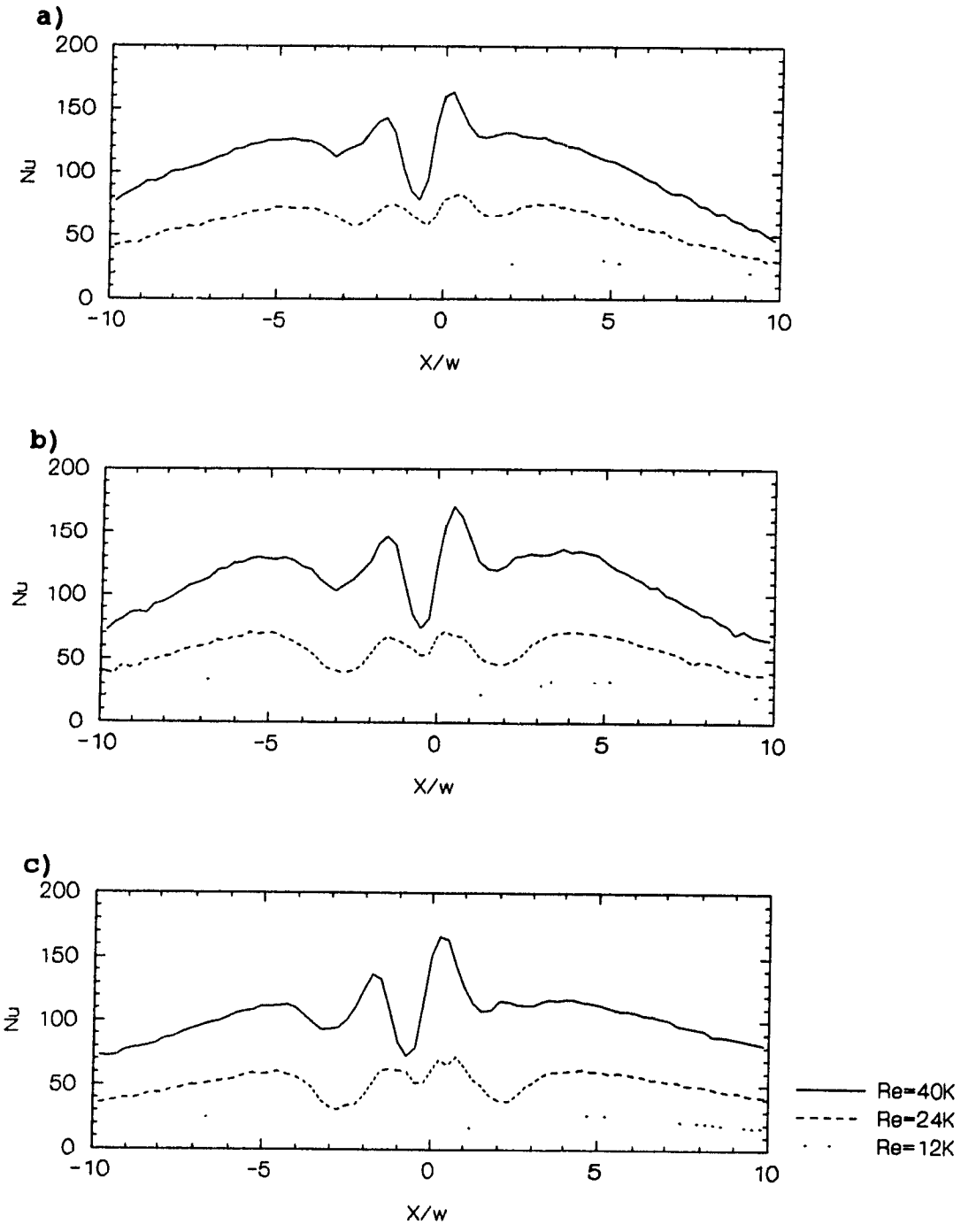

Figure 4.17 Profiles of local Nu for w=12mm, tg=0: a) H=37mm; b) H=24mm; c) H=12mm.

turbulent jet flow is highly undeveloped. Thus even at the lowest Reynolds number, each profile of fig. 4.17 shows off-stagnation minimum and secondary maximum peaks in the Nusselt number profile, which become larger as H/w becomes smaller. It is well established from the research of Martin (1977) and numerous others, that these off-stagnation features indicate transition from a laminar to a turbulent boundary layer.

Figure 4.18 shows profiles for the largest nozzle, w=25, at the three values of H and three values of Re. At the higher flowrates, the minima are larger yet and the secondary maxima are greater than the stagnation point peak, a phenomenon well documented by van Heiningen (1982) and Polat (1988).

4.4.1.2 Average Heat Transfer

Just as profiles of local turbulence intensity in the previous section, while being informative of the flow field, do not provide a direct measure of the turbulence conditions experienced by an impingement surface moving under such jets, local heat transfer profiles such as figures 4.17 and 4.18 do not indicate directly the impingement heat transfer for such a moving surface. In the important continuous process of paper drying under impinging jets, the moving surface, i.e. the sheet being dried, travels under the entire profile of each impinging jet. Thus the effective impingement heat transfer

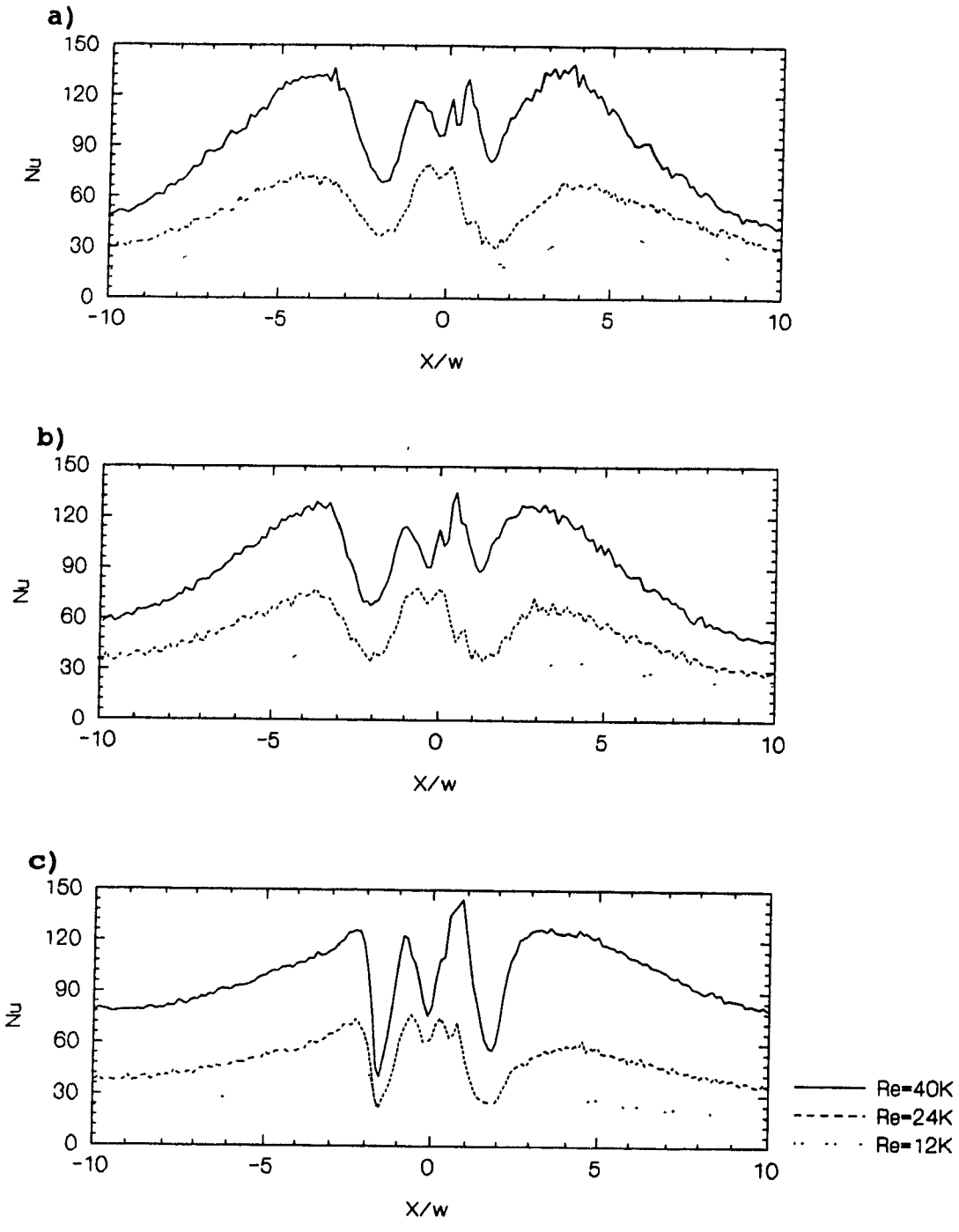

Figure 4.18 Profiles of local Nu for w=25mm, tg=0: a) H=37mm; b) H=24mm; c) H=12mm.

for the moving impingement surface is the integrated average, $\overline{Nu}$, of the profile of local heat transfer. Thus $\overline{Nu}$ for heat transfer is analogous to $\bar{I}$ for turbulence intensity.

The heat transfer averaging area has been defined in previous work in terms of S, the half width of the impingement area, i.e. the extent of the impingement surface as measured laterally from the stagnation point at the centreline of the jet flow. This width is non-dimensionalised as S/w. Figure 4.19 shows profiles of the average Nusselt number, $\overline{Nu}$, as a function of S/w for the same nozzle parameters as in fig. 4.17. Likewise fig. 4.20 shows the average Nusselt number profiles corresponding to the local profiles of fig. 4.18.

For the basic objective of comparing mean $\overline{Nu}$ with and without turbulence generation at the nozzle exit, it is necessary to consider the choice of the extent of the impingement surface over which this average is calculated. In industrial paper dryers employing impinging jets, the ratio of nozzle area to confinement surface area, a ratio commonly referred to as "open area", is in the range of 5%. For slot nozzles, an open area of 5% corresponds to a width of impingement surface S/w=10 on each side of the nozzle centreline. Inspection of the Nu profiles of figs 4.19-4.20 shows that a region 10w on either side of the jet centreline covers the impingement region of high Nu. For conditions which produce off-stagnation minima and secondary maxima in profiles of local Nu, a distance of 10w out from the centreline, figs.

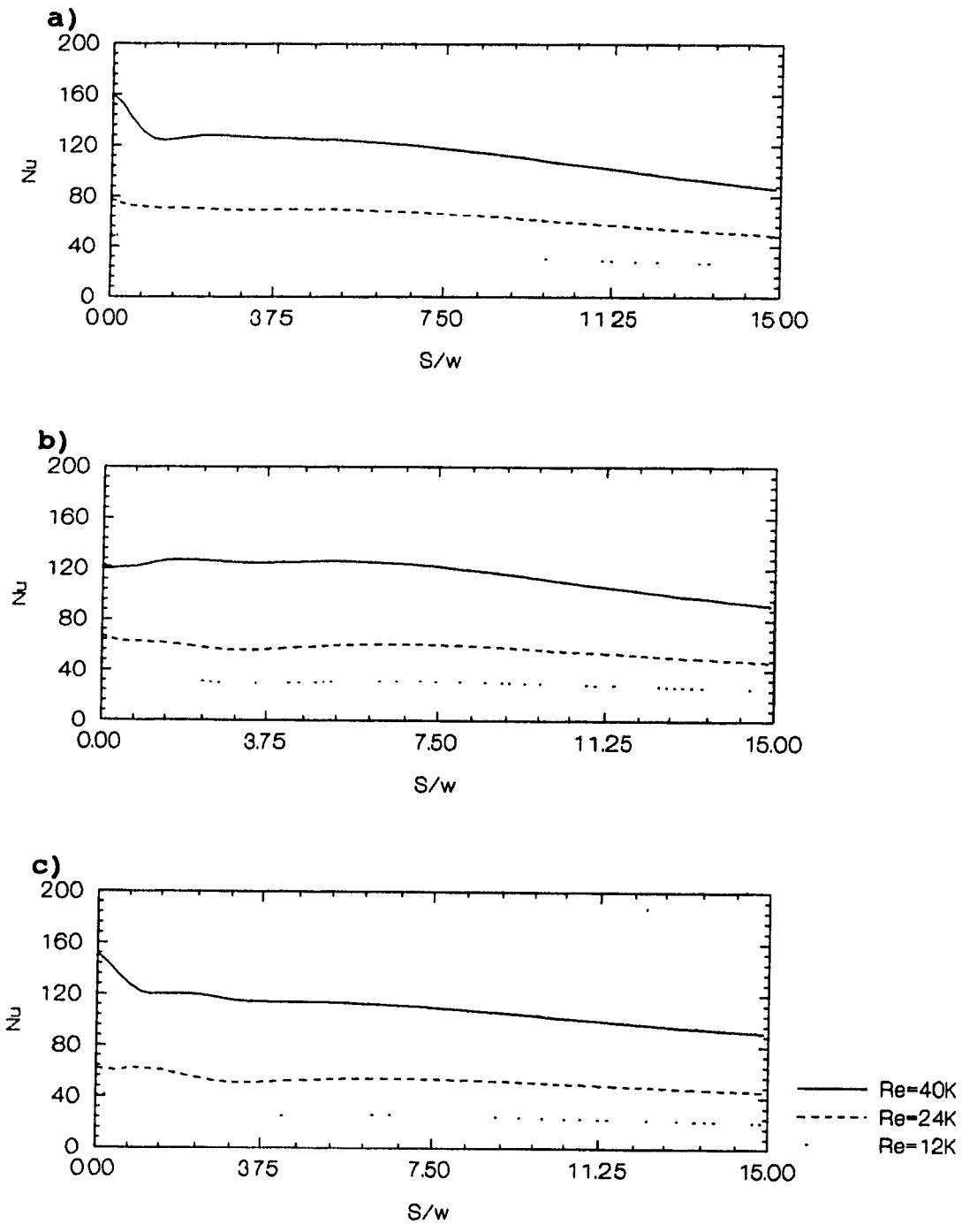

Figure 4.19 Profiles of average Nu for w=12mm, tg=0: a) H=37mm; b) H=24mm; c) H=12mm.

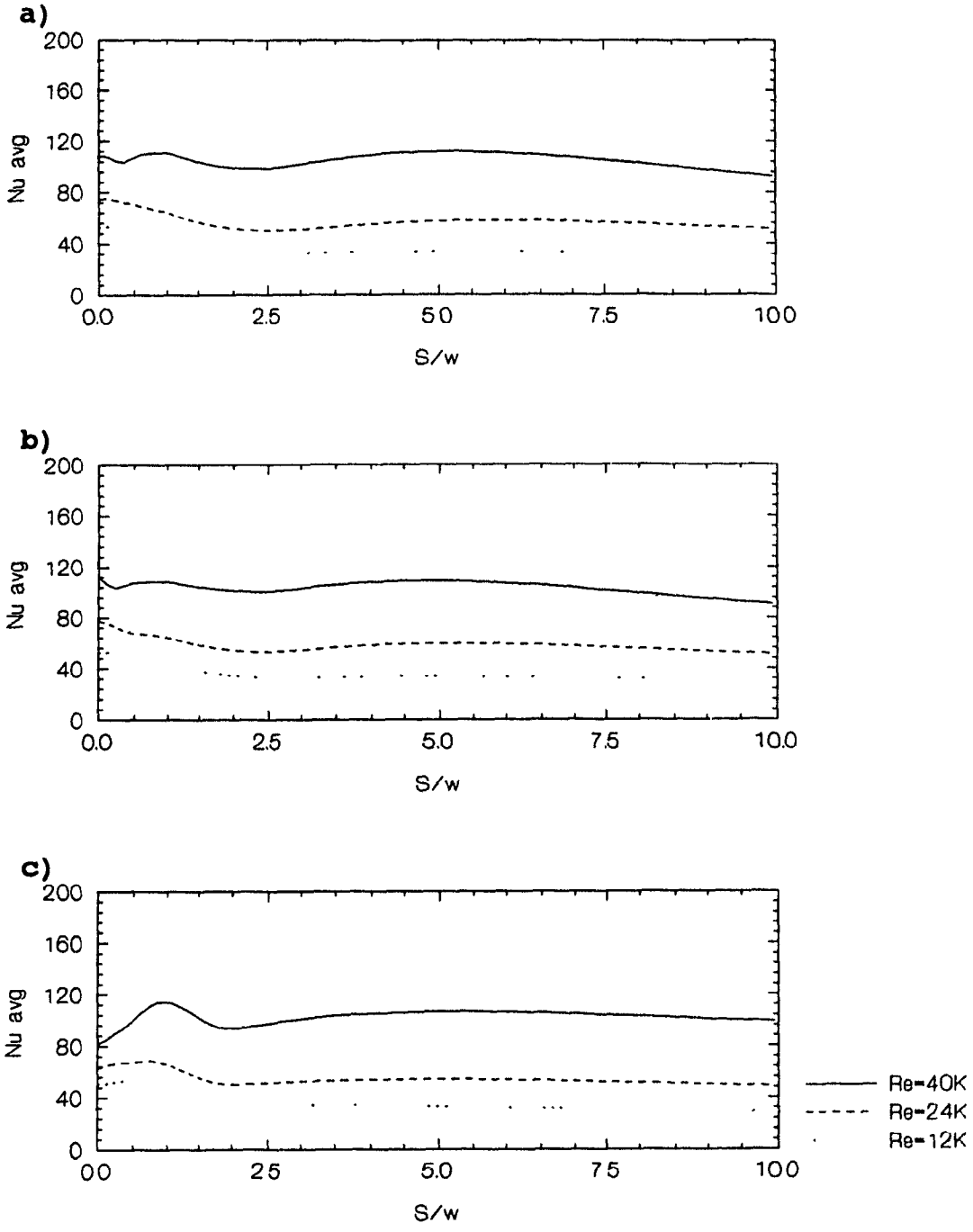

Figure 4.20 Profiles of average Nu for w=25mm, tg=0: a) H=37mm; b) H=24mm; c) H=12mm.

4.17 and 4.18, easily includes these secondary maxima. Thus S=10w represents a reasonable extent of heat transfer area over which to compute the reference average Nusselt number. As various values of S will be appropriate for specific industrial applications, the results of this study are presented in Appendices B and C as a function of S/w, with values ranging up to at least S/w=10.

4.4.2 Heat Transfer with Turbulence Generation

4.4.2.1 Local Heat Transfer

Figure 4.21 shows profiles of local heat transfer with the addition of #10 wire mesh as a turbulence generating grid to the nozzle for which fig. 4.17 gives the profiles for the plain nozzle. The turbulence generation eliminates the off-stagnation minima and secondary maximum peaks. The conclusion is that the enhanced turbulence has moved the location of the transition from laminar to turbulent boundary layer from about 2w from the stagnation point, fig. 4.17, to sufficiently close to the stagnation point that this transition is lost in the central peak of fig. 4.21.

Figure 4.22 is a comparison of the three metho - of turbulence generation used with the widest nozzle. The ı.ıes marked tg=0 correspond to the three profiles shown in fig. 4.19a. Comparison with the same geometrical and flow parameters with no turbulence generation shows that all types

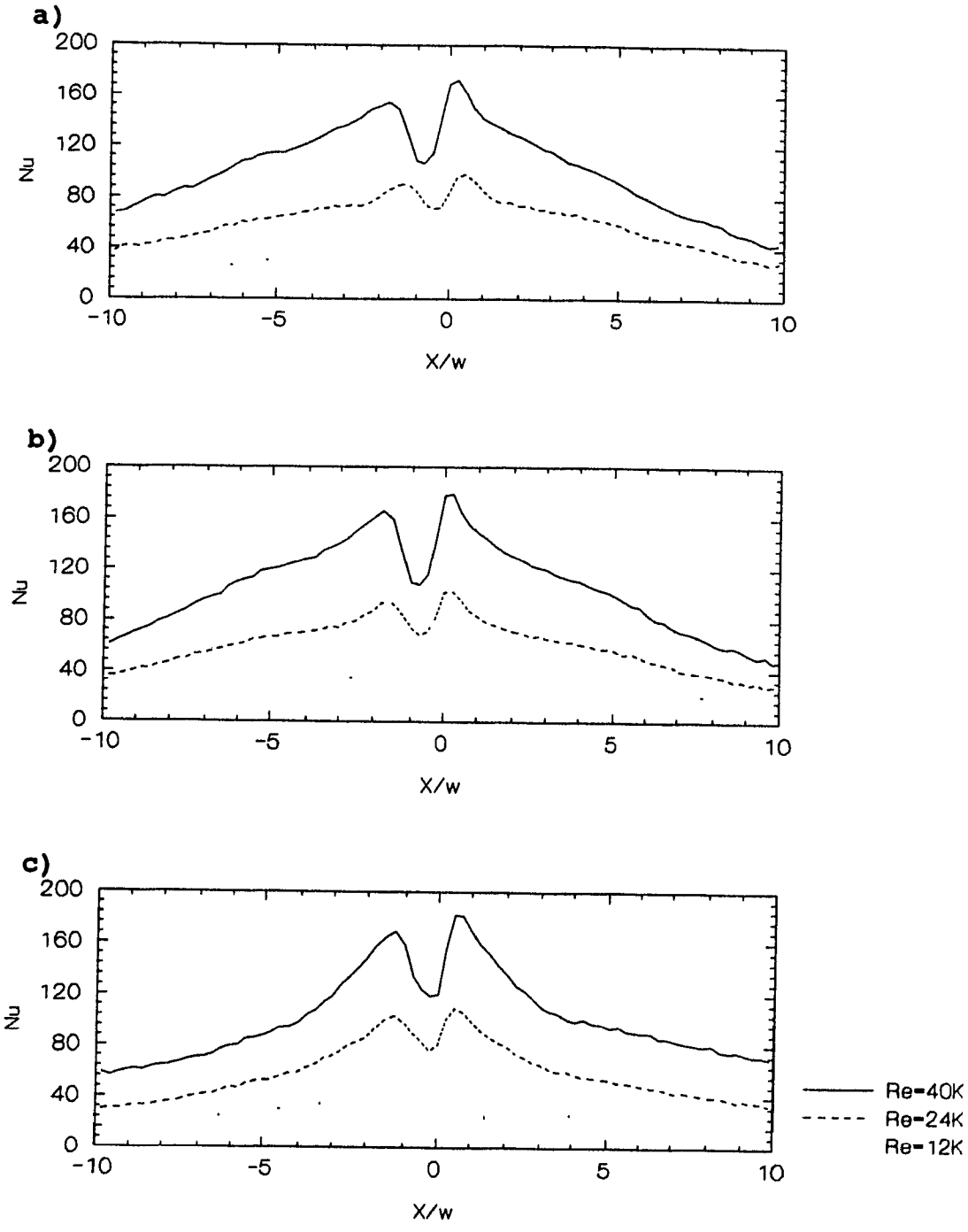

Figure 4.21 Profiles of local Nu for w=12mm, tg=10: a) H=37mm; b) H=24mm; c) H=12mm.

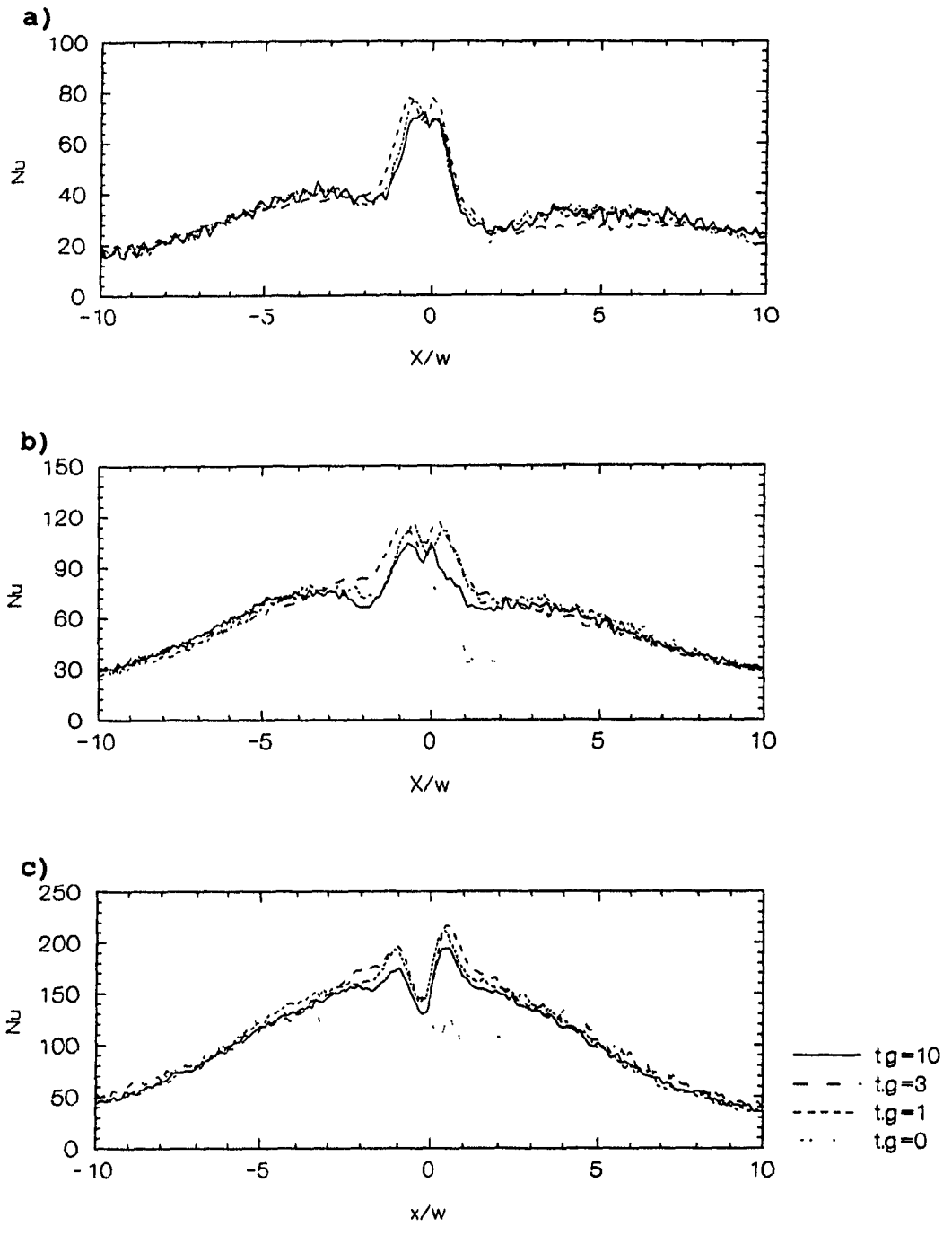

Figure 4.22 Profiles of local Nu for H=37mm, w=25mm: a) Re_j=12000; b)Re_j=24000; c) Re_j=40000.

of enhancement used here have increased the Nu profiles and have eliminated the off-stagnation features otherwise found in the Nusselt number profiles. These changes in local Nu show that the changes in the flow field initiated at the nozzle exit are felt at the impingement surface.

This series of six sets of results, figures 4.21-4.22, shows that turbulence generation at the nozzle exit can greatly shorten the transition from a laminar to turbulent boundary layer, with consequently higher heat transfer rates in the region close to the stagnation point. Beyond about 3w - 4w from the stagnation point the profiles of local Nu are unchanged by the turbulence generation at the nozzle exit.

A set of figures analogous to fig. 4.22 for all combinations of parameters studied is provided in Appendix C.

4.4.2.2 Average Heat Transfer

A comparison of the curves for average Nusselt number, $\overline{Nu}$, for the 12 mm nozzle with and without the wire mesh, i.e. comparing fig 4.23 to fig. 4.19, shows the increase in $\overline{Nu}$ produced by the turbulence generation. The enhancement in $\overline{Nu}$ is particularly evident for S less than 5w. Figure 4.24 displays this comparison explicitly through profiles of $\overline{Nu}$ for the three turbulence generation methods, along with the base case of the $\overline{Nu}$ profile for the open nozzle. Although the enhancement in $\overline{Nu}$ is substantial for all types of turbulence

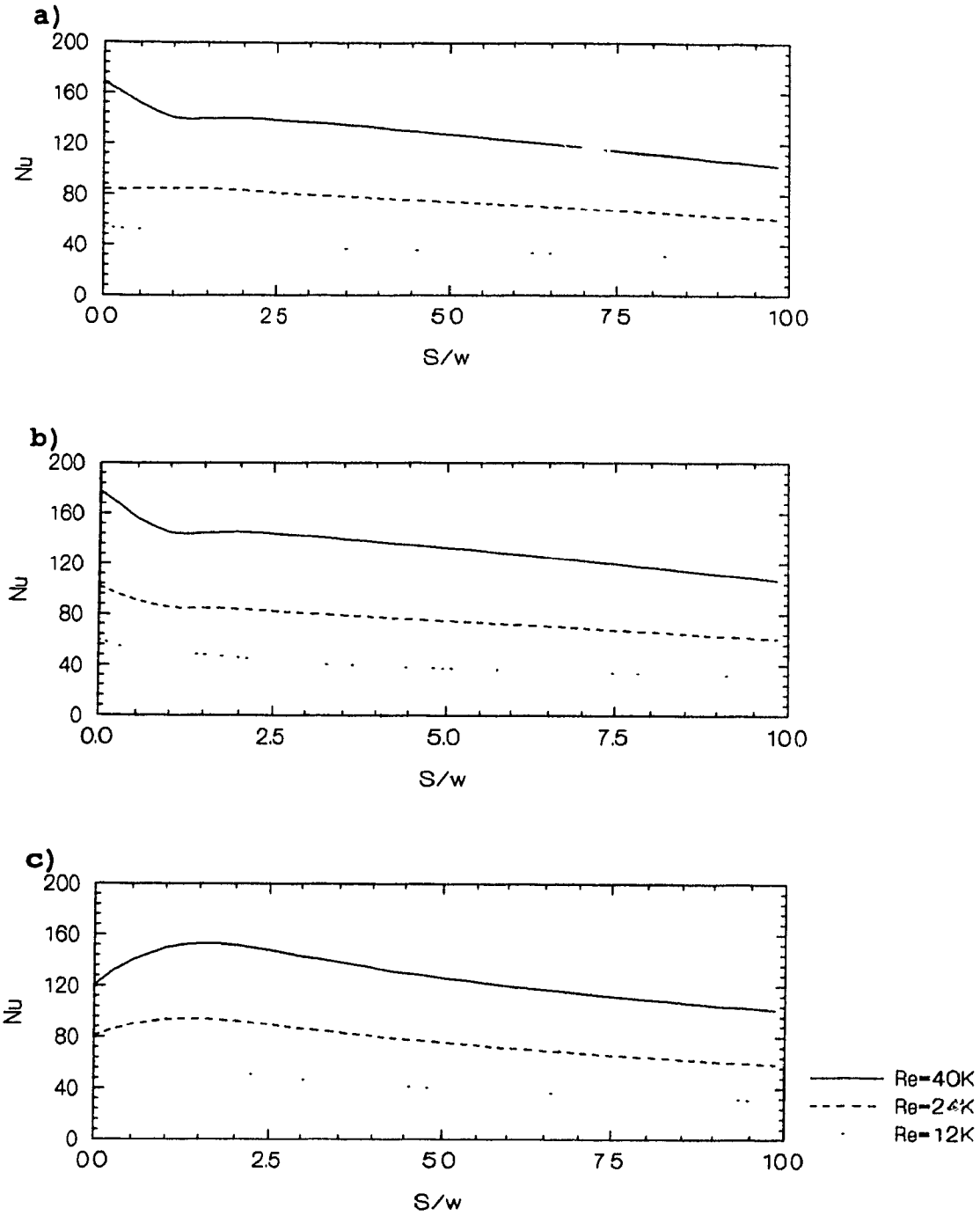

Figure 4.23 Profiles of average Nu for w=12mm, tg=10: a) H=37mm; b) H=24mm; c) H=12mm.

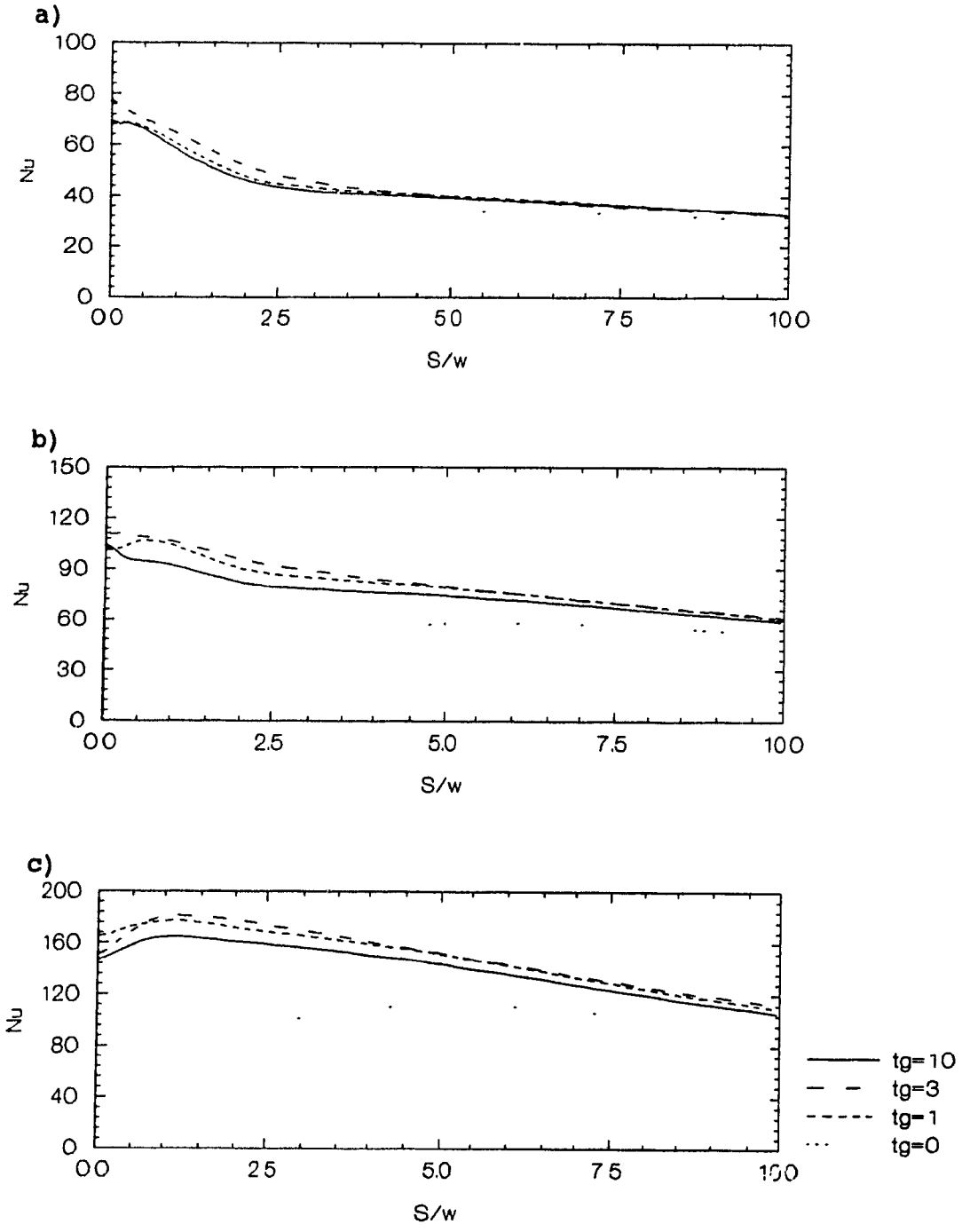

Figure 4.24 Profiles of average Nu for H=37mm, w=25mm: a) Re_j=12000; b) Re_j=24000; c) Re_j=40000.

generator used, the three bar nozzle produces the highest profile, followed by the single bar nozzle and then the #10 mesh screen. This distinction is clear for the lower range of values of impingement surface width, i.e. S less than about 5w, but diminishes for wider impingement surfaces. As fig. 4.22 showed that the enhancement in local Nu was in the impingement zone within about 4w from the nozzle centreline, these trends in fig. 4.24 are as expected.

A set of figures analogous to fig. 4.24 for all experiments is given in Appendix C.

Although representation of results in the form shown as fig 4.24 and in Appendix C show the sensitivity of the enhancement in $\overline{Nu}$ as a function of the extent of the impingement surface, it is also useful to examine the dependence of this enhancement on the nondimensional nozzle-to-surface spacing, H/w. To show this it is necessary to select a particular value of the extent of the impingement surface, S/w. An averaging width of S/w=10 corresponds to an open area of 5%, which is in the range used in industrial impinging jet dryers for paper. Thus for S/w=10 and with the largest nozzle, figure 4.25 shows comparisons for each jet Reynolds number of the increases in $\overline{Nu}$ over the plain nozzle that are produced by the three types of turbulence generation used. As a technique for enhancing $\overline{Nu}$, the wire mesh is outperformed by the bars at all but the closest nozzle to surface spacing. As industrial use of confined impinging jets

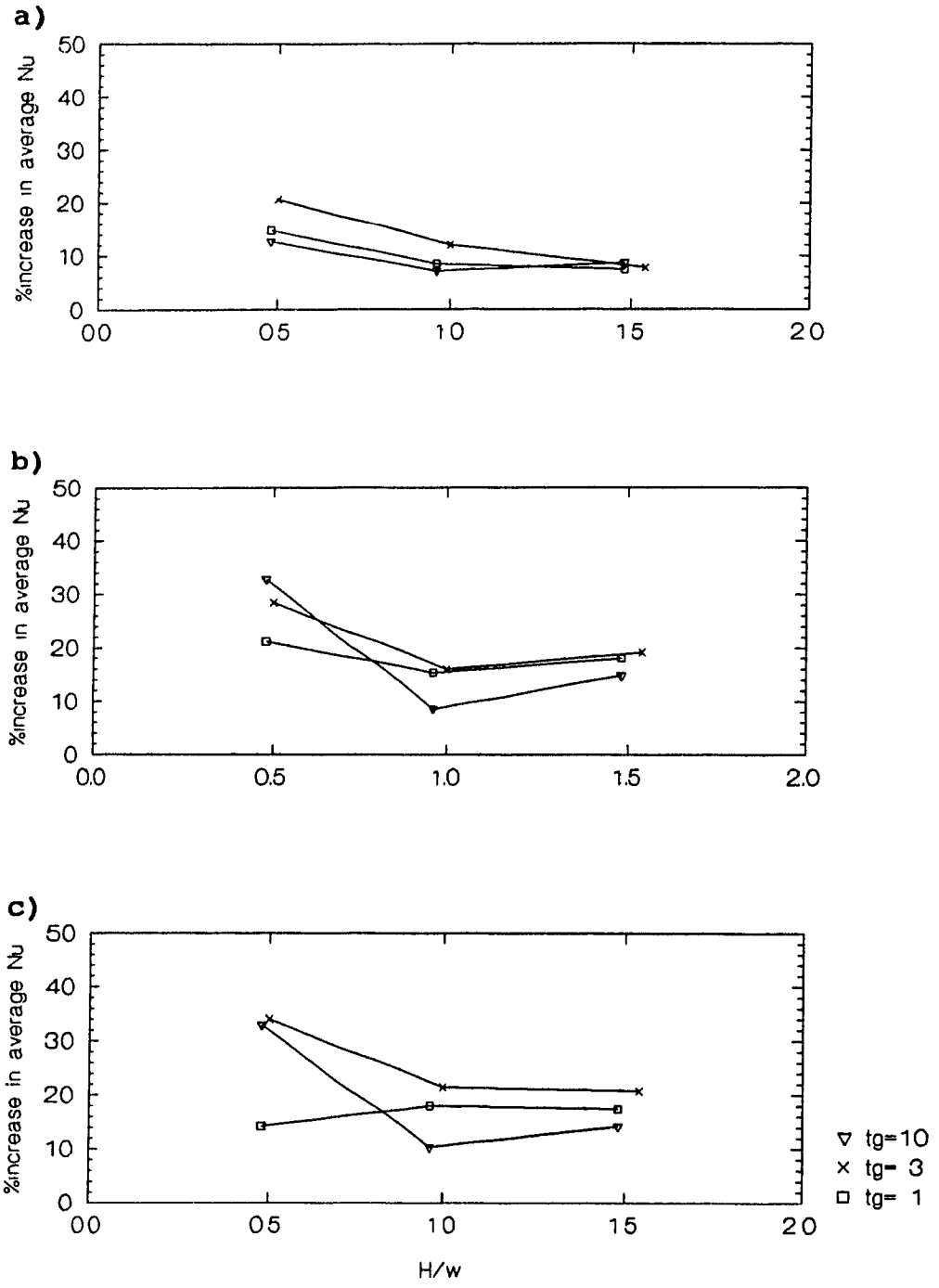

Figure 4.25 Increase in average Nu at S/w=10 over a plain nozzle forthree turbulence generation methods, a)Re_j=12000; b)Re_j=24000; c)Re_j=40000.

does not normally employ spacings as small as H/w=0.5, it is the larger spacings which are of more practical relevance. At nozzle spacings in the range of H/w=1.0-1.5, the small scale turbulence produced by the 0.66 mm diameter wire of the #10-mesh screen grid is less effective at enhancing heat transfer rates than the larger scale turbulence from a single bar 3 mm in diameter. In the range of H/w of 1.0-1.5, the enhancement of $\overline{Nu}$ for S/w=10 is generally better for the three-bar than the one-bar nozzle, fig. 4.25. However, as the enhancement given by the one-bar nozzle is only marginally less than that from the three-bar nozzle, considerations of simplicity and cost suggest the one-bar nozzle as the practical choice.

The enhancement of average heat transfer rate increases with increasing jet Reynolds number. If the values of enhancement of $\overline{Nu}$ for the 1- and 3-bar nozzles are combined for H/w=1.0 and 1.5, the Reynolds number effect is seen in table 4.4. These Reynolds numbers are in the range of those used in industrial drying of paper under impinging jets.

Table 4.4 Increase in average heat transfer for 1- and 3-bar nozzles.

Re	Increase of $\overline{Nu}$ at S/w=10 over plain nozzle
12000	10%
24000	19%
40000	21%

Figure 4.26 compares data from this study with results

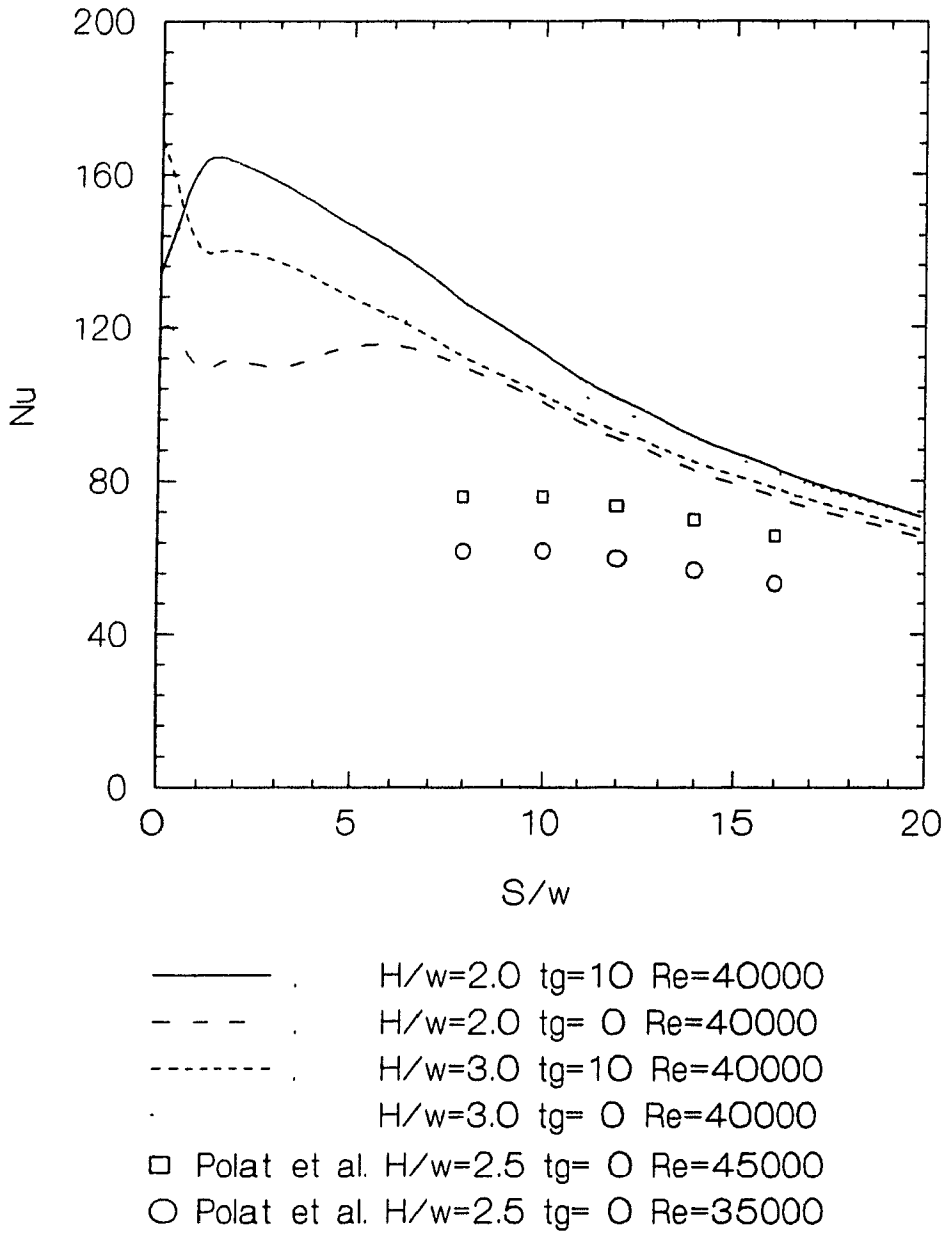

Figure 4.26 Comparison of mean Nusselt number from present study and that of Polat et al. (1991).

from contoured-entry rather than a sharp-edged nozzle. Polat et al. (1991) used a confined slot jet with a nozzle entry contoured to ASME standard specifications. At the same Reynolds number and without additional turbulence generation, the plain sharp edged nozzle produces average heat transfer rates which, over the range of S/w of 8-16 tested by Polat et al. (1991), are 30-65% higher than those for the standard ASME contoured-entry nozzle. This comparison demonstrates the impressive extent to which the turbulence generated by sharp edged nozzles acts to enhance $\overline{Nu}$. Notwithstanding that substantial advantage of plain, sharp-edged nozzles, the summary in table 4.4 shows that at S/w=10 and Re=40000, $\overline{Nu}$ can be increased by a further 21% by the simple expedient of adding a single bar along the nozzle centreline.

Appendix B lists Nu_o and the $\overline{Nu}$ for S/w=5 and S/w=10 for all 64 runs.

4.5 Relation Between Turbulence and Heat Transfer

A prime objective of the present study is the relation between turbulence in the impinging jet flow field and impingement heat transfer rate. For the types of turbulence generation at the nozzle used here, table 4.3 summarizes the development of average turbulence intensity, $\bar{I}$, from the nozzle exit to the approach to the impingement surface. The relationship may now be examined between these measurements of

$\bar{I}$ and the values of percent increase in $\overline{Nu}$ at S/w=10 as represented on fig. 4.25.

As $\bar{I}$ was determined at various axial positions, the choice of axial position is considered first. In the examination of turbulence measurements, section 4.2, it was noted that the development of $\bar{I}$ downstream of the nozzle exit varies greatly with the nature of the turbulence structure at the nozzle exit. For example, from Table 4.3 it was seen that from the nozzle exit to the axial midpoint (position 2), $\bar{I}$ increases greatly from a plain nozzle, but only moderately when there is wire mesh at the nozzle. Thus $\overline{Nu}$ at the impingement surface should not be expected to relate directly nozzle exit $\bar{I}$ or perhaps even to $\bar{I}$ at the midplane.

Ideally, an $\overline{Nu}$-$\bar{I}$ relationship should be based on the value of $\bar{I}$ close to the impingement surface where the heat transfer occurs. Thus it would be logical to examine the $\overline{Nu}$-$\bar{I}$ relationship at the near approach to the impingement surface, axial position 3 or 3*. The relation cannot however be examined with measurements at axial position 3 because of the incompleteness of the data, for the instrumental reasons described earlier. The $\overline{Nu}$-$\bar{I}$ relation can be examined with the data obtained at position 3*, but with the reservation noted earlier because of the substantial lateral component in mean velocity at that axial position. However, as this effect influences values of $\bar{I}$ for all of the data similarly at position 3*, the $\overline{Nu}$-$\bar{I}$ relation may be examined for relative

effects of $\bar{I}$, keeping in mind that the absolute value of $\bar{I}$ in these cases is affected by this measurement limitation.

The $\overline{Nu}$-$\bar{I}$ relation was therefore examined with $\bar{I}$ values from two axial positions; at the midpoint location, position 2, and at position 3* near the impingement surface. With respect to $\overline{Nu}$ values, fig. 4.25 indicated that there is no consistent effect of H/w over the range of 1.0 to 1.5. Therefore the values of $\overline{Nu}$ used for this analysis are the average of the values determined for these two nozzle spacings. The values of $\overline{Nu}$ apply for S/w=10, corresponding to a nozzle area which is 5% of the impingement surface area, i.e. an open area of 5%.

For the three types of turbulence generation - screens, one and three bars - figs 4.27 and 4.28 show that there is a remarkably direct dependence of $\overline{Nu}$ on the value of $\bar{I}$, whether $\bar{I}$ is measured at the near approach to the impingement surface (fig. 4.27) or at the axial midpoint (fig. 4.28). Although the positive $\overline{Nu}$-$\bar{I}$ dependence extends to the limiting case of the plain nozzle if $\bar{I}$ is determined at the near approach to the surface, fig. 4.27, this is not the case for $\bar{I}$ at the midpoint, fig. 4.28. As it was noted in section 4.2 that turbulence intensity increases much more in the region just after the nozzle exit for the plain nozzle, $\bar{I}$ from plain nozzles is unusually high at the midpoint position. This behaviour leads to the very high values of $\bar{I}$ for tg=0 on fig. 4.28. The conclusion is that the $\overline{Nu}$-$\bar{I}$ relation is best used

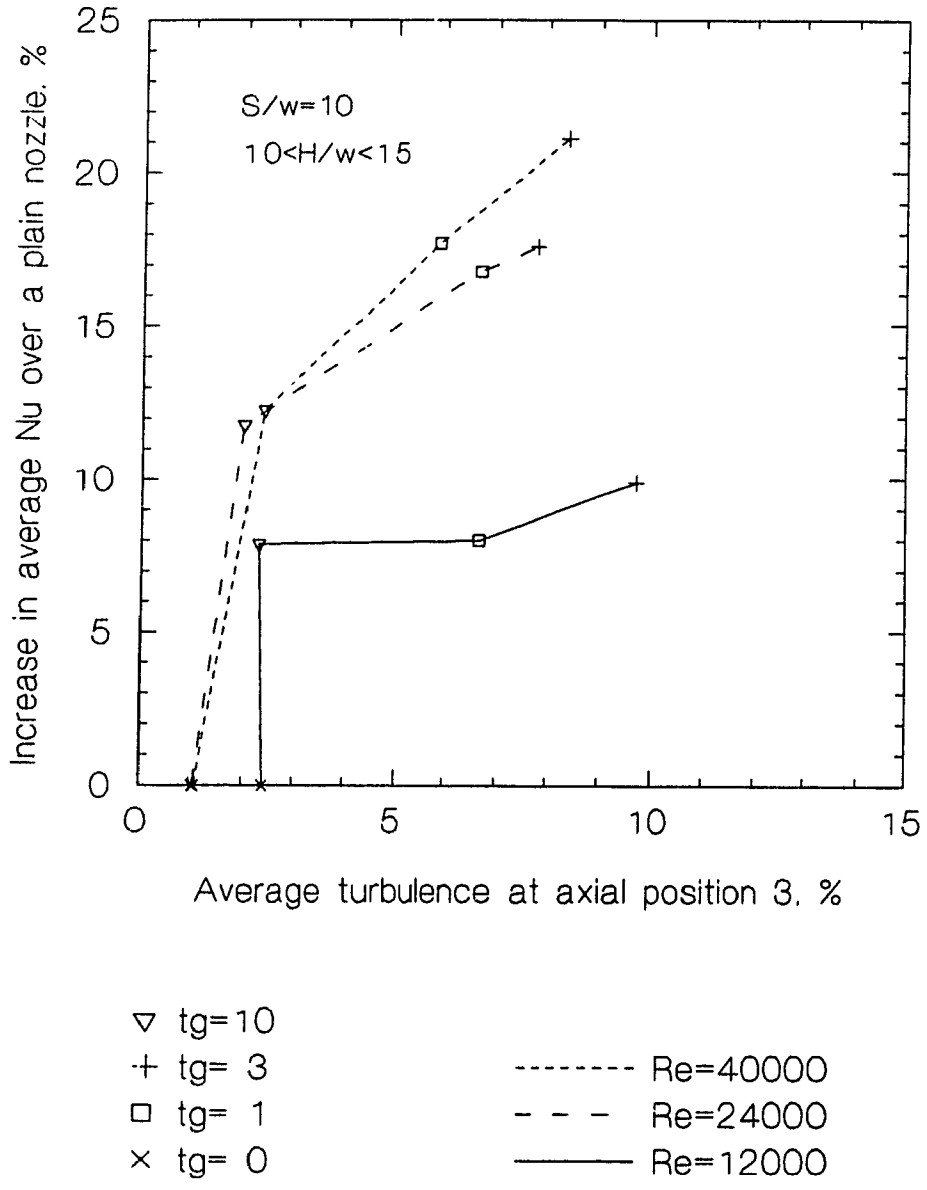

Figure 4.27 $\overline{Nu}$-$\bar{I}$ relation for $\bar{I}$ measuread at the approach to the impingement surface.

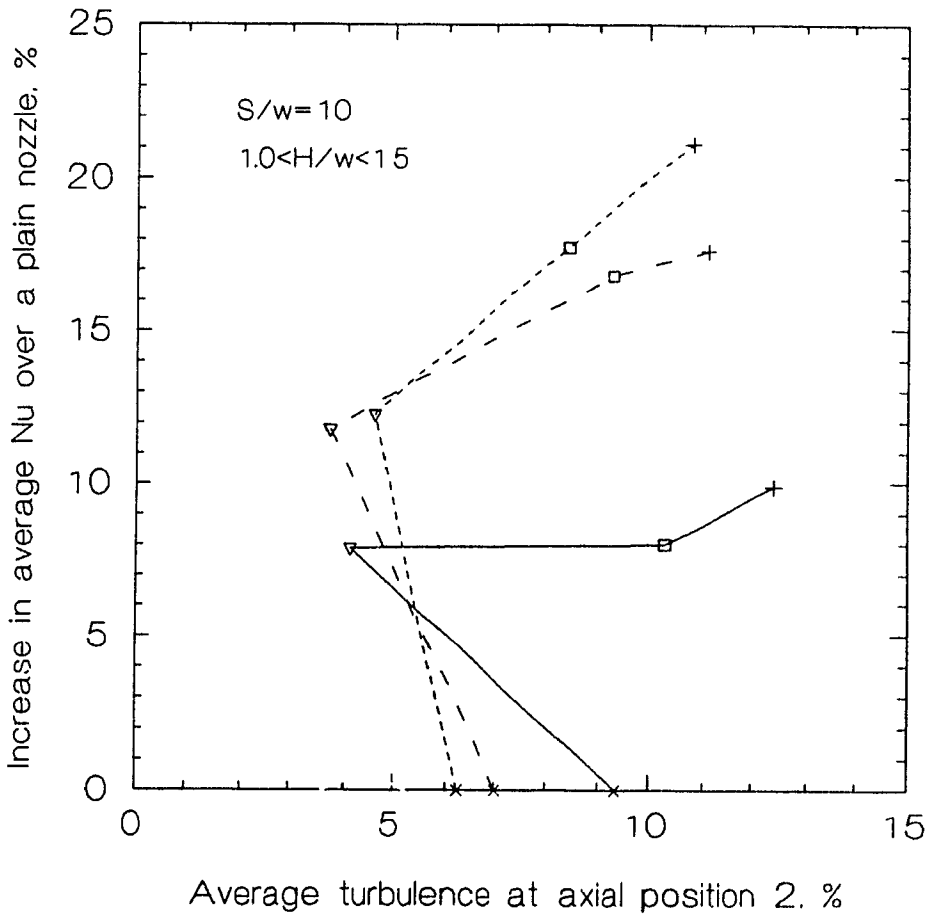

Figure 4.28 $\overline{Nu}$-$\bar{I}$ relation for $\bar{I}$ measuread at the midpoint between the nozzle exit and the impingement surface.

with $\bar{I}$ evaluated at the near approach to the impingement surface, as shown in fig 4.27. Fig. 4.27 further indicates that a change which produces a small increase in $\bar{I}$ near the impingement surface produces a relatively larger increase in $\overline{Nu}$ than changes which produce large increases in $\bar{I}$.

The type of turbulence generation is therefore not a parameter in the $\overline{Nu}$-$\bar{I}$ relationship established by fig. 4.27, as each line includes the results of all three types of turbulence enhancement used, as well as the base case of the plain nozzle without turbulence generation. Thus the variable of mean turbulence, $\bar{I}$, as defined in the present study unifies the data for all four types of nozzle when $\bar{I}$ is determined at the near approach to the impingement surface. Only jet Reynolds number is a parameter, with the $\overline{Nu}$ enhancement increasing with Re, although fig. 4.27 suggests little further increase in this effect above Re=40000.

As experimental studies of turbulence establish that a number of characteristics such as scale and spectrum of turbulence are important, it is impressive to find that a simple parameter, $\bar{I}$, the mean turbulence intensity as defined here, integrates the heat transfer results for all four types of nozzle used. Figure 4.27 shows that the increase of $\overline{Nu}$ with $\bar{I}$ is very nonlinear, with the sensitivity of $\overline{Nu}$ to $\bar{I}$ decreasing as mean turbulence intensity increases. The results of the present study suggest that a potentially large increase in impingement heat transfer rate may be obtained by

turbulence generation, especially in applications for which the higher range of jet Reynolds number is practical.

As the turbulence measurements made in this study were restricted to one-dimensional turbulence intensity, an in-depth documentation of the flow field, a subject for a major investigation in itself, was clearly not intended. None the less it is impressive that the evaluation of average Nusselt number for the four types of nozzle correlate well with the mean intensity of axial turbulence at the approach to the impingement surface, using the empirical definition of mean turbulence intensity defined here.

In developing a correlation between impingement heat transfer and turbulence intensity, the jet Reynolds number effect was divided into two terms, representing separately the Reynolds number dependence of Nusselt number and the coupled effect of Reynolds number and turbulence intensity. The latter is evident from the representation of the results shown in fig. 4.27, and turbulence studies have noted a Reynolds number effect coupled with the turbulence (Bayley and Priddy, 1981) or used the product I*Re as a parameter (Hoogendoorn 1977). The equation obtained here is:

$$\frac{\overline{Nu}_{10}}{Re_j^{0.8}} = 0.0091\,(\bar{I}_3 Re_j)^{0.12} \qquad (4.3)$$

with a correlation $R^2 = 0.991$.

The Nusselt number dependence on Reynolds is given by the 0.8 exponent based on the results of previous turbulent impingement heat transfer studies.

Figure 4.29 shows a plot of the above correlation. Figure 4.30 is a comparison of the measured values of $\overline{Nu}_{10}$ with those calculated using equation 4.3.

Earlier it was noted that most experiments with turbulent impinging jets employ contoured entry nozzles with no jet confinement and large H/w values. In addition, studies of turbulence tend to measure centreline values alone, and correlations are produced relating centreline turbulence to stagnation point Nusselt number, Nu_o. No previous studies have attempted to relate an average jet turbulence intensity with an average Nusselt number. Thus there are no previous results for comparison with the present work.

In his study of heat transfer and turbulence for an unconfined round jet impinging on a flat plate, Hoogendoorn (1977) used a combined turbulence-Reynolds number parameter in the form $I*Re^{0.5}$ for a correlation of stagnation point Nusselt number. By contrast the present study is concerned with an average Nusselt number. Examination of the local and average Nusselt number profiles, figs 4.22 and 4.24, shows that the effect of turbulence generation is greatest in the stagnation region, with the effect decreasing as the area of averaging

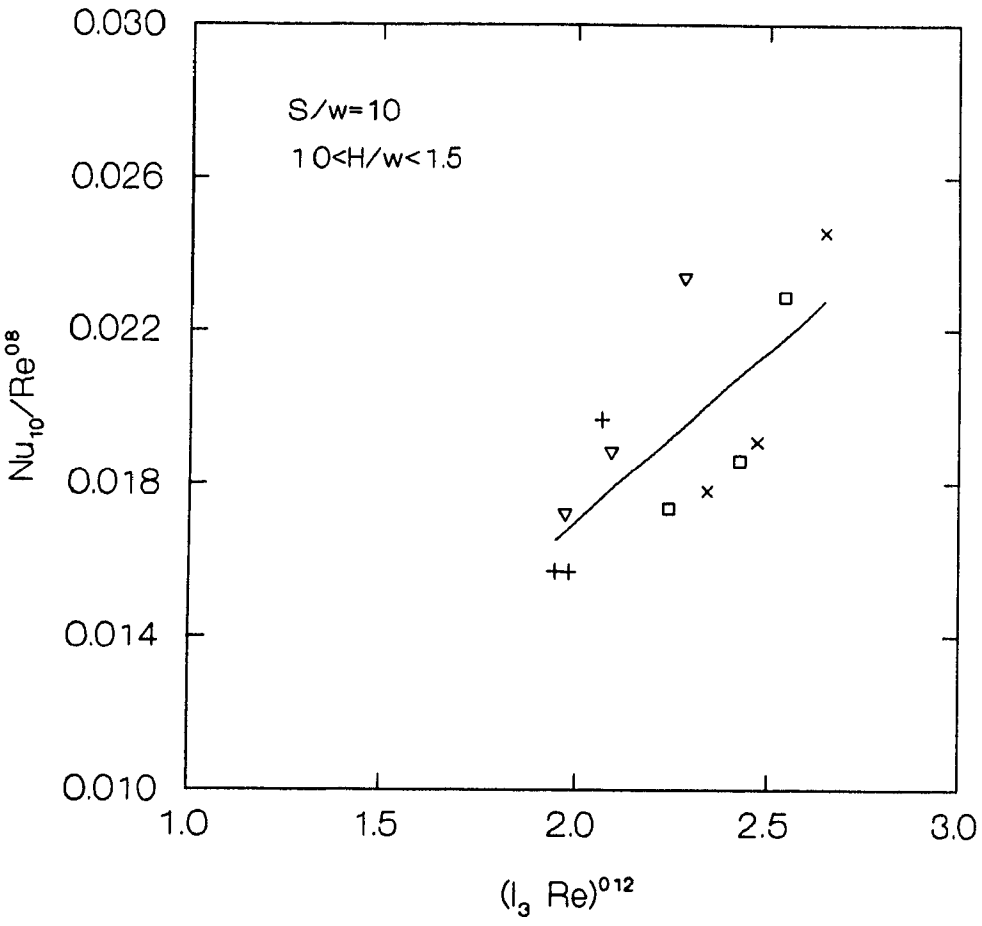

▽ tg=10
\+ tg= 3
□ tg= 1
× tg= 0

Figure 4.29 $\overline{Nu}$-Re-$\overline{I}$ correlation.

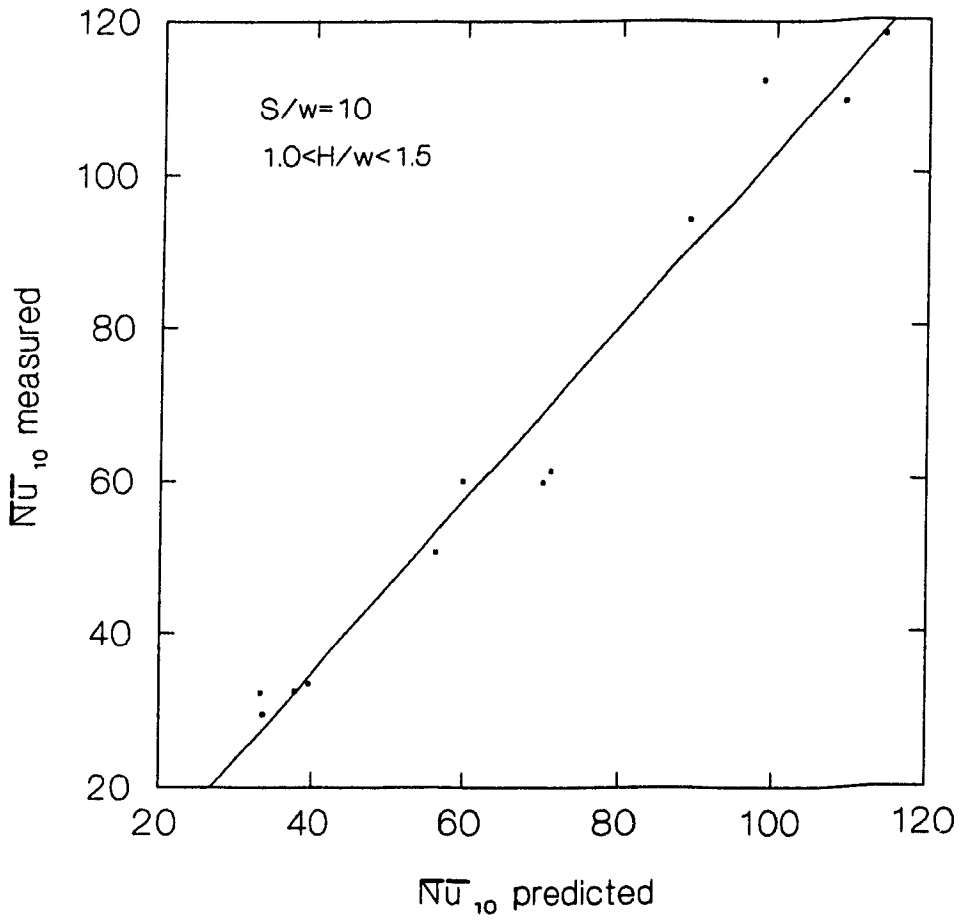

Figure 4.30 Comparison of predicted vs. measured $\overline{Nu}^{10}$.

increases. Therefore it follows that the exponent for $\overline{\text{Re}}$ would be less for $\overline{Nu}_{10}$, integrated for 10w on either side of the nozzle centreline, than for the stagnation value, Nu_o.

4.6 Relation Between Pressure Drop and Heat Transfer

The placing of obstructions in a nozzle to generate increased turbulence will inevitably increase pressure drop. Another objective of the present study was to compare the effectiveness of increasing impingement heat transfer rate in this way with the associated effect of increasing pressure drop. Increased heat transfer rates can be obtained, but at the price of an increased pressure drop which in engineering applications cannot be ignored.

This cost/benefit relationship is shown in figure 4.31. The pressure drop data has been averaged for the largest nozzle at the two highest values of H, 24 and 37 mm. The results are plotted as a comparison between the increase in mean heat transfer rate attained for turbulence enhanced nozzles over the plain nozzle, relative to the increase in pressure caused by the addition of the turbulence generator. The advantages of all of the turbulence generation methods for heat transfer are clearly seen. But it is also apparent that the wire mesh is the least effective method, producing the lowest increase in $\overline{Nu}$ yet at the highest price in increased operating pressure. Figure 4.31 further shows that the 3-bar

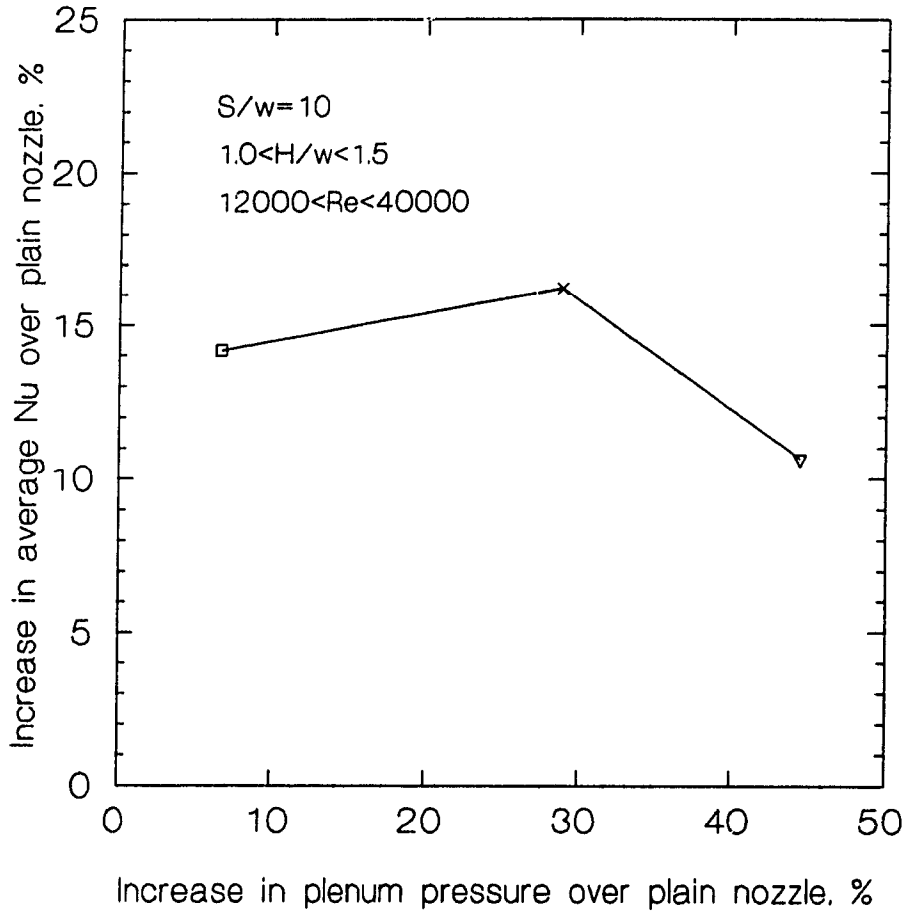

▽ tg=10
× tg= 3
□ tg= 1

Figure 4.31 Nozzle pressure - heat transfer relation for three types of turbulence enhanced nozzle.

turbulence generation gives only a marginally greater increase in impingement heat transfer over the 1-bar alternative, but at the cost of about 4 times the increase in pressure upstream of the nozzle. Of the three types of turbulence enhancement tested the simplest, the single bar, would clearly be the most practical choice, giving a 14% increase in $\overline{Nu}$ at the cost of only about 7% increase in air pressure to the nozzle. Because of the pressure recovery phenomenon discussed in section 4.3, the final increase in pressure would be less than 7%.

In applying this heat transfer enhancement technique to an industrial application such as impingement drying of paper, the average heat transfer rate is a one measure of overall dryer effectiveness. A 10% increase in average impingement heat transfer rate, for example, would lead to a corresponding increase in production capacity for an existing dryer, or to a correspondingly smaller dryer for a specified production rate. On the other hand, the extra cost incurred by increased pressure drop is only one part of the overall operating cost of the dryer. Thus one percentage point increase in pressure drop does not correspond to an equivalent increase in operating costs. Thus in each individual case the economic attractiveness of heat transfer rate enhancement would be a very specific function of such factors as the electrical energy costs for the fan supplying the drying air to the impingement hood, the cost incurred in modifying the nozzle plates for turbulence enhancement, the importance of equipment

cost for a new dryer, and the value of the potential increased production for such a retrofit implementation.

4.7 Summary and Conclusions

A sharp-edged nozzle used here produces much higher average impingement heat transfer rates than does the ASME standard contoured-entry nozzle, the results of which have been documented by numerous authors. The turbulence suppression property of the contoured nozzle produces a low turbulence level flow at the nozzle exit which is counterproductive to high heat transfer rates at the impingement surface.

The addition to a sharp edged slot nozzle of the turbulence generation techniques tested in the present study, i.e. the addition of 1 bar or 3 bars along the length of the nozzle, or a wire mesh over the nozzle, increases the local Nusselt number substantially within the impingement region out to about 4w from the stagnation point. Within the impingement region this increase in local Nu can be in the order of 50%. Farther from the stagnation point the local Nu is unaffected by any change in the flow structure at the nozzle exit.

In the industrial application of heat transfer from impinging jets under a confinement hood, the impingement drying of paper moving at high speed under confined jets is of major commercial importance. Whenever the impingement surface

moves under the jets it is the integrated average Nusselt number, $\overline{Nu}$, which determines the overall heat transfer or drying rate. As the enhancement of local Nu is limited to the impingement region, it follows that the enhancement of $\overline{Nu}$ by turbulence generation at the nozzle exit will decrease with increasing impingement surface width used to compute $\overline{Nu}$. As an impingement surface width, S, of 10w on each side of the nozzle centreline corresponds to 5% nozzle open area, a value in the range possible for industrial impingement dryers of paper, the comparisons were made for values of $\overline{Nu}$ computed at S/w=10.

In the range of nozzle spacing, H/w, of 1.0-1.5, and for an averaging width S/w=10, nozzles with one or three bars give significantly higher enhancement of $\overline{Nu}$ than does #10 mesh screen at the nozzle. For this H/w and S/w, the enhancement in $\overline{Nu}$ given by all nozzles was a function of jet Reynolds number. With one or three bars the enhancement increased from 10% at Re=12000 to 21% at Re=40000. A 10-mesh screen gave only about 2/3 - 3/4 the enhancement in $\overline{Nu}$ that is given by the use of either one or three bars at the nozzle. The lower effectiveness of the screen is consistent with the more rapid decay of the small scale turbulence generated by the 0.66 mm diameter wire of #10 mesh screen than for the larger scale turbulence generated by one 3mm bar or three 1 mm bars.

Turbulence intensity of the jet flow field was found to be a very important variable for the increase in impingement

heat transfer rate. It was found that the use of a single parameter, mean intensity of axial turbulence, $\overline{I}$, integrated the results of mean impingement heat transfer, $\overline{Nu}$, for all four types of nozzles used. This unification of the results was most complete when $\overline{I}$ was evaluated at the near approach to the impingement surface. Thus for each of the three levels of jet Reynolds number used, Re of 12000, 24000 or 40000, the values determined for $\overline{Nu}$ for all four nozzle types used display a smooth trend with $\overline{I}$ as the independent variable. The increase of $\overline{Nu}$ with $\overline{I}$ is quite nonlinear, with the sensitivity of $\overline{Nu}$ to $\overline{I}$ decreasing as mean turbulence intensity increases.

The results are presented in two forms. The percentage increase in mean Nusselt number is provided as a graphical function of mean intensity of turbulence at the three experimental levels of jet Reynolds number, fig. 4.27. Also, an empirical correlation was obtained in the following form:

$$\frac{\overline{Nu}_{10}}{Re^{0.8}} = a\,(\overline{I}_3 Re_j)^n$$

for S/w=10 (5% nozzle open area) and for dimensionless nozzle spacing, H/w, in the range of 1.0 to 1.5. The $Re^{0.8}$ term represents the dependence of Nusselt number for turbulent jets, and the $\overline{I}$Re product reflects the $\overline{I}$-Re coupling observed

experimentally here and the use of this parameter in studies of turbulence. With the mean intensity of turbulence, $\bar{I}$, evaluated near the impingement surface the following correlation parameters were determined:

$a = 0.0091$, $n = 0.12$

with a very satisfactory statistical fit to the experimental data.

The effectiveness of increasing impingement heat transfer rate by turbulence enhancement at the jet nozzle is achieved at an increased operating cost for the higher pressure drop associated with the presence of turbulence generators. Analysis of the results showed that the #10 wire mesh screen would be the poorest practical choice, as it gives the lowest heat transfer enhancement but the highest increase in the pressure upstream of the nozzle. Of the other two turbulence generation techniques tested, the 3-bar nozzle produced marginally higher heat transfer rate than the 1-bar nozzle, but at the cost of about 4 times the increase in upstream pressure. For S/w=10, or 5% nozzle open area, the single bar nozzle provided a 14% increase in $\overline{Nu}$ for only a 7% increase in pressure in the nozzle, while the actual increase in pressure would be lower yet due to the pressure recovery phenomenon for confined impinging jets. Therefore, of the three types of turbulence generation tested, the simplest one, the nozzle with a single bar, has the best cost/benefit performance and would be the practical choice.

References

Bayley F.J., and Milligan R.W., The effect of free stram turbulence upon heat transfer to turbine blading. AGARD PEP Conference on High Temperature Problems in Gas Turbine Engines, Paper No. 37, (1977).

Bayley F.J., and Priddy W.J., Effects of free stream turbulence intensity and frequency on heat transfer to turbine blading. J. Eng. Power, Trans ASME, 103, 7, (1981), 60-64.

Cadek F.F., A Fundamental Investigation of Jet Impingement Heat Transfer. Ph.D. Thesis, University of Cincinnati, (1968).

Chance J.L., Experimental investigation of air impingement heat transfer under an array of round jets. Tappi 57, 6, (1974), 108-112.

Chen G., Impingement Heat Transfer with Re-entry Channel Nozzles. M.Eng. Thesis, McGill University, (1989).

Comings E.W., Clapp J.T., Taylor J.F., Air Turbulence and Transfer Processes. Ind. Eng. Chem., 40, 6, (1948), 1076-1082.

Gardon R. and Akfirat J.C., The Role of Turbulence in Determining the Heat Transfer Characteristics of Impinging Jets. Int. J. Heat Mass Transfer 8, (1965), 1261-1272.

Gardon R. and Akfirat J.C., Heat Transfer Characteristics of Impinging Two Dimensional Jets. J. Heat Transfer, Trans. ASME, 88, (1966), 101-108.

Gauntner J.W., Livingood J.N.B., Hrycak P., Survey of Literature on Flow Characteristics of a Single Turbulent Jet Impinging on a Flat Plate, NASA Technical Note TN-5652, (1970).

Gutmark E., Wolfshtein M., Wygnanski I., The plane turbulent Impinging Jet. J. Fluid Mechanics, 88, 4, (1978), 737-756.

Groth J. and Johansson A.V., Turbulence Reduction by Screens. J. Fluid Mech. 197, (1988), 139-155.

Hardisty H. and Can M., An Experimental Investigation into the Effects of Changes in the Geometry of a Slot Nozzle on the Heat Transfer Characteristics of an Impinging Air Jet. Proc. Inst. Mech. Eng. 197, (1983) 7-13.

Hinze J.O., Turbulence, McGraw-Hill, New York (1975).

Hoogendoorn C.J., The Effect of Turbulence on Heat Transfer at a Stagnation Point. Int. J. Heat Mass Transfer 20, (1977) 1333-1338.

Huang B., Heat Transfer Under an Inclined Slot Jet Impinging on a Moving Surface. Ph. D. Thesis, McGill University, (1988).

Kestin J., The effect of Free-stream turbulence on heat transfer rates. Advances in Heat Transfer, 3, (1966)

Korger M., and Krizek F., Mass transfer coefficient in impingement flow from slotted jets. Int. J. Heat Mass Transfer 9, (1966), 337-344.

Inoue S., Eguchi K., Imamoto T, Development of High Thermal Efficiency Impinging Jet Nozzle for Hot Air Drying of Gravure Printing. J. Chem. Eng. Japan 21, 6, (1988) 569-575.

ISO, Measurement of Fluid Flow in Closed Conduits, ISO Handbook #15, International Standards Organization, Switzerland (1983).

Kataoka K., Hrada T., Sahara R., Mechanism for enhancement of Heat transfer in turbulent impinging jets. Current Res. Heat Mass Transfer (1986), 81-96.

Kataoka K., Mihata I., Maruo K., Suguro M., and Chigusa T., Quasi-Periodic Large Scale Structure Responsible for the Selective Enhancement of Impinging Jet Heat Transfer, Proc. Eighth Intnatl. Heat Transfer Conf., (1986).

Maisel D.S., and Sherwood T.K., Evaporation of liquids into turbulent gas streams. Chem. Eng. Progress 46, 3, (1950), 131-138.

Maisel D.S., and Sherwood T.K., Effect of air turbulence on rate of evaporation of water. Chem. Eng. Progress 46, 4, (1950), 172-175.

Martin H., Heat and Mass Transfer Between impinging Gas Jets and Solid Surfaces. Advances in Heat and Mass Transfer 13 (1977).

Obot N.T., Flow and Heat Transfer for Round Turbulent Jets Impinging on Permeable and Impermeable Surfaces. Ph.D. thesis, McGill University, (1980).

Obot N.T., Mujumdar A.S., Douglas W.J.M., Design Correlations for Heat and Mass Transfer Under Various Turbulent Impinging Jet Configurations, Drying '80, Vol1: Developments in Drying. Hemisphere Publishing Corp, (1988) 388-402.

Perry A.E., Hot-wire Anemometry, Oxford University Press, Oxford, (1982).

Polat S., Transport Phenomena Under Jets Impinging on a Moving

Surface with Throughflow. Ph.D. Thesis, McGill University, (1988).

Polat S., Mujumdar A.S., Douglas W.J.M., Impingement Heat Transfer Under a Confined Slot Jet. Part I: Effect of Surface Throughflow, Can. J. Chem. Eng. 69, (1991), 266-273.

Polat S., Mujumdar A.S., Douglas W.J.M., Impingement Heat Transfer Under a Confined Slot Jet. Part II: Effects of Surface Motion and Throughflow, Can. J. Chem. Eng. 69, (1991), 274-280.

Roach P.E., The Generation of Nearly Isotropic Turbulence by Means of Grids. Heat and Fluid Flow (1986) 82-92.

Saad N.R., Flow and Heat Transfer for Multiple Turbulent Impinging Slot Jets. Ph.D. thesis, McGill University (1981).

Saad N.R., Mujumdar A.S., Douglas W.J.M., Heat Transfer Under Multiple Slot Jets Impinging on a Flat Plate, Drying '80, Vol1: Developments in Drying. Hemisphere Publishing Corp, (1988) 422-430.

Van Dressar N.T., Mayle R.E., Stagnation Transfer Rates for Incident Flow with High Turbulence Intensities. Symposium on Fundamentals of Forced Convection Heat Transfer, ASME (1988)

VanFossen G.J., Simoneau R.J., A Study of the Relationship Between Free-stream Turbulence and Stagnation Region Heat Transfer. NASA Conference Publication 2386 (1984).

van Heiningen A.R.P., Heat Transfer Under an Impinging Slot Jet. Ph.D. Thesis, McGill University (1982).

Wedel G.L., Air Impingement Heat Transfer. Tappi 63 8 (1980) 89-92.

Yokobori S., Kasagi N., Hirata M., Nishwaki N., Role of Large Scale Eddy Structure on Enhancement of Heat Transfer in Stagnation Region of Two-Dimensional, Submerged, Impinging Jet. 6th International Heat Transfer Conference (1978) 305-310.

Appendix A Heat Flux Sensor Construction and Calibration

A.1 Sensor Construction

A new fast response heat flux sensor was constructed following techniques described by van Heiningen (1982) and Polat (1988).

The material chosen for the sensor substrate was Macor, a machinable fluorine based ceramic from Corning. The substrate was prepared by machining a piece to the dimensions of a slot which had been machined in the impingement cylinder. The top surface of the substrate was polished with silicone/carborundum.

The sensor was made by vacuum depositing gold onto the substrate using a mask of a straight line, 1mm wide by 80mm long. Several depositions were attempted using 0.116g of 99.99% pure gold until a sensor with a resistance of approximately 180 ohms was produced.

The sensor was aged in an oven at 110°C until a stable resistance was acheived, after 10 days of heat treatment.

For the heat transfer calculations, the following thermal properties for Macor were obtained from Corning:

THERMAL CONDUCTIVITY

1.29 W/m °K (constant over the experimental temperature range)

HEAT CAPACITY

$755.6 + 1.05(T) - 0.00105(T)^2$ J/kg °K

DENSITY

2520 kg/m^3 (constant over the experimental temperature range)

A.2 Calibration

The final calibration of the sensor was conducted in situ. The sensor was with the mounted with the sensor surface level with that of the impingement cylinder. A bead of RTV silicone was used to cement the sensor in place eliminate flow discontinuities between the impingement surface and that of the sensor.

The sensor was connected data acquisition equipment. An E-type thermocouple was mounted on the impingement cylinder surface so that the bead was centred approximately 1mm above the sensor. The sensor was located at the centre of the heated jet and the resistance was monitored as the jet temperature was increased.

The sensor was calibrated by measuring resistance (R) versus temperature (T) several times during the course of the experiments. A typical calibration curve is shown in fig A.1 All of the calibration curves obtained were linear, with a slope of 0.244 ohms/°C. The intercepts for the curves were different as the base resistance changed slightly over time. The room temperature resistance was measured and used with the slope of the calibration equation to produce the conversion equation for the day's experiments.

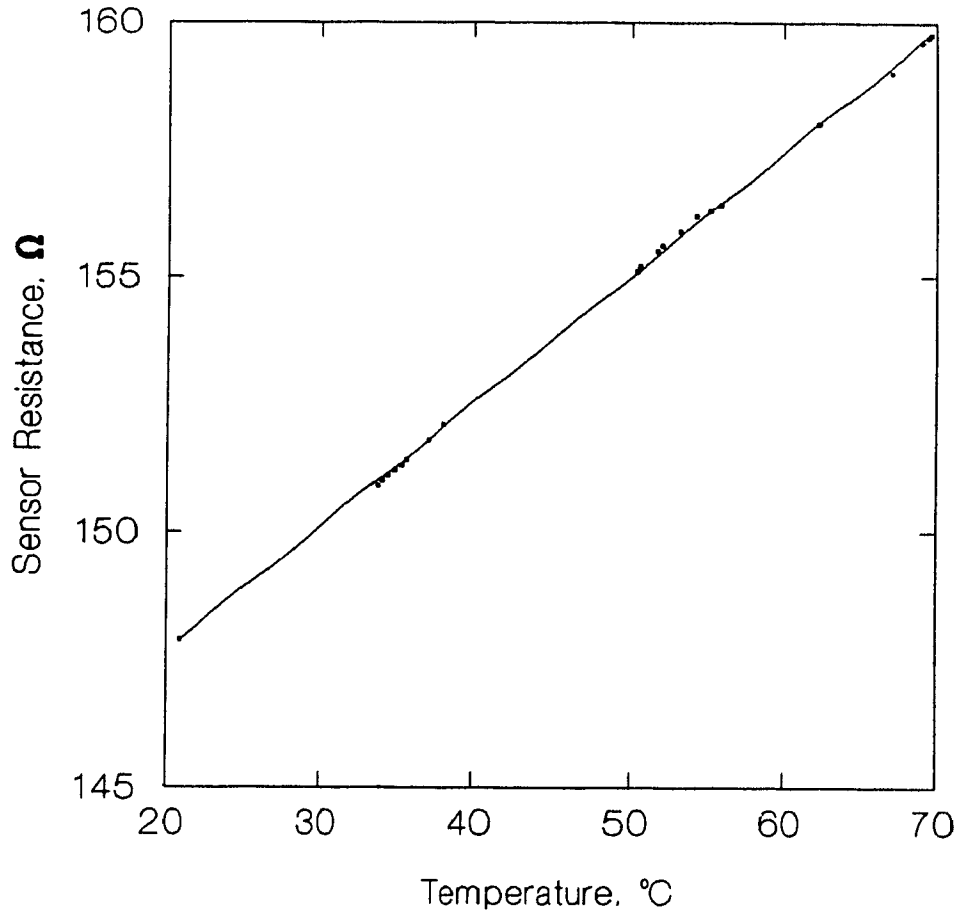

Figure A.1 Heat flux sensor calibration curve.

Appendix B Pressure, Turbulence, and Heat Transfer data for all Experiments.

H	w	tg	Re_j Nom	Re_j HT	Re_j TI	P_j HT	P_j TI	I_1	I_2	I_3	Nu_0	Nu_5	Nu_{10}
12	6	0	24000	24167	24010	32.70	36.40	1.65	.	.	39.00	56.14	50.08
12	6	0	12000	12692	12129	8.00	8.59	2.34	.	.	33.37	32.69	29.01
12	6	10	24000	24033	24486	28.30	30.10	1.01	.	.	88.63	64.35	51.54
12	6	10	12000	12239	12110	8.90	6.21	0.80	.	.	45.68	36.53	27.95

H	w	tg	Re_j Nom	Re_j HT	Re_j TI	P_j HT	P_j TI	I_1	I_2	I_3	Nu_0	Nu_5	Nu_{10}
12	12	0	40000	39841	40360	24.20	27.10	1.40	.	.	72.74	113.71	102.54
12	12	0	24000	24106	24296	8.90	10.00	1.52	.	.	51.64	53.47	50.94
12	12	0	12000	12736	12126	2.10	2.60	1.58	.	.	40.06	26.00	23.93
12	12	10	40000	40249	40428	28.00	28.91	1.54	.	.	119.25	125.78	100.58
12	12	10	24000	24171	24261	11.60	11.21	1.69	.	.	75.93	75.34	58.06
12	12	10	12000	12725	11876	2.90	3.21	1.98	.	.	56.24	40.04	30.24

H	w	tg	Re_j Nom	Re_j HT	Re_j TI	P_j HT	P_j TI	I_1	I_2	I_3	Nu_0	Nu_5	Nu_{10}
12	25	0	40000	38297	40234	12.00	11.60	1.81	.	.	75.84	106.26	98.94
12	25	0	24000	23445	24227	4.60	4.20	0.97	.	.	60.54	53.98	48.89
12	25	0	12000	12329	12330	1.50	1.20	1.76	.	.	48.54	32.96	28.39
12	25	1	40000	38827	40048	13.20	13.00	3.33	.	.	110.79	137.50	112.96
12	25	1	24000	23476	24168	5.20	5.21	1.71	.	.	61.22	74.39	59.25
12	25	1	12000	12381	12095	1.30	1.20	3.76	.	.	49.24	41.57	32.64
12	24	3	40000	39169	40307	12.40	13.60	4.38	.	.	155.74	166.53	132.55
12	24	3	24000	25844	24321	5.90	4.30	10.48	.	.	87.21	81.78	62.76
12	24	3	12000	12536	12127	1.00	1.40	7.57	.	.	62.78	44.98	34.37
12	25	10	40000	40176	40575	14.40	13.70	5.50	.	.	130.32	160.70	131.41
12	25	10	24000	24133	23669	5.40	5.00	5.46	.	.	82.54	82.93	64.91
12	25	10	12000	12766	12126	1.20	1.50	6.93	.	.	56.27	41.40	32.07

H	w	tg	Re_j Nom	Re_j HT	Re_j TI	P_j HT	P_j TI	I_1	I_2	I_3	Nu_0	Nu_5	Nu_{10}
24	12	0	40000	39791	40428	28.80	24.40	2.34	.	5.24	74.34	126.03	110.95
24	12	0	24000	23997	24190	10.10	8.00	1.51	.	5.94	52.99	59.60	55.94
24	12	0	12000	12659	12081	2.80	2.31	1.16	.	7.01	42.09	31.03	29.17
24	12	10	40000	39391	40566	30.80	25.79	2.66	.	3.23	107.59	133.33	105.60
24	12	10	24000	23891	23915	12.30	9.00	2.38	.	3.09	68.29	75.18	59.92
24	12	10	12000	12680	11902	3.00	2.60	2.06	.	3.07	49.61	37.79	30.72

H	w	tg	Re_j Nom	Re_j HT	Re_j TI	P_j HT	P_j TI	I_1	I_2	I_3	Nu_0	Nu_5	Nu_{10}
24	25	0	40000	39729	39997	7.20	6.80	1.26	.	0.78	90.86	108.96	91.18
24	25	0	24000	24811	24181	2.80	2.60	1.01	.	0.74	69.45	59.68	51.56
24	25	0	12000	12625	12058	0.50	0.69	1.51	.	1.00	52.96	33.87	29.77
24	25	1	40000	39733	40414	8.50	7.60	3.26	.	5.54	120.08	144.47	106.93
24	25	1	24000	24813	24443	3.00	2.90	2.66	.	5.02	89.33	78.98	59.52
24	25	1	12000	12616	12115	0.40	1.00	2.95	.	4.87	61.63	39.89	32.36
24	24	3	40000	39743	40190	10.00	10.00	4.13	.	8.27	124.90	149.25	110.15
24	24	3	24000	24091	24256	3.60	3.81	3.32	.	7.46	89.35	79.89	59.81
24	24	3	12000	12702	12126	0.80	1.31	3.87	.	10.21	58.63	42.40	33.42
24	25	10	40000	39998	40003	10.20	10.00	3.18	.	2.22	131.61	136.63	100.60
24	25	10	24000	23863	24145	3.70	5.99	3.07	.	2.08	92.01	73.88	56.02
24	25	10	12000	12626	12114	0.90	0.81	3.86	.	2.37	67.03	39.21	31.95

H	w	tg	Re_j Nom	Re_j HT	Re_j TI	P_j HT	P_j TI	I_1	I_2	I_3	Nu_0	Nu_5	Nu_{10}
37	12	0	40000	39377	40499	28.80	25.00	1.92	6.84	8.20	78.76	125.27	107.43
37	12	0	24000	24814	24288	11.00	8.99	1.69	7.83	9.52	58.63	69.92	59.72
37	12	0	12000	12558	11590	2.60	2.00	0.86	9.63	10.40	46.94	34.69	29.80
37	12	10	40000	38876	39992	32.30	29.50	3.66	5.23	6.19	106.62	128.64	102.29
37	12	10	24000	24578	24129	12.20	11.70	2.97	5.27	6.47	71.17	74.55	59.72
37	12	10	12000	12564	12066	2.70	2.50	3.27	5.18	6.36	52.03	34.91	29.06
37	12	18	40000	.	40401	.	38.31	3.02	4.24	4.26	.	.	.
37	12	18	24000	.	24034	.	14.21	2.50	4.80	4.47	.	.	.
37	12	18	12000	.	12184	.	3.80	2.67	4.41	4.71	.	.	.

H	w	tg	Re_j Nom	Re_j HT	Re_j TI	P_j HT	P_j TI	I_1	I_2	I_3	Nu_0	Nu_5	Nu_{10}
37	18	0	40000	39205	40127	17.00	11.61	3.31	10.17	5.57	79.39	115.37	100.90
37	18	0	24000	23940	24123	6.40	4.30	2.82	9.48	5.18	58.24	54.30	50.65
37	18	0	12000	12661	12069	1.60	1.19	1.43	9.45	6.19	48.10	30.53	28.52
37	18	10	40000	40292	40104	17.00	14.80	3.47	4.28	2.88	115.80	146.50	113.59
37	18	10	24000	24771	23915	5.10	5.60	3.24	3.94	2.96	78.23	76.61	61.40
37	18	10	12000	12573	11937	1.00	1.90	4.55	5.15	3.37	60.90	38.24	32.08

H	w	tg	Re_j Nom	Re_j HT	Re_j TI	P_j HT	P_j TI	I_1	I_2	I_3	Nu_0	Nu_5	Nu_{10}
37	25	0	40000	39404	40124	6.90	6.00	2.09	6.22	1.37	96.12	112.20	93.01
37	25	0	24000	23799	24236	2.50	4.00	1.52	7.01	1.37	70.94	57.45	51.32
37	25	0	12000	12608	12327	0.60	0.91	1.85	9.35	3.79	51.51	33.86	30.42
37	25	1	40000	39290	40114	7.80	6.80	3.88	8.43	6.22	141.76	152.36	109.77
37	25	1	24000	23860	23821	2.80	2.60	3.56	9.30	8.25	97.47	79.08	60.61
37	25	1	12000	12629	12081	0.60	1.00	4.29	10.29	8.49	67.77	40.16	32.77
37	24	3	40000	40229	40161	9.10	8.00	6.95	10.81	8.51	144.74	152.80	111.98
37	24	3	24000	23950	24369	3.60	3.00	6.18	11.15	8.06	101.11	79.96	61.15
37	24	3	12000	12666	12149	1.00	0.40	5.44	12.44	9.18	68.41	40.29	32.62
37	25	10	40000	39880	40238	9.60	6.00	3.55	4.56	2.53	129.53	144.15	105.97
37	25	10	24000	23835	23863	3.60	7.00	3.31	3.71	1.89	92.45	74.45	58.96
37	25	10	12000	12785	11951	0.80	1.00	3.47	4.15	2.24	65.74	39.59	32.96

Appendix C. Local (left) and average (right) Nusselt number profiles for all experiments.

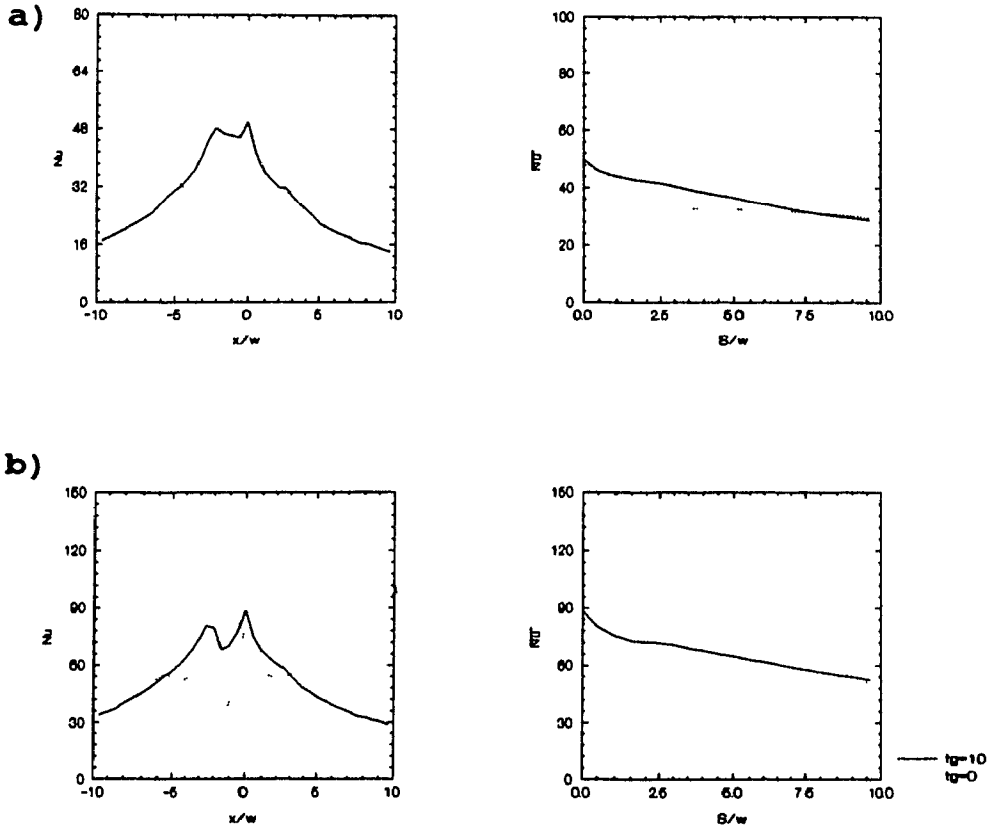

Figure C.1. Profiles of local and average Nu for H=12mm, w=6mm:
a) Re_j=12000; b) Re_j=24000.

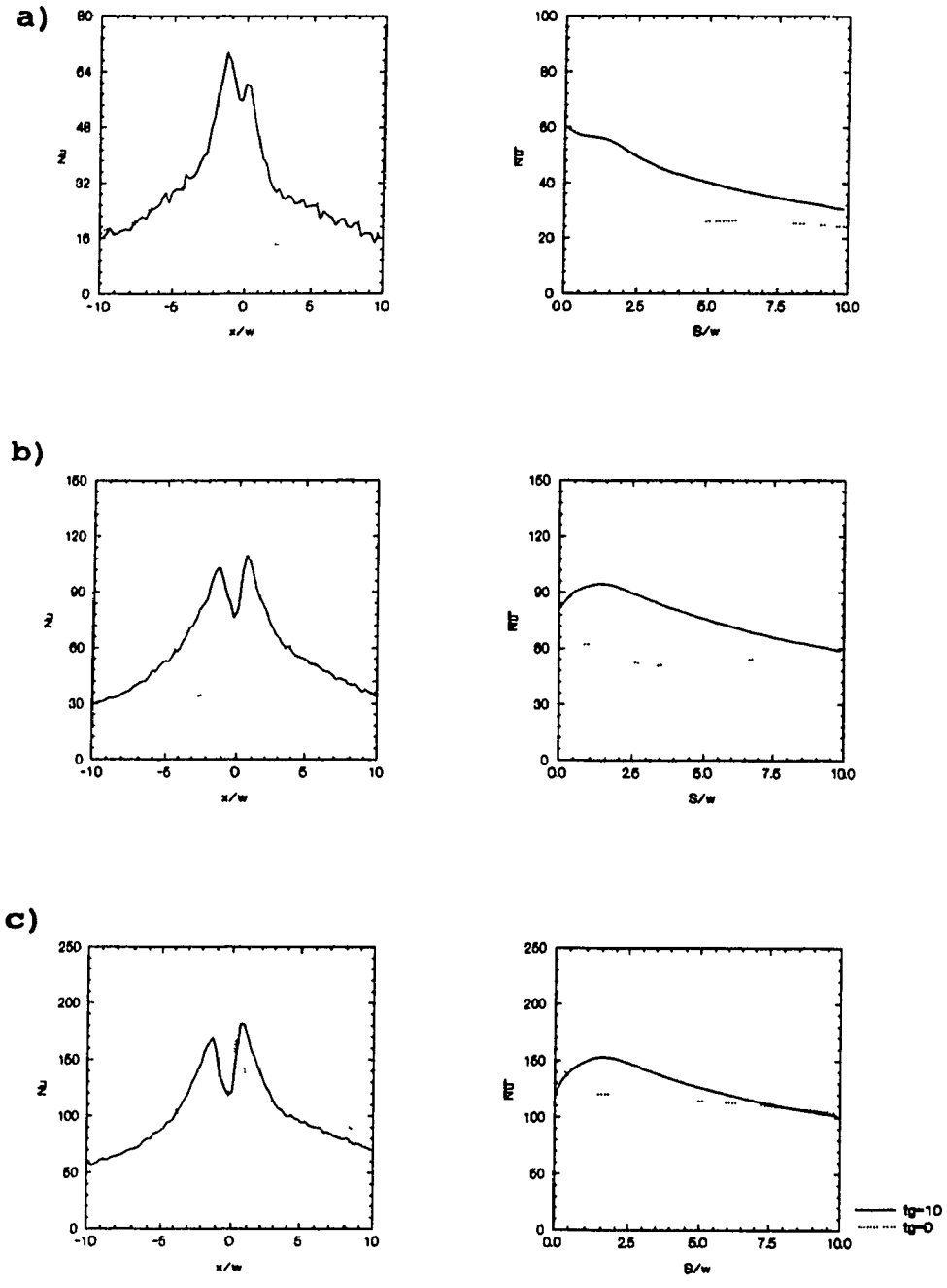

Figure C.2 Profiles of local and average Nu for H=12mm, w=12mm:a) Re_j=12000; b)Re_j=24000; c) Re_j=40000.

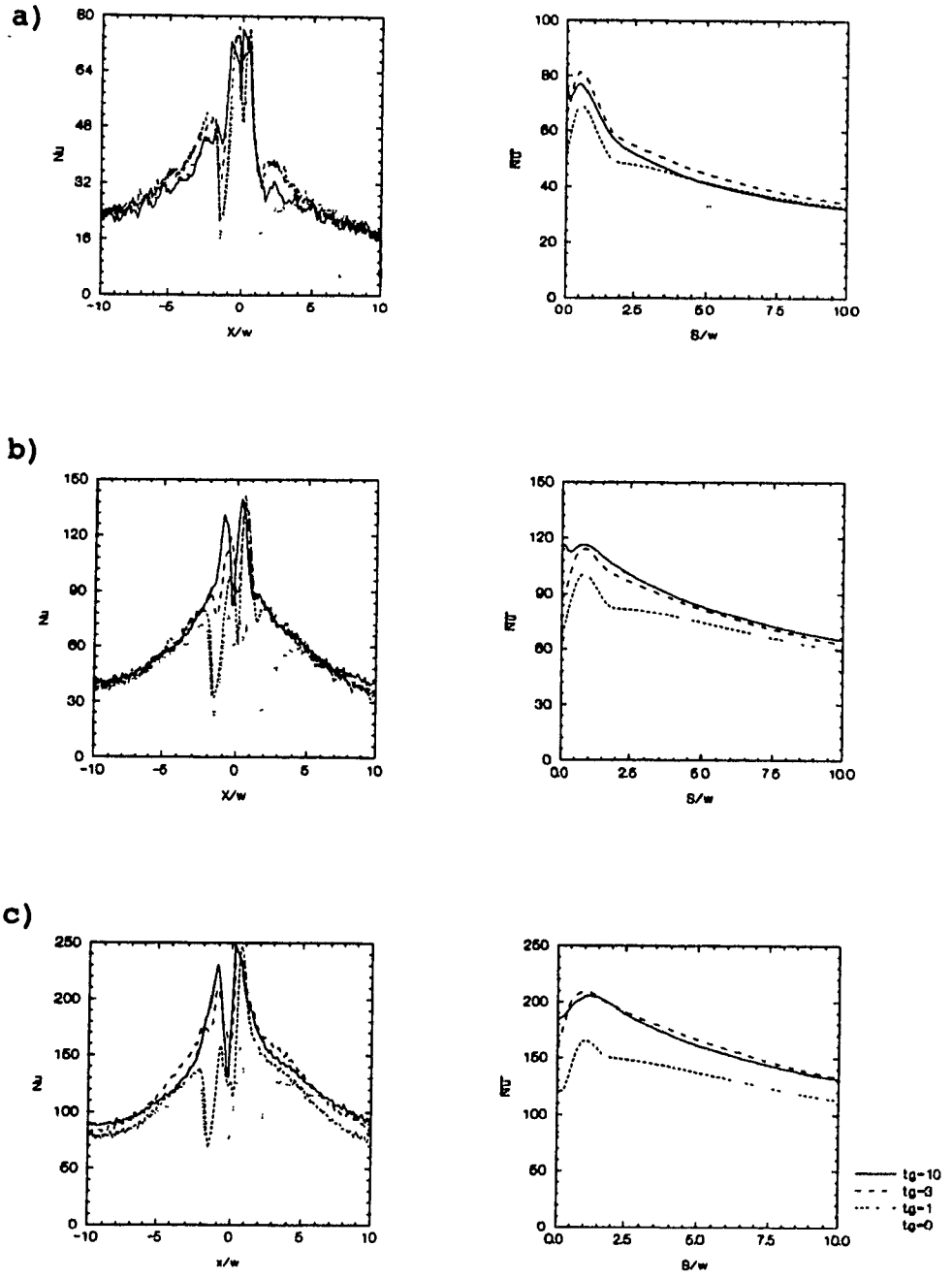

Figure C.3 Profiles of local and average Nu for H=12mm, w=25mm: a) Re_j=12000; b)Re_j=24000; c) Re_j=40000.

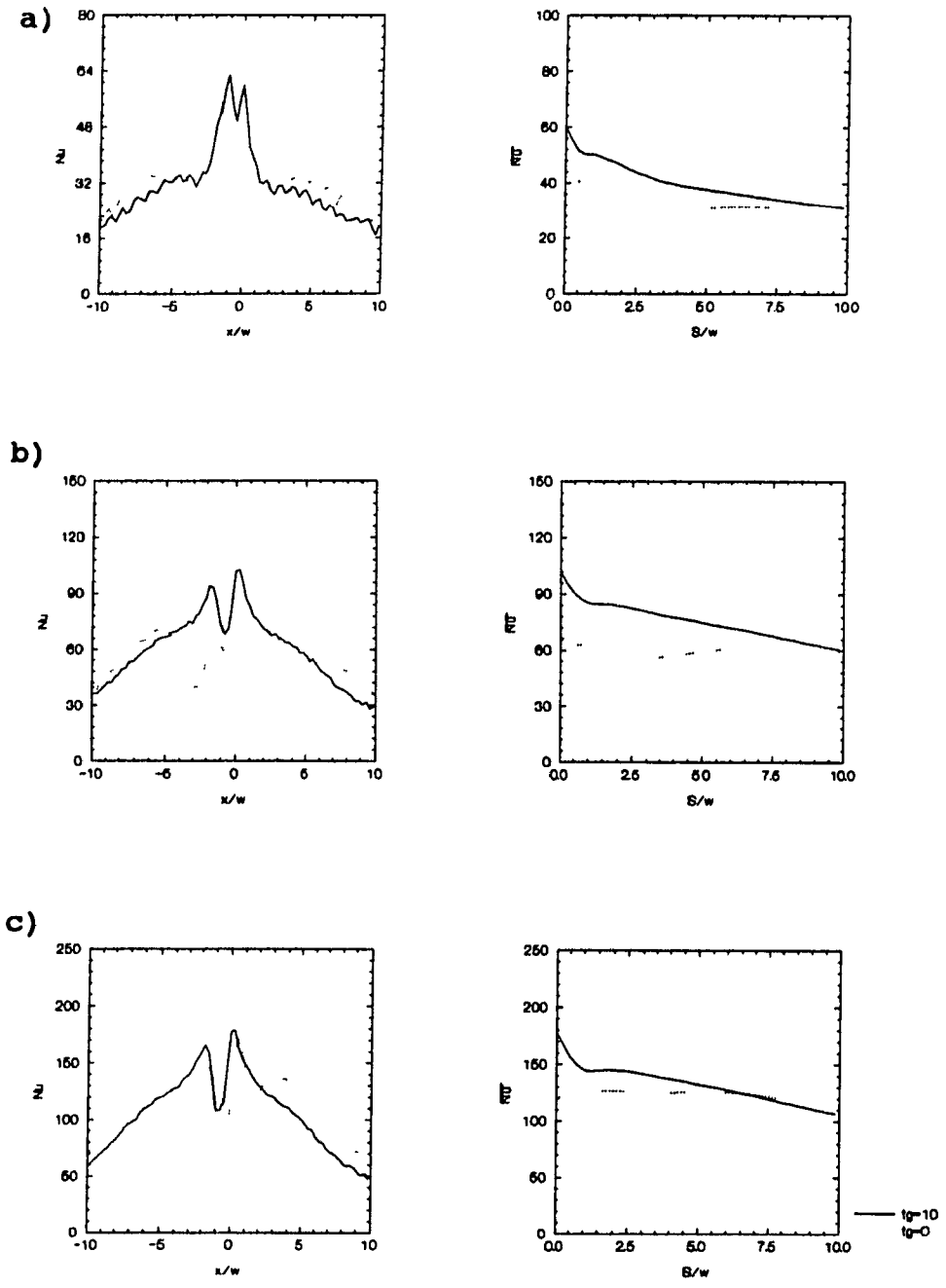

Figure C.4 Profiles of local and average Nu for H=24mm, w=12mm: a) Re_j=12000; b)Re_j=24000; c) Re_j=40000.

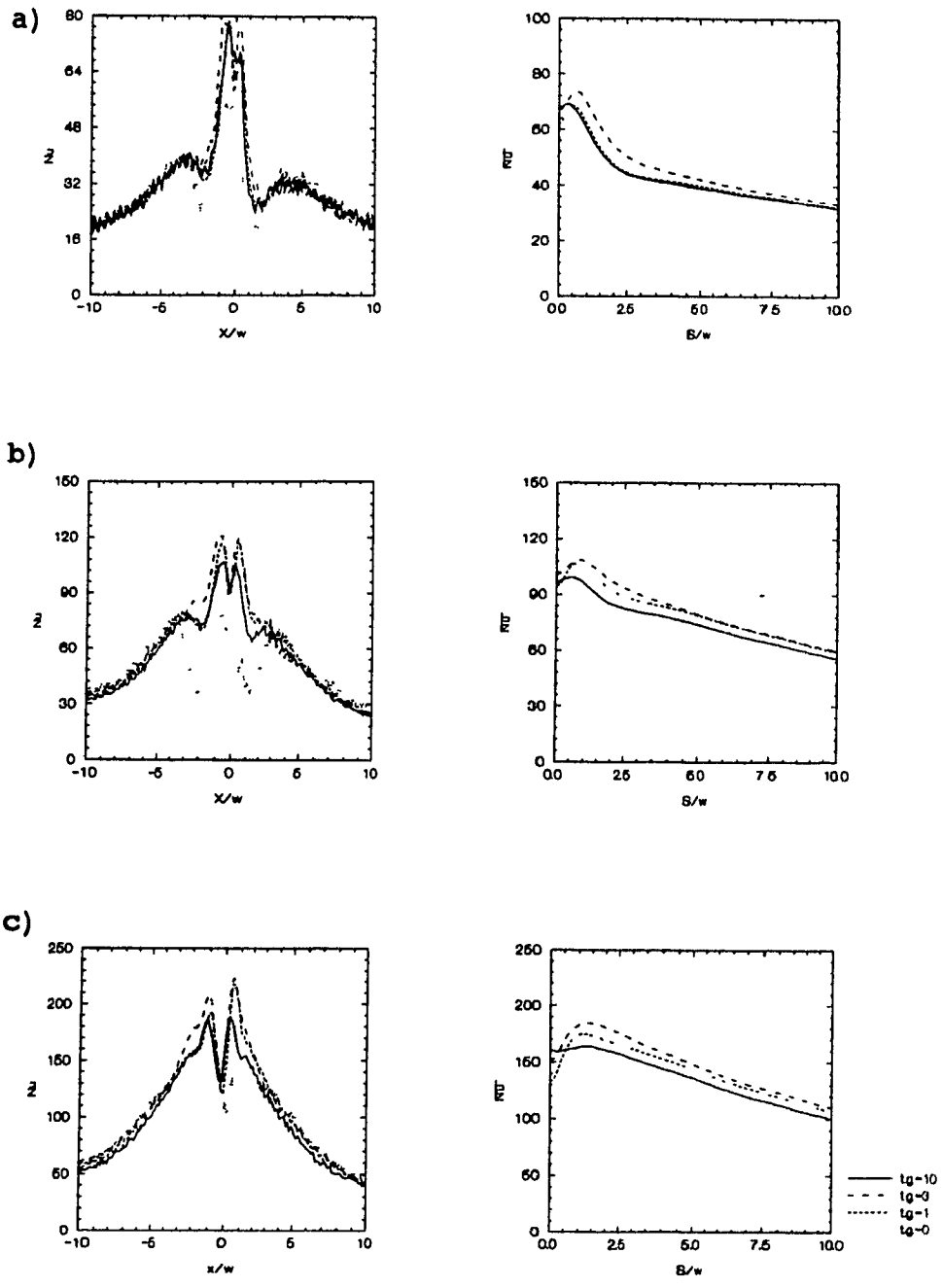

Figure C.5 Profiles of local and average Nu for H=24mm, w=25mm: a) Re_j=12000; b)Re_j=24000; c) Re_j=40000.

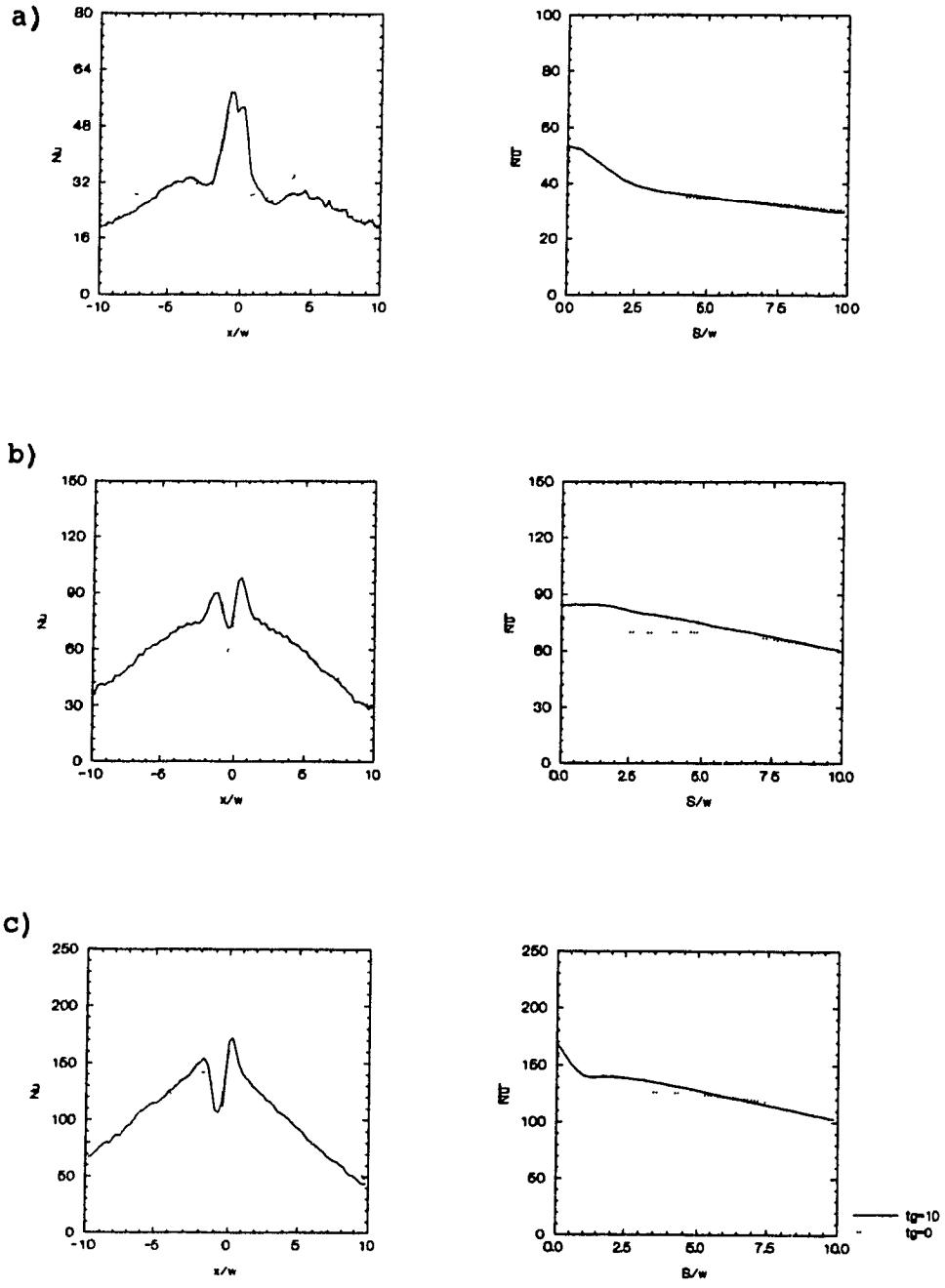

Figure C.6 Profiles of local and average Nu for H=37mm, w=12mm: a) Re_j=12000; b)Re_j=24000; c) Re_j=40000.

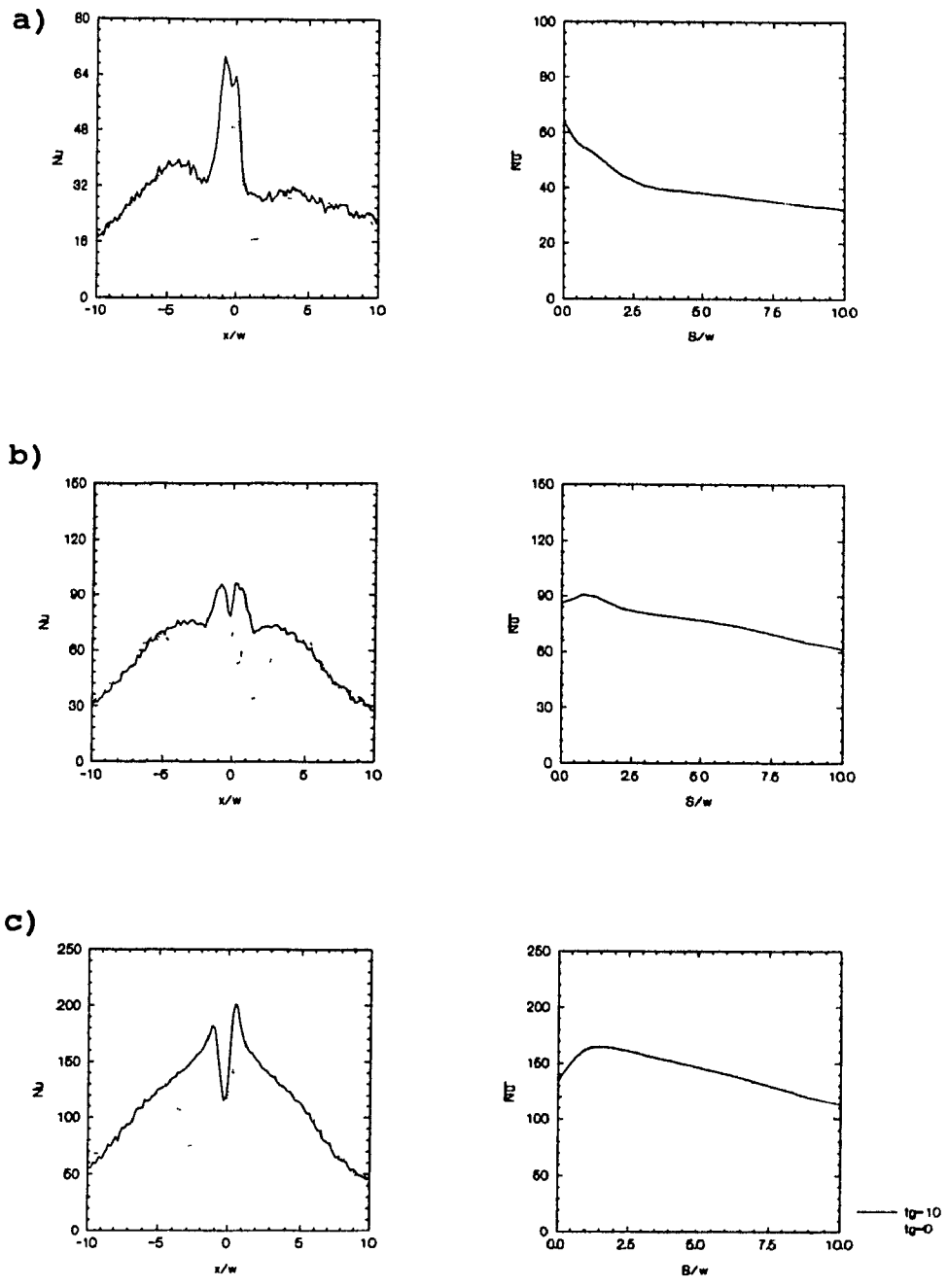

Figure C.7 Profiles of local and average Nu for H=37mm, w=18mm: a) Re_j=12000; b) Re_j=24000; c) Re_j=40000.

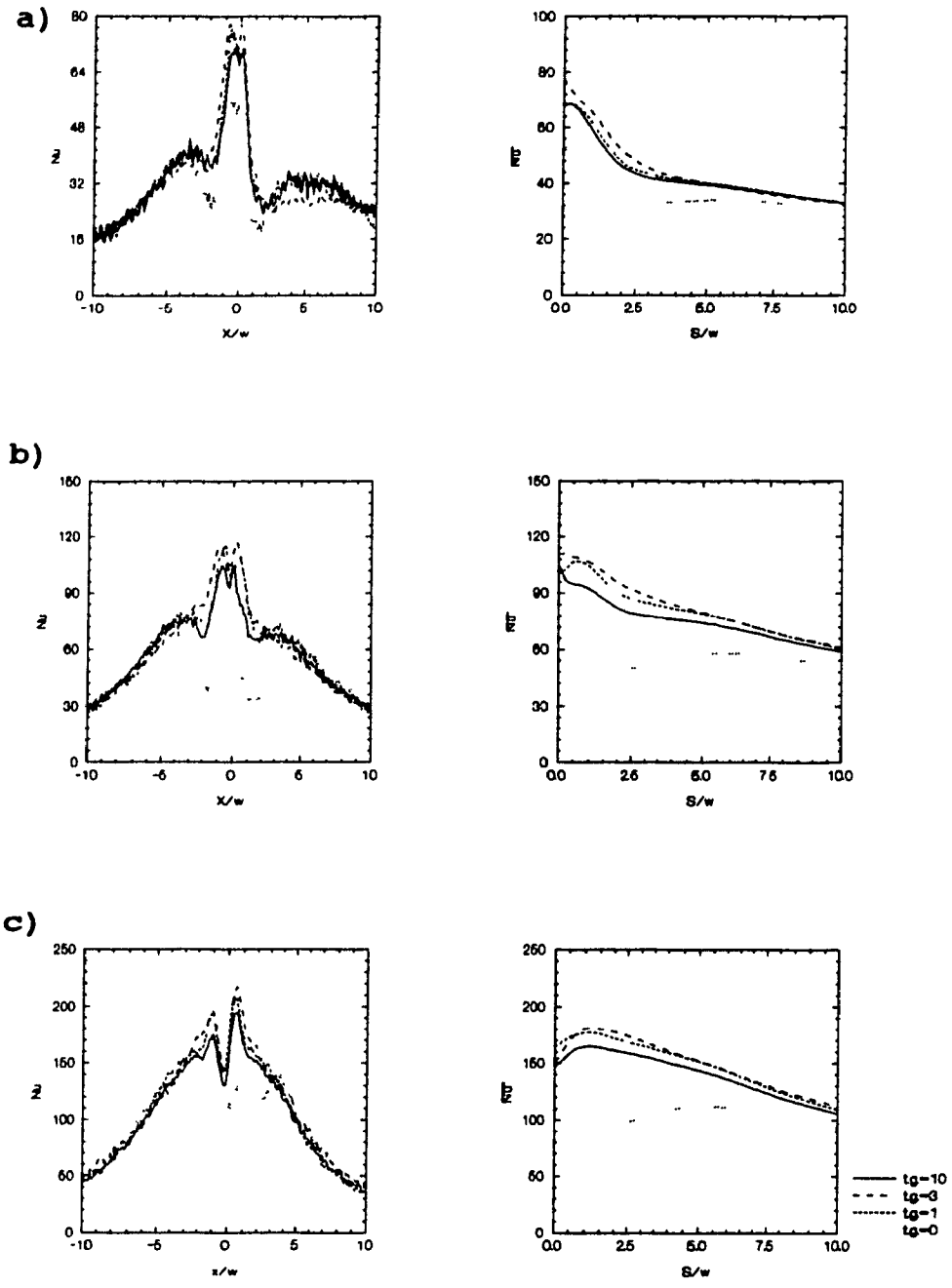

Figure C.8 Profiles of local and average Nu for H=37mm, w=25mm: a) Re_j=12000; b) Re_j=24000; c) Re_j=40000.